2014

Synthesis and Analysis of Copper Beta-Diketonate Complexes

Jonathan Stephen Casey
Louisiana State University and Agricultural and Mechanical College, jcase16@tigers.lsu.edu

SYNTHESIS AND ANALYSIS OF COPPER BETA-DIKETONATE MOLECULAR COMPLEXES

A Thesis

Submitted to the Graduate Faculty of the
Louisiana State University and
Agricultural and Mechanical College
in partial fulfillment of the
requirements for the degree of
Master of Science

in

The Department of Chemistry

by
Jonathan Stephen Casey
B.S., University of New Orleans, 2010
August 2014

Acknowledgements

I want to express my gratitude and appreciation to my parents Christopher and Andree Casey for their unrelenting support of my academic pursuits. Personally and financially, it is because of your assistance I have achieved a certain level of professional success.

I would like to thank my two academic advisors for their patience and dedication to helping me achieve my goals. Dr. Maverick, thank you for your infinite patience with my variety of different questions. The time you spent explaining and going over concepts was invaluable and instrumental towards advancing the research and my knowledge of chemistry. Additionally, you exhibited a genuine kindness which was much appreciated especially in the research world. Dr. Russo, I appreciate the hard-nosed approach and self-reliance you advocated. Intellectual autonomy and contrasting ideas is as every bit important to advancing science as I believe cooperation is. I also wish to acknowledge Dr. Pokharel (Dr. Maverick's group) and Wayne Huberty (Dr. Russo's group) with the time each has given me in the respected labs. Both of your assistance was instrumental in becoming competent and knowledgeable about each of the respected fields.

My thesis document was a sizeable undertaking that took much time to complete and finish. Thank you Dr. Mavierck, Dr.Russo, Dr. Cornelia Rosu, and Dr. Melissa Collins for the hours/days spent making suggestions and comments on my thesis. Considering how much of your own time went into it, I cannot express enough gratitude for your assistance with this project. Again thank you for your generosity with this task.

I would like to thank Dr. Garno and her group for the AFM analysis on our compounds. Thank you especially Tian Tian and Xianglin Zhai for analyzing the complexes. Thank you to Kitty Liu from Dr. Licata's lab for assistance in learning how to operate the AUC machine. I wish to express my gratefulness to Mrs. Susan Saale of the tutor center at LSU's Middleton library. Much of the mathematics involved for the project were not immediately understood and were at times esoteric.

Thank you for taking your own time and energies to help me understand the mathematical concepts involved with this project. I would also like to express my gratitude to Mrs. Connie David for the analysis of our copper complexes by ESI-TOF mass spectrometry and MALDI. You have given much of your own time with the variety of questions I had regarding mass spectrometry. I learned a great deal about mass spectrometry and much of it was because of the time you gave in helping me understand it.

Dr. Marzilli, Dr. Duran, and Dr. Eades thank you for agreeing to be on my committee and accepting all of the obligations that comes along with it. I realize it takes a good deal of your own time and energy to do this; therefore I cannot express enough gratitude for the time you have dedicated to this. Thank you again.

Acknowledging those who helped me get adjusted to Baton Rouge life: Mr. Kyle Cupit, Dr. Frank Schalow (University of New Orleans), and Dr. John Pojman. Anytime there are major shifts in life, there are difficulties and challenges becoming adapted to new environments; thank you especially for helping me getting adjusted to new surroundings.

Finally I would like to thank all of my family and friends who have assisted me in my academic pursuits. Thank you all that have contributed to my goals and academic progress.

Table of Contents

Abstract

This research addresses the synthesis and characterization of Cu(II) complexes of silicon-based multidentate β-diketonate ligands. The possible products of the synthesis include (where L represents the coordinated ligand) cube $Cu_{12}L_8$, decahedron $Cu_{24}L_{16}$, and dodecahedron $Cu_{30}L_{20}$. This study aims to determine the structure of these discrete molecules, which may have applications in drug delivery, fuel storage, and chemical retention.

Different techniques were involved in the characterization of Cu(II) complexes: Electrospray Ionization Time of Flight Mass Spectrometry (ESI-TOF MS), Atomic Force Microscopy (AFM) and Analytical Ultracentrifugation (AUC).

In ESI-TOF MS, the exact mass of the molecules was attempted to be determined by experimenting if multiply charged ions could occur with these complexes. Although no multiply charged ion peaks were discovered, different experimental conditions yielded different ESI-TOF MS spectra. Additionally in ESI-TOF MS, peaks having large m/z values containing copper atoms were discovered.

In AFM studies, heights of multiple copper complexes were measured to see if the discrete molecules of cube (2 nm), decahedron (3.5-4.5 nm), and dodecahedron (5 nm) could be identified. In creating an AFM histogram, the frequency of heights could be used to determine what kind of complexes were being formed and in what percentage. In the studies conducted, there were common occurrences of the samples at or around the heights of the projected structures (e.g. cube, decahedron, and dodecahedron). Additionally, there was a substantial occurrence of measured heights (i.e. 8 nm and 10 nm) that indicated possible aggregation of the discrete molecules.

The AUC technique was used to determine whether the samples contained a pure compound or a mixture of discrete molecules, and also to estimate their molecular weight. What was found in the AUC studies of the Cu(II) complexes of silicon-based multidentate β-diketonate ligands were molecular weights similar to the empirical formula of the molecules (i.e. $Cu_3(MeSi(phac)_3)_2$: 1322.07 g/mol;

$Cu_3(MeSi(phpr)_3)_2$: 1567.80 g/mol) and samples that were polydisperse. No evidence from AUC showed the discovery of compounds which had molecular weights similar to the proposed polyhedra. The numbers are based on assumed densities of 1.138 g/mL.

Chapter 1: Porous Metal Organic Materials (MOMs)

1.1 Properties of Metal Organic Materials

Zeolites are porous minerals made of aluminosilicates [1]. They are known as molecular sieves; Just as garden sieve separate unwanted stones from topsoil allowing nutritive soil through [2], molecular sieves (zeolites) pass some molecules through but not others. These minerals were discovered hundreds of years ago in rock formations, and initially had little practical use in industrial settings [3]. Since then, zeolites have grown as a field of research with applications in water treatment [4-7], petroleum refinement [8-10], and catalysis [11-13].

Union Carbide was one of the first companies to help elucidate the structure of zeolites (i.e. Faujasite) and promoted their industrial applications between 1940-1960 [14]. Zeolite X (Faujasite's) structure was determined by X-ray crystallography by Robert M. Milton of Union Carbide [14]. Today Faujasite is used as an absorbent [15]. Even though zeolites are extensively used, limitations associated with their structure can restrict their application. The pore sizes of zeolites are typically small (due to their strictly inorganic components), and therefore zeolites are used for specific functions (i.e. filtration, purification, refinement, etc.). Metal organic materials (MOMs) have expanded the versatility of porous compounds by their unique properties soon to be discussed [1].

Much progress has been made over the past two decades in the development of metal-organic materials (MOMs) [1]. MOMs have diverse applications and can be used as gas storage devices [16, 17], in catalysis [18-21], and in other applications such as drug delivery [22, 23]. MOMs are created by the self-assembly of a metal ion and an organic ligand [24]. When the metal and ligand are bound together, the desired structure (or pore) can be formed. In addition, having both inorganic and organic modules affect the retention of guest molecules in MOMs compared to zeolites. A comparison of H_2 retention for zeolites compared to metal organic material retention was performed by Isaeva and coworkers [25]. They found different properties of MOMs made hydrogen retention more effective. One feature of

MOMs compared to zeolites was the metal organic materials ordered structure making H_2 uptake more effective [25].

Catenation is a phenomenon which can affect the retention of guest molecules. It takes place when there is an entanglement between metal organic materials which can decrease the size of the pore [26]. For example, Fujita and coworkers showed the catenation of discrete polyhedral cages of palladium based compounds reduced the pore size of the metal organic polyhedron (MOPs) [27]. Catenation is not common among metal organic polyhedra and is more common with metal organic frameworks, but cited literature studies have shown catenation can occur with MOPs [28].

Another property of MOMs that affects retention of different hosts is the metal center. When the metal cation is unsaturated, it is open to other attachments [26]. An example is the research performed by Long and coworkers on the MOFs of $Mn_3(BDT)_2Cl_2(DEF)_6$ and Mn_4-$(BDT)_3(NO_3)_2(DEF)_6$ (BDT^{2-} = 1,4-benzeneditetrazolate; DEF = N,N-diethylformamide [29]. When the tetrazolate ligands were removed from the MOF containing manganese metal, the retention of H_2 increased significantly. Depending on the metal center, this will have an effect on host retention of guest molecules [25, 30].

Additionally, organic ligands play a role in the absorption of molecues [26]. Having electron donating groups on the metal center is one way to increase the retention of H_2 [26]. One way to improve hydrogen storage for instance, is to increase the aromaticity of organic ligands [31-33]. For example, Kuang and coworkers showed groups of $Zn_4O(CO_2)_6$ linked together with organic ligands with greater aromaticity were able to adsorb more H_2 than less aromatic ligands [31].

1.2 Silicon-Based Multidentate β-Diketonate Ligands and Copper β-diketonate Complexes

The ligands used in this research were $MeSi(phacH)_3$, $MeSi(phprH)_3$, and $MeOC_6H_4(CH_2)_3Si(phacH)_3$. Their structures appear in Figure 1.1.

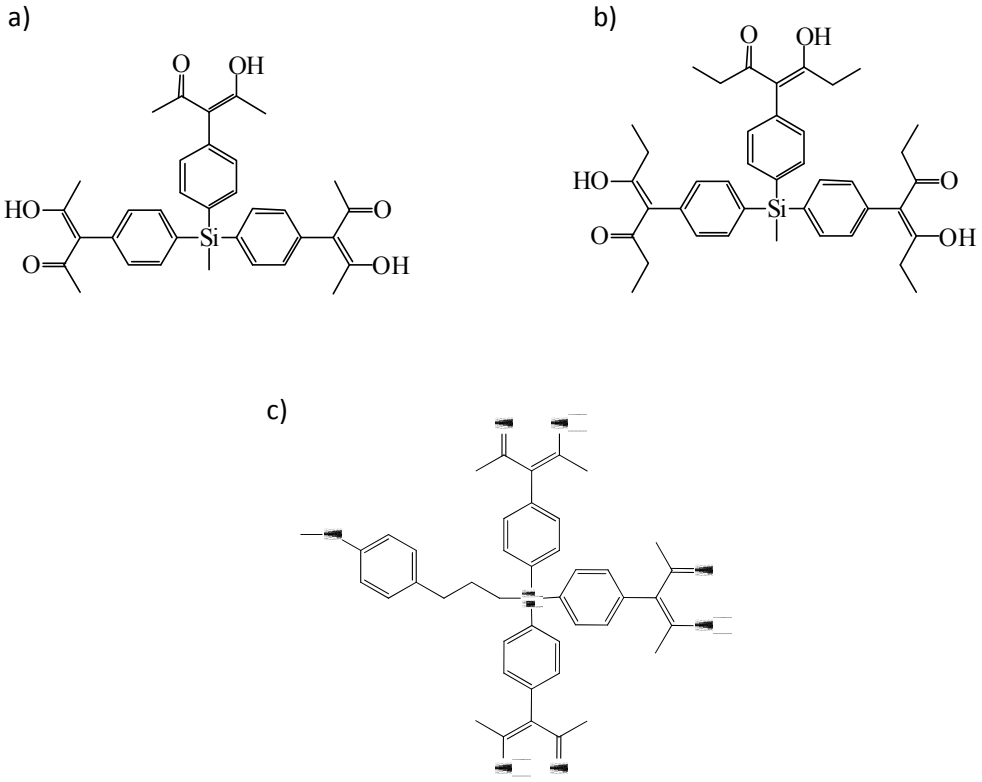

Figure 1.1- Silicon-based multidentate β-diketonate ligands.
a) $MeSi(phacH)_3$
b) $MeSi(phprH)_3$
c) $MeOph(CH_2)_3Si(phacH)_3$

The ligands in Figure 1.1 were used in the synthesis to yield three-dimensional complexes. The geometry of these structures is unknown and is the focus of this research. Projected structures were made using the program HyperChem (Hypercube Inc., Gainesville Florida) by Dr. Andrew Maverick of Louisiana State University and are shown in Figure 1.2. The ratio between the copper (II) metal and the ligand in the reaction is 3:2. The empirical formula of these complexes is expressed as Cu_3L_2, where L represents one of the ligands shown in Figure 1.1. Figure 1.2 displays 3D structures possibly forming from the synthesis (e.g. cubic, decahedron, and dodecahedron).

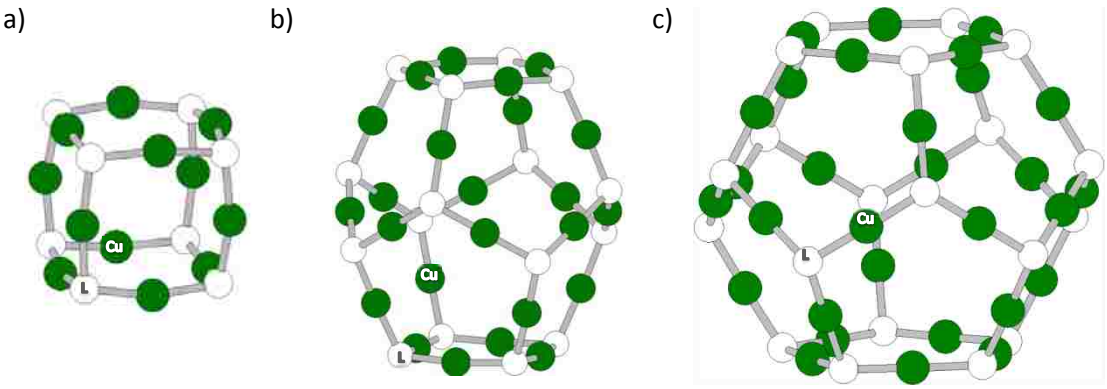

Figure 1.2- Copper β-Diketonate Molecular Complexes. Green = Cu atoms; White = ligands.
a) Cube- $Cu_{12}(L)_8$
b) Decahedron- $Cu_{24}(L)_{16}$
c) Dodecahedron- $Cu_{30}(L)_{20}$

These images are based on molecular modeling of $Cu_{12}(L)_8$, $Cu_{24}(L)_{16}$, and $Cu_{30}(L)_{20}$. The green spheres represent the Cu(II) center, and the white spheres a whole silicon-based β-diketonate ligand. The grey bond signifies the coordinated β-diketonate to the Cu metal. Figure 1.3 shows an example of the silicon based ligand coordinating to the Cu metal.

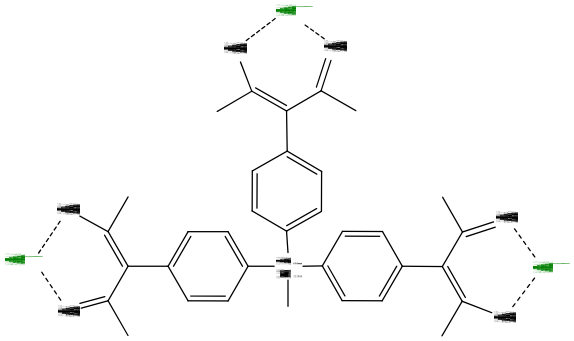

Figure 1.3- Example of β-diketonate ligand $MeSi(phacH)_3$ coordinating to copper metal.

The three β-diketonate groups form ~109.5° angles at the Si atom and bind effectively to the unsaturated metal center [34]. The chealating unit bound to the copper ion (Figure 1.3) increases the

stability of the complex. Chealation increases stability by having two instead of one atom bound to the metal center.

1.3 Characterization of Metal Organic Materials (MOMs) and Copper β-Diketonate Complexes

Silicon-based β-diketonate copper complex have shown to be resistant to some methods of structural elucidation, but have shown possibility of analysis by others. For instance the unknown copper complexes have properties resistive to common forms of analysis such as X-ray crystallography and nuclear magnetic resonance (NMR). Other characterization techniques used in this research show the possibility of determining the structure of the molecules. The techniques used for the research are electrospray ionization time of flight mass spectrometry (ESI-TOF MS), atomic force microscopy (AFM), and analytical ultracentrifugation (AUC).

For crystalline MOMs, X-ray analysis is sufficient to elucidate their structure [35]. Maverick and coworkers synthesized copper β-diketonate molecular squares which were able to be characterized using X-ray crystallography [35]. Unlike the copper β-diketonate complexes analyzed in previous research, these silicon-based β-diketonate complexes do not form crystals which are able to be characterized by X-ray crystallography.

Nuclear magnetic resonance (NMR) has shown potential for characterization of paramagnetic compounds [36]. Pierattelli and coworkers demonstrated copper(II) proteins able to be structurally elucidated by NMR [36]. Although progress has been made in using NMR to characterize paramagnetic compounds, other obstructions limit NMR's effectiveness at elucidating different materials. In the case of these copper organic complexes, NMR has been ineffective. These supramolecular structures are difficult to analyze by NMR due to the high symmetry of the complexes. The resulting NMR would have similar peaks for the cube, decahedron, and dodecahedron since these complexes would be expected to have similar resonances; it would be difficult to assign them to specific complexes.

Nevertheless, attempts have been made to collect NMR spectra on $Cu_3(MeSi(phac)_3)_2$. An NMR spectrum was taken with the known compound of copper(II) acetylacetonate ($Cu(acac)_2$) shown in the Appendix C section of the thesis.

The structure of $Cu(acac)_2$ is in Figure 1.4 below:

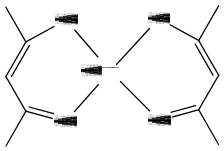

Figure 1.4- Copper(II) acetylacetonate ($Cu(acac)_2$)

The ^1H NMR spectrum of $Cu(acac)_2$ showed only one very broad resonance. Similar spectra of $Cu_3(MeSi(phac)_3)_2$ did not show any resonances attributable to the metal-organic molecules.

Electrospray Ionization Time of Flight Mass Spectrometry (ESI-TOF MS) may be a useful technique in determining the structure of the copper complexes. Copper's natural isotopic abundance (^{63}Cu, 69.17%; ^{65}Cu, 30.83%) [37] leads to distinctive mass spectrometry patterns. This may be a way to identify the copper complexes that are forming. ESI-TOF MS gives the exact mass of the compound, and since copper leaves an isotopic "thumbprint", it may be possible to determine the exact ratio of copper to ligand. If the copper complexes become multiply charged in mass spectrometry, then it may be possible to determine its structure. Multiply charged ions would bring the complexes in a range mass spectrometry could analyze (the range of the ESI-TOF MS instrument is 3000 amu), since values given by this technique are mass-to-charge (m/z).

In atomic force microscopy (AFM) the size of the copper organic material is analyzed providing support to the idea of 3D complexes being formed. In these AFM studies, a milligram amount of sample is analyzed by the instrument. Several points on the AFM substrate are measured, and an AFM

histogram is made. AFM could be useful in giving an estimate of the proportion of copper complexes being made with each of these syntheses.

Another technique being used to characterize the copper complexes is Analytical Ultracentrifugation. AUC utilizes the properties of sedimentation and diffusion of a substance to determine its molecular weight. Analytical Ultracentrifugation could give the molecular weight of the copper complexes as well as the sedimentation coefficient. This will be the topic of discussion for the next chapter.

Chapter 2: Analytical Ultracentrifugation

2.1 Introduction

Analytical Ultracentrifugation (AUC) is a powerful tool in analyzing compounds. It utilizes the properties of sedimentation and diffusion of a substance to determine the molecular weight of a sample and if the sample contains multiple species. In addition, AUC can be used to examine interactions of different molecules with each other. For instance, Correia and coworkers used AUC to demonstrate the binding affinity of Eribulin (E7389) and ER-076349 (anti-mitotic drugs) with tubulin to determine their effect on microtubule assembly [38]. By using the sedimentation coefficient (explained in section 2.4) of the solute in AUC, the interaction between the anti-mitotic drug and tubulin were able to be quantified. In this research, the different species possibly contained in solution and their molecular weights is what is being determined.

Chapter 2 is divided into various sections explaining how AUC operates. Section 2.2 will go into a brief history of the ultracentrifuge and give a description of the mechanics of the AUC instrument. The laws governing sedimentation and diffusion are contained in Section 2.3 and 2.4. This section is important to understanding the hydrodynamic principals which allow for experimental values to be ascertained. In Section 2.4, velocity ultracentrifugation is described in detail as a way to determine the sedimentation coefficient. The sedimentation coefficient is important as it can allow for other characteristics of the molecule (i.e. molecular weight) to be discovered. Section 2.5 describes equilibrium ultracentrifugation and the equations involved. This will provide explanation of how the molecular weights of compounds can be established using a different form of AUC.

AUC velocity and AUC equilibrium experiments with BSA are in Section 2.6. These experiments were performed on a molecule already characterized by AUC to ensure the reliability of the results for the unknown copper complexes. Section 2.7 contains simulated data used to replicate situations of ideal samples to get an idea of what experimental test would resemble.

2.2 Analytical Ultracentrifuge Instrument

Theodor H. E. Svedberg was a Swedish chemist who invented the ultracentrifuge in the 1920s at Uppsala University [39]. The invention of ultracentrifugation came from his study of colloidal particles with the goal of determining the size of colloids in solution. He won the Nobel Prize in chemistry in 1926 for his work in this area [39]. An illustration of a modern analytical ultracentrifuge is in Figure 2.1 below.

Analytical Ultracentrifugation operates on the principles of sedimentation and diffusion of molecules in solution. A sample in solution is inserted into a sector-shaped cell (see Figure 2.2) and is analyzed. The sector-shaped cell is placed inside a metal rotor (usually titanium or aluminum) and spun at extremely high speeds (e.g. AUC velocity typically spins at 38 krpm and AUC equilibrium usually spins at 11 krpm) where it is then analyzed [40]. The sample sediments over time to the bottom of the cell and the change in concentration of the sample give the information necessary to determine the physical characteristics of the molecules.

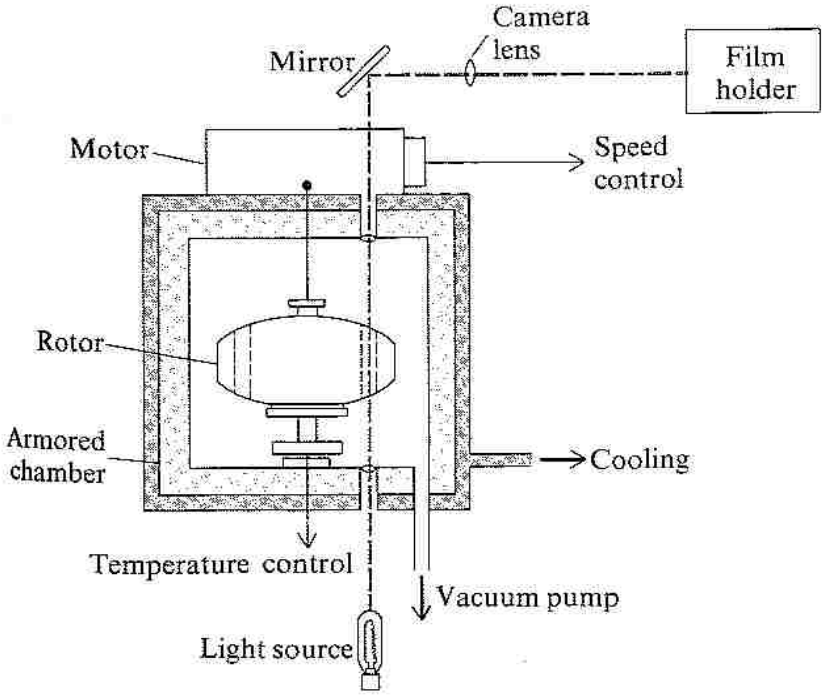

Figure 2.1- Schematic of Analytical Ultracentrifugation Apparatus [41].

The chamber housing the rotor is under vacuum due to the high speed at which the rotor spins preventing the formation of superheated air. Additionally, the rotor is encased in a guarded chamber in the case of mechanical failure [40]. To protect the instrument, balancing the rotor load is a necessity. The shaft where the rotor sits can become distorted under the asymmetric force. The maximum mass difference between the experimental cell and the counter balance is 0.5 g [40].

The cells where the samples are analyzed are sector-shaped pieces (Figure 2.2). The pieces come in a single-sector cell, double-sector cell, and six-sector cell pieces. In the experiments performed on the copper complexes, a double-sector cell made of aluminum was used. The amount of sample placed in the cells can vary, but it typically ranges from 0.1 to 1 mL of sample in solution [40].

The cells are designed to be sector-shaped, because of the sedimentation of the sample. If the cells were square or rectangular, the sample would curve inwards and affect the analysis. If the cells were too trapezoidal, then the solute sample would curve inwards. The following are diagrams of the geometry of different cells in Figure 2.2 [40]:

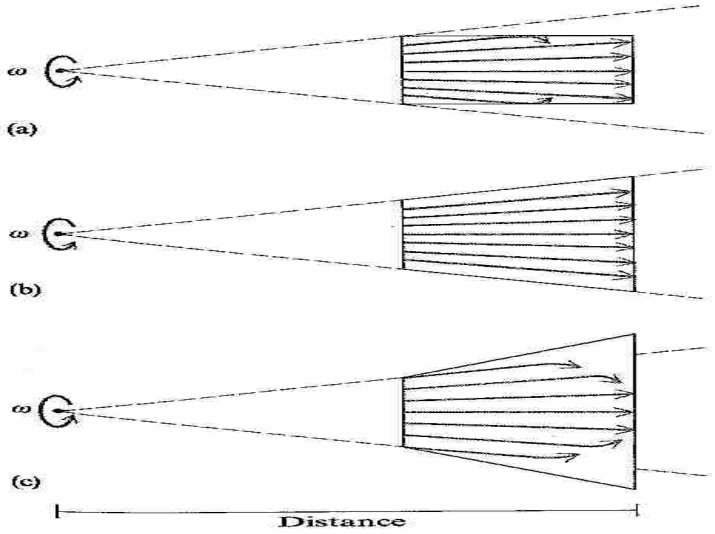

Figure 2.2- Fluid Dynamics of Solute Molecules in the Ultracentrifuge Cell.-
a) Rectangular cell
b) Sector-shaped cell
c) Trapezoidal cell [42]

2.3 Diffusion

Brownian motion, the random motion of particles in solution, is often used to describe diffusion. The first experiment to demonstrate this was performed in 1828 by Robert Brown [43] when he observed the motion of pollen grains in water using a microscope [44]. Over time, particles (pollen grain) suspended in solution became evenly distributed throughout. Diffusion of molecules minimizes concentration gradients [43]. Figure 2.3 is an example of diffusion:

Figure 2.3 Diffusion of molecules in solution. [45]

Fick's first law describes the one-dimensional diffusional properties of concentration and distance. Fick's first law is [43]:

$$J = -D\left(\frac{\partial C}{\partial x}\right) \qquad \text{Equation 2.1}$$

In equation 2.1, *J* is the flow, *D* is the diffusion coefficient, and ∂C/∂x is the rate of concentration change with respect to distance [43]. The equation states the higher the concentration and the larger the distance, the greater the flow will be. Fick's first law is used for one-dimensional analysis [45]. It is the diffusion of a substance in planar areas such as in gels or films. The continuity equation expands

this, as it takes into account the three-dimensional characteristics of position and the one-dimension of time [43]. The continuity equation is expressed in equation 2.2:

$$\Delta w = J(x)A\Delta t - J(x + \Delta x)A\Delta t \qquad \text{Equation 2.2}$$

For the continuity equation, Δw is the change in mass, *J*(x) is the flow rate, *J*(x+Δx) is the flow rate of mass out of a volume, A is the perpendicular cross-sectional area to the direction of flow, Δt is the change in time, and AΔx is the total volume of the object. Figure 2.4 illustrates the flow of mass in and out of a volume:

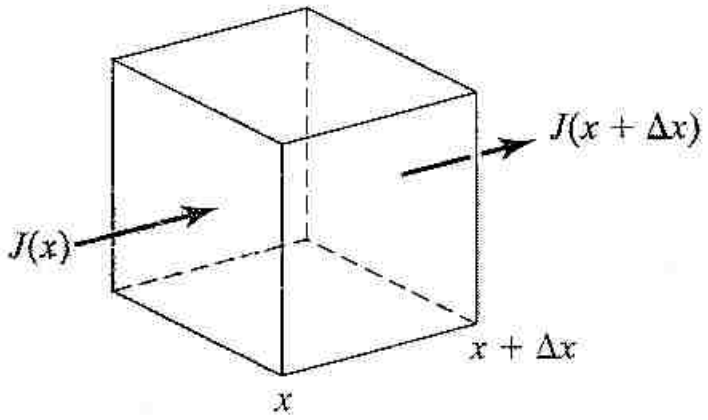

Figure 2.4- A three dimensional object demonstrating the continuity equation expressing flow of material in an object and flow out of an object [45].

The change in concentration (ΔC) can be determined by the change of mass divided by the total volume of the object:

$$\Delta C = \frac{\Delta w}{A\Delta x} \qquad \text{Equation 2.3}$$

When the continuity equation is divided by the total volume of the object (AΔx), the change in concentration can be determined (ΔC). This is seen in the equations below:

$$\frac{\Delta w}{A\Delta x} = \frac{J(x)A\Delta t - J(x + \Delta x)A\Delta t}{A\Delta x} \qquad \text{Equation 2.4}$$

$$\Delta C = \frac{J(x) - J(x + \Delta x)}{\Delta x}\Delta t \qquad \text{Equation 2.5}$$

$$\frac{\Delta C}{\Delta t} = \frac{-\Delta J}{\Delta x} \qquad \text{Equation 2.6}$$

The concentration is dependent on the flow in and flow out [43]. The combination between the continuity equation and Fick's first law results in Fick's second law:

$J = -D\left(\frac{\partial C}{\partial x}\right)$ Fick's First Law

$\frac{\partial C}{\partial t} = \frac{-\partial J}{\partial x}$ The Continuity Equation

$$\left(\frac{\partial C}{\partial t}\right) = \frac{-\partial}{\partial x}\left(-D\left(\frac{\partial C}{\partial x}\right)\right) \qquad \text{Equation 2.7}$$

$$\left(\frac{\partial C}{\partial t}\right) = D\left(\frac{\partial^2 C}{\partial x^2}\right) \qquad \text{Equation 2.8}$$

Fick's second law describes all one dimensional diffusional properties [43]. Beyond the parameters of diffusion, there are other considerations to take into account. The shape and morphology of the molecules studied as well as the frictional coefficient is a feature of this. The relationship between the diffusion coefficient and frictional coefficient is expressed in Equation 2.9 [43]:

$$D = \frac{kT}{f} = \frac{RT}{\mathcal{N}f} \qquad \text{Equation 2.9}$$

Where k is Boltzmann constant, T is temperature, $\mathcal{N}$ is Avogadro's number, R is the ideal gas constant, and f is the frictional coefficient [43]. The frictional coefficient is a resistant force experienced by molecules moving through solution and depends on both the morphology of the molecule and the properties of the solvent [43]; For spherical molecules Stoke's law is applied [43]:

$$f_0 = 6\pi\eta a \qquad \text{Equation 2.10}$$

Where f_0 is the frictional coefficient, η is the viscosity of the solvent, and a is the radius of a sphere [43].

$$D_0 = \frac{RT}{6\pi\mathcal{N}\eta a} \qquad \text{Equation 2.11}$$

Depending on the shape of the molecule, the frictional coefficient can be determined by using the appropriate equation. Table 2.1 gives examples of the different shapes with the corresponding frictional coefficients [43]:

Table 2.1 [43] -The frictional coefficients for various shapes. The α value is half the length of the major axis, the β value is the radius of the minor axis.

Morphology	Frictional Coefficient
Prolate ellipsoid	$f_0 = 6\pi\eta(\alpha\beta^2)^{1/3}$
Oblate ellipsoid	$f_0 = 6\pi\eta(\alpha^2\beta)^{1/3}$
Long rod	$f_0 = 6\pi\eta\left(\frac{3\alpha\beta^2}{2}\right)^{1/3}$

2.4 Centrifugal Sedimentation and Velocity Ultracentrifugation

Two types of sedimentation are known: gravity sedimentation and centrifugal sedimentation [44]. The research deals exclusively with centrifugal sedimentation and this will be the primary focus of discussion.

Centrifugal sedimentation can be used to determine the molecular mass of molecules smaller than 1 μm. The rate at which the particles settle is affected by the size and shape of the molecules. Diffusion affects the rate of sedimentation and is inversely related to the mass of the molecules [44]. Centrifugal sedimentation is the motion of molecules in solution away from the rotation axis [44]. This occurs when the centrifugal force is applied to the solution. In centrifugal sedimentation, three primary forces are involved: centrifugal, buoyancy, and frictional force. Figure 2.5 illustrates the three forces involved in centrifugal sedimentation:

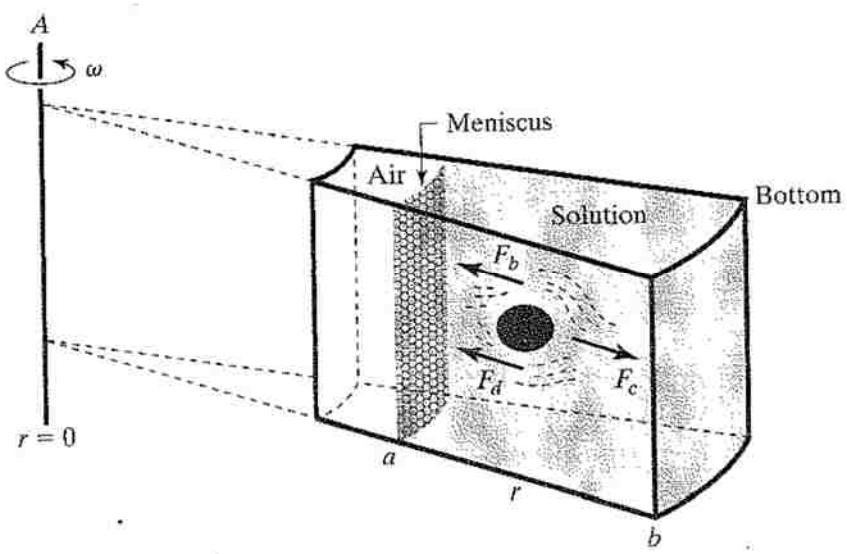

Figure 2.5-Schematic of centrifugal sedimentation: F_c, F_b, and F_d are centrifugal, buoyancy, and frictional force [45].

Centrifugal force is the force applied by the spinning rotor:

$$\mathrm{F_c} = \omega^2 \mathrm{rm} \qquad \text{Equation 2.12}$$

Where ω is the angular velocity (radians per second), r is the distance from the rotation center, and m is the mass of the sample. The centrifugal force is the angular momentum squared times the mass and the distance from the rotation center [43].

Buoyancy force is the force pushing on the molecule from the displaced solution. This force is equal to the force the solution is displaced:

$$\mathrm{F_b} = -\omega^2 \mathrm{rm_0} \qquad \text{Equation 2.13}$$

In this case, m_o would be the mass of the solvent displaced. The buoyancy force is negative since it is a counter force to F_c [43].

Frictional force is the other counter force to centrifugal force, it is the frictional coefficient times the velocity (v) of the particle [43]:

$$\mathrm{F_d} = -\mathrm{fv} \qquad \text{Equation 2.14}$$

When a molecule is at rest, the net force will be zero due to the cancellation of all of the forces. The equation will then be set to zero:

$$F_c + F_b + F_d = 0 \qquad \text{Equation 2.15}$$

$$\omega^2 rm - \omega^2 rm_0 - fv = 0 \qquad \text{Equation 2.16}$$

In the buoyancy force expression, the mass of the solvent displaced m_o, can be substituted with the mass of the sample times the partial specific volume ($\bar{v}$) and the density of the solution (ρ). The partial specific volume can be described as the inverse density of the molecule examined [43]. The equation gives:

$$\omega^2 rm - \omega^2 rm\bar{v}\rho - fv = 0 \qquad \text{Equation 2.17}$$

Rearrangement of terms in Equation 2.17 gives:

$$\omega^2 rm(1 - \bar{v}\rho) - fv = 0 \qquad \text{Equation 2.18}$$

$$\omega^2 rm(1 - \bar{v}\rho) = fv \qquad \text{Equation 2.19}$$

$$\frac{\omega^2 rm\,(1 - \bar{v}\rho)}{f} = v \qquad \text{Equation 2.20}$$

When this equation is multiplied by Avogadro's number (to convert it to molar form) the equation becomes the following:

$$\frac{M\,(1 - \bar{v}\rho)}{\mathcal{N}f} = \frac{v}{\omega^2 r} = s \qquad \text{Equation 2.21}$$

The sedimentation coefficient (s) is equal to the velocity of the sample divided by the momentum squared times the distance from the rotation center [43]. The $\omega^2 r$ make up the centrifugal field. Sedimentation is measured in units of Svedberg (S), which are 1×10^{-13} sec [43]. The Svedberg unit was named after the founder of the ultracentrifuge, Theodore Svedberg, and the sedimentation value of 1×10^{-13} sec was agreed upon by the values common occurrence in experimental measurements.

2.5 Equilibrium Ultracentrifugation

Sedimentation equilibrium occurs when the sedimentation of the molecules is equal to the diffusion of molecules. Sedimentation flow (J_s) is a component of sedimentation equilibrium. This is illustrated in Equation 2.22.

$$J_s = v_s C = \frac{M(1-\bar{v}\rho)\omega^2 r\, C}{\mathcal{N} f} \qquad \text{Equation 2.22}$$

The sedimentation flow is the speed (v_s) at which the molecules sediment times the concentration (C) of the solution [43]. The equation is reminiscent of the sedimentation coefficient. When equilibrium is achieved, the total flow will be equal to zero and Fick's first law of diffusion can be used. The reason for this is when a system reaches equilibrium, concentration is not a function of time, only a function of distance [43]. In terms of equilibrium, sedimentation flow (J_S) subtracted by diffusional flow (J_D) is zero. This is represented by the following equations:

$$J = J_s + J_d \qquad \text{Equation 2.23}$$

$$J = \frac{M(1-\bar{v}\rho)\omega^2 r\, C}{\mathcal{N} f} - D\left(\frac{dC}{dr}\right) \qquad \text{Equation 2.24}$$

At equilibrium the flow J is equal to zero:

$$0 = \frac{M(1-\bar{v}\rho)\omega^2 r\, C}{\mathcal{N} f} - D\left(\frac{dC}{dr}\right) \qquad \text{Equation 2.25}$$

Because $D = \frac{RT}{\mathcal{N} f}$ the equation can be further modified:

$$\frac{RT}{\mathcal{N} f}\left(\frac{dC}{dr}\right) = \frac{M(1-\bar{v}\rho)\omega^2 r\, C}{\mathcal{N} f} \qquad \text{Equation 2.26}$$

$$\left(\frac{dC}{dr}\right) = \frac{M(1-\bar{v}\rho)\omega^2 r\, C}{RT} \qquad \text{Equation 2.27}$$

According to the power rule, you get $\frac{d}{dx}(x^n) = nx^{n-1}$ [46]. Taking the derivative of r^2 you receive:

$$\frac{d}{dr}(r^2) = 2r \qquad \text{Equation 2.28}$$

$$d\,(r^2) = 2rdr \qquad \text{Equation 2.29}$$

$$\frac{d\,(r^2)}{2} = rdr \qquad \text{Equation 2.30}$$

When this equation is applied to equation 2.27 you receive the following:

$$\left(\frac{dC}{dr^2}\right) = \frac{M(1-\bar{v}\rho)\omega^2 C}{2RT} \qquad \text{Equation 2.31}$$

Dividing dC by C one obtains dln(C) you get by the chain rule [46],

$$\frac{d}{dx}(\ln x) = \frac{1}{x} \qquad \text{Equation 2.32}$$

When the chain rule is substituted in for dC you receive the following equation:

$$\frac{d\ln(C)}{d(r^2)} = \frac{M(1-\bar{v}\rho)\omega^2}{2RT} \qquad \text{Equation 2.33}$$

Taking the integration of both sides will remove the derivative from the left side of the equation and makes ($r^2 - r_b{}^2$) a variable on the right side of the equation:

$$\int\frac{d\ln(C)}{d(r^2)} = \int\frac{M(1-\bar{v}\rho)\omega^2}{2RT} \qquad \text{Equation 2.34}$$

$$\ln\left[\frac{C(r)}{C(r_b)}\right] = \frac{M(1-\bar{v}\rho)\omega^2}{2RT}\,(r^2 - r_b{}^2) \qquad \text{Equation 2.35}$$

$$2.303 \times \log\left[\frac{C(r)}{C(r_b)}\right] = \frac{M(1-\bar{v}\rho)\omega^2}{2RT}\,(r^2 - r_b{}^2) \qquad \text{Equation 2.36}$$

$r_b{}^2$ is the point of the meniscus, and r^2 is the end point of the solution.

$$\frac{C(r)}{C(r_b)} = e^{\frac{M(1-\bar{v}\rho)\omega^2}{2RT}(r^2 - r_b{}^2)} \qquad \text{Equation 2.37}$$

From these equations the molecular weight can be determined (see section 2.6 for actual data analyzed). One form gives the concentration of the sample as a linear function of distance. The other equation places it in exponential form. By knowing the concentration of the sample and its position in the cell, the molecular weight can be determined. Examples of this will be demonstrated in the next section.

2.6 AUC Equilibrium and Velocity Experiments with Bovine Serum Albumin

AUC experiments were performed on the protein bovine serum albumin (BSA). BSA is a well-characterized and known protein whose molecular weight is known (66kDa [47]). Test runs with BSA were performed by analytical ultracentrifugation. AUC experiments were conducted on a well-behaved sample to set the parameters for the unknown copper complexes.

In order to understand what is occurring in the AUC data, it is beneficial to understand how the data is correlated to the physical sample being examined. Figure 2.6 below illustrates an AUC curve with a drawing of the sample in the sector shaped cell:

a) b)

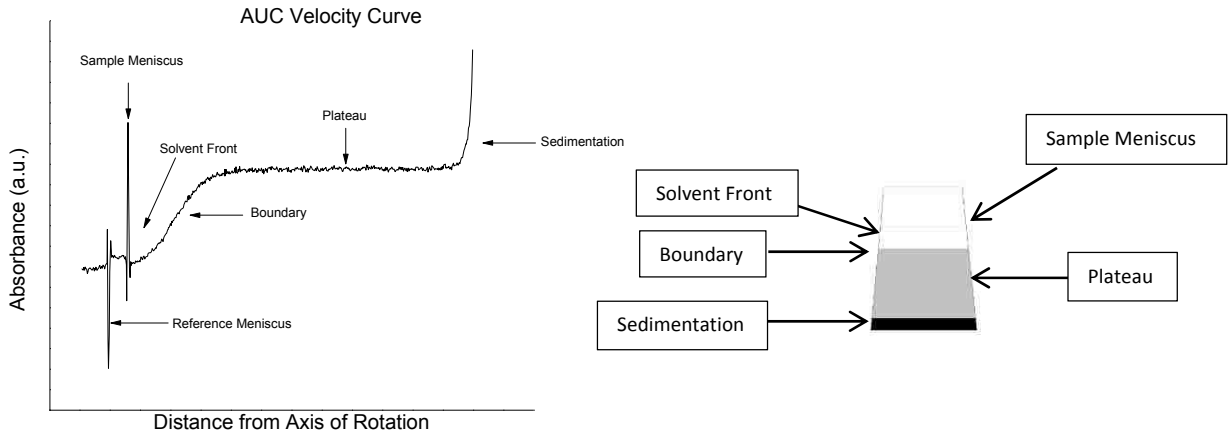

Figure 2.6- AUC Curve and its illustration. a) Real AUC Velocity Data of the sedimentation of Bovine Serum Albumin (BSA) in phosphate buffer saline solution. b) An illustration of the sample section of the AUC sector shaped cell. The sample meniscus is at the top of sample solution; when the light from the AUC instrument hits this area the light is refracted, as indicated by the sharp peak. The solvent front is the area where the solvent contains little or no solute and thus has a low absorbance. The solvent front becomes larger as the sample sediments over time. The boundary area is the area between the solvent front and the plateau region. The plateau region is the region where the sample is approximately uniformly dispersed in the cell. The bottom of the cell is the sedimentation of the sample, and hence its peak upward in the graph.

Velocity AUC and equilibrium AUC were performed on the protein BSA. Below is Figure 2.7, the absorption spectrum of BSA:

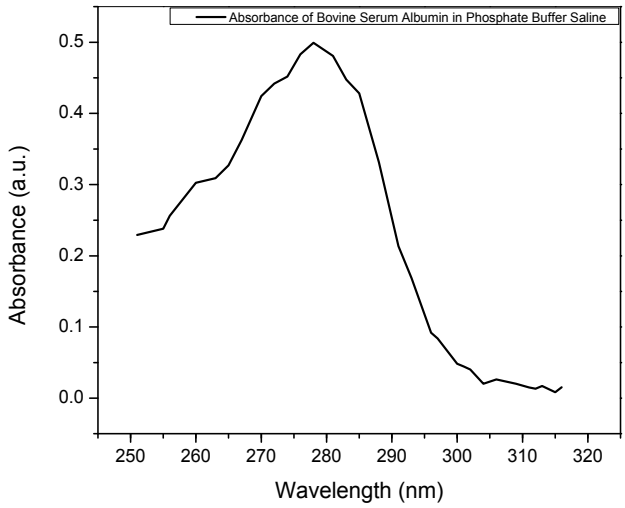

Figure 2.7- BSA absorption spectrum (9.02 x 10^{-6}M in PBS buffer, pH 7.02) at a rotational speed of 3000 rpm.

In the AUC velocity BSA experiment, the sedimentation coefficient was determined for the protein. The velocity scans of BSA were taken every 1000 s at the λ_{max} value of 280 nm, and the speed was set at 38krpm (the ω^2 value was 1.5 x 10^7 rad^2/sec^2). Figure 2.8 below shows the velocity scans beginning at 50 minutes, and each succeeding scan measured 30-35 minutes apart.

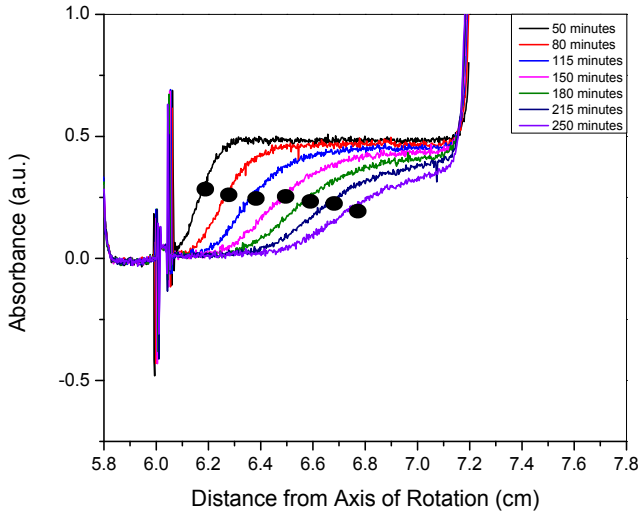

Figure 2.8- BSA AUC velocity data; The wavelength used was 280 nm (λ_{max}); Measurements were at 30-35 minute intervals beginning with an initial 50 minute scan. The black spheres on the curve are the boundary positions where the Ln(R_b) points were taken. Over time the boundary region of the curve becomes broader. This is due to diffusion. As the sample sediments, the concentration increases toward the bottom, and diffusion becomes more of a competing force.

The points measured are where the absorbance reaches half of its boundary value and below the plateau region which is "consistent" in the absorbance (See Figure 2.6). From these points, the graph Ln(R_b) vs. time *w^2r was constructed, as shown in Figure 2.9:

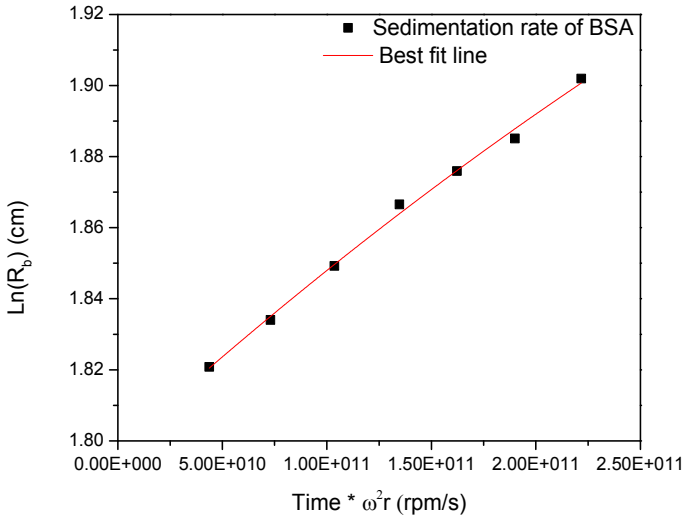

Figure 2.9- Linearized data of BSA AUC velocity. The slope $\frac{v}{\omega^2 r}$ is used to determine the sedimentation coefficient of the protein.

The slope of the graph Ln(R_b) vs. time *ω^2r gives the sedimentation coefficient. This can be seen from the equation 2.38:

$$\frac{v}{\omega^2 r} = s \qquad \text{Equation 2.38}$$

The distance the sample moves Ln(R_b) over time gives the velocity. The value over the $\omega^2 r$ (the centrifugal field) allows for the sedimentation coefficient to be determined. The sedimentation coefficient of the BSA was 4.51 x 10^{-13} s. The literature reported value is 4.50 x 10^{-13} s [48]. The sedimentation coefficient can be used as a quantitative tool in examining interactions between molecules, and can also be used with the diffusional coefficient to determine the molecular weight of a molecule. In order to determine molecular weight with AUC alone, AUC equilibrium is performed.

In the AUC equilibrium BSA experiment, the molecular weight was determined for the protein. The equilibrium scans of BSA were taken every 5 hours at the λ_{max} value of 280 nm, and the speed was

set at 11 krpm (i.e $\omega^2 = 1.3 \times 10^6$ rad^2/sec^2). Figure 2.10 below shows the equilibrium scans beginning at the end of the ~4 hour AUC velocity run (the speed was de-accelerated from 38 krpm to 10 krpm), 10 hours after diffusion, and 20 hours when equilibrium was reached.

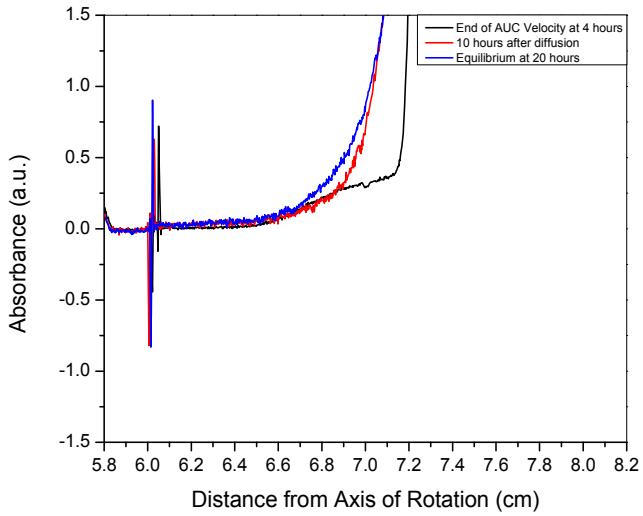

Figure 2.10- BSA AUC Equilibrium; the wavelength used was 280 nm (λ max); the equilibrium speed was set at 10 krpm after being de-accelerated from 38 krpm from the AUC velocity run. The graph indicates the black curve at the end of AUC velocity, the red curve 10 hours after diffusion, and finally the blue curve when equilibrium at 20 hours was reached.

Equilibrium is achieved when sedimentation balances diffusion and no net flow of the sample occurs. The sample is spun at a speed sufficient to cause a measurable perturbation of the concentration, but not enough to cause complete sedimentation. In the software output, the scanned curves will appear on top of one another; this is a reflection of what happened with the AUC equilibrium of BSA. In Figure 2.10, the curves in the figure represent BSA approaching and finally reaching equilibrium.

In order to determine the molecular weight after equilibrium, the raw data was linearized for analysis in Figure 2.11 (See equation 2.35). The area of the curve analyzed was 6.667-7.2cm (r_b value), this region was used for analysis due to concentration of the BSA in the area. Figure 2.11 is the linearized representation of Figure 2.10 (for the equilibrium curve):

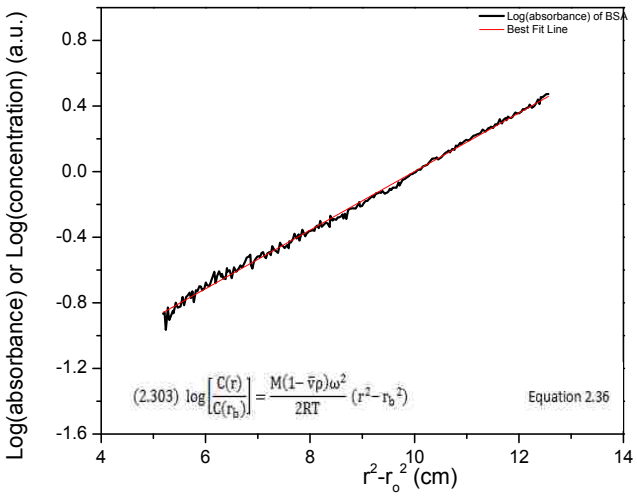

Figure 2.11- Log_{10}(absorbance) vs. rb^2-rm^2 data for AUC equilibrium experiment on BSA. The slope of this graph, multiplied by 2.303, is used to determine the molecular weight of the protein. Linearized data of BSA AUC equilibrium.

According to Eq. 2.36, the slope of Figure 2.10 is proportional to M. The r is the distance from the axis of rotation at a particular point in the cell. r_o is the distance from the meniscus level to the axis of rotation. The equation used to determine the molecular weight from the analysis is below:

$$(2.303)\ \log\left[\frac{C(r)}{C(r_b)}\right] = \frac{M(1-\bar{\nu}\rho)\omega^2}{2RT}\ (r^2 - {r_b}^2) \qquad \text{Equation 2.39}$$

The molecular weight of the BSA was determined to be 66 kDa (the actual value of BSA is ~66.5 kDa). Performing preliminary runs on the BSA was essential in order to ensure reliable results for the unknown copper complex performed later.

2.7 Simulation of One and Two Component Samples

Simulations of one and two component samples were made in order to imitate actual experiments. These mockups were made to give an idea of how ideal systems operate, and what the results would look like given set parameters (i.e. density of solvent, density of compound, etc.). These models were then used to project sedimentation of the unknown copper complexes to give an idea of what the unknown copper complex's results would look like.

The equations used for the simulations were an approximate solution to the Lamm equation; the Lamm equation is as follow [49]:

$$\frac{dc}{dt} = \frac{1}{r}\frac{d}{dr}\left[rD\frac{dc}{dr} - s\omega^2 r^2 c\right] \qquad \text{Equation 2.40}$$

The Lamm equation is used to analyze solutes in solution in a sector-shaped cell. The variables in the Lamm equation are as follows: c is the concentration, t is time, r is the radius from the axis of rotation, D is diffusion, s is the sedimentation coefficient, and ω is the angular velocity. This equation takes in the properties of sedimentation and diffusion to be able to determine the change in concentration over the change in time $\frac{dc}{dt}$.

Two different sedimentation models were made for AUC. The first simulation was for a single-component solute, and the second simulation was for a two-component solute. These equations are a variant of the Lamm equation, and were determined by H. Faxen in 1929 [49]. The Faxen version of the Lamm equation expresses change of concentration distribution c(r,t) of a sample in a sector shaped cell [49]. It requires the sedimentation coefficient (s) and the diffusion coefficient (D) of the sample. The equation can simulate the change in concentration over time in an idealized system. Below are the equations used for the simulations:

One-sedimentation simulation:

$$c(r,t) = \left(\frac{c_o e^{-2sw^2 t}}{2}\right)\left[1-\phi\left[\frac{r_m(\omega^2 st + \log(r_m) - \log(r))}{2\sqrt{Dt}}\right]\right] \qquad \text{Equation 2.41 [41]}$$

Two sedimentation simulation:

$$\begin{aligned} &c(r,t) \\ &= \left(\frac{{c_o}^A e^{-2s^A w^2 t}}{2}\right)\left[1-\phi\left[\frac{r_m(\omega^2 s^A t + \log(r_m) - \log(r))}{2\sqrt{D^A t}}\right]\right] \\ &+ \left(\frac{{c_o}^B e^{-2s^B w^2 t}}{2}\right)\left[1-\phi\left[\frac{r_m(\omega^2 s^B t + \log(r_m) - \log(r))}{2\sqrt{D^B t}}\right]\right] \end{aligned} \qquad \text{Equation 2.42}$$

In Figure 2.12-AUC Simulation for Single Sedimentation below, different values were placed in Equation 2.40. The r_m is the radius at the meniscus; s is the sedimentation coefficient; D is the diffusion coefficient; c_0 is the concentration of the sample in solution. ϕ is the error function of the equation and is required for the simulation; this is a function of specific differential equations (i.e. Lamm equation) [50]. The error function does not measure error; it is a function dealing with the distribution of the entire sample. It [50] is used for sigmoidal shaped curves , and the equation is as follows:

$$\mathrm{erf}(x) = \frac{2}{\sqrt{\pi}} \int_0^x e^{-t^2} dt \qquad \text{Equation 2.43}$$

For both of the simulations, the values were assumed for purposes of demonstration and they have not been derived from the properties of any particular macromolecule.

The variables were given the following values: r_m= 6.2 cm ; ω^2= 1.5 x 10^7 $1/s^2$; s = 4.5 x 10^{-13}; D = 7.1 x 10^{-7} cm^2/s; c_0 = 0.5 mg/mL. The time for the graph was the variable in the equation and changed every 1000s. The simulated data had a start value at 6.2 cm and the end of the cell at 7.2 cm, the mockup data for the length from the axis of rotation (rb) was increased by increments of 5.0 x 10^{-3} cm. In actual AUC experiments, the cell is scanned between 1.0 x 10^{-3} cm – 3 x 10^{-3} cm. This is done to ensure the reliability and consistency of results. The simulation used 5.0 x 10^{-3} cm increments for the AUC experimental. Figure 2.12 below is a simulation of a one component sample:

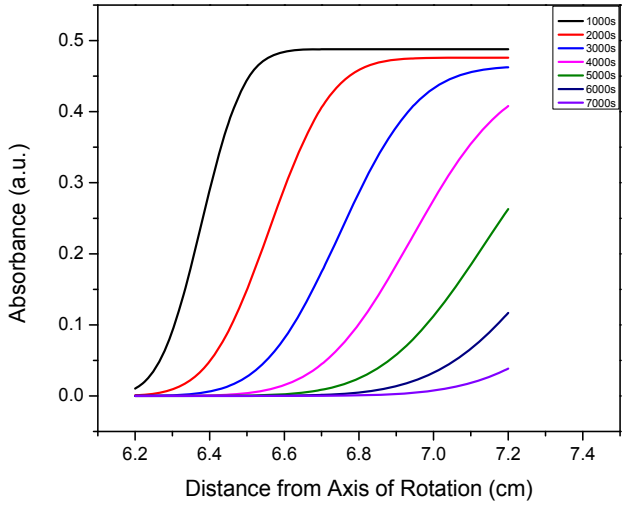

Figure 2.12- Single Component AUC Simulation. The simulation shows 7 scans at 1000s intervals.

In Figure 2.13-AUC Simulation for Two-Sedimentation, Equation 2.41 was used to simulate data. Equation 2.40 represents a single component; when two components are being simulated, the equation becomes additive. This means for each component in the mixture, the equation adds on another Lamm equation. This is seen in Equation 2.41.

For the first component, the following values were given: r_m= 6.2 cm; ω^2 = 2.7 x 10^7 $1/s^2$; s^A = 4.5 x 10^{-13}; D^A = 5.7 x 10^{-8} cm^2/s; c_0^A = 0.5 mg/mL. For the second component, the following values were given: r_m= 6.2 cm ; ω^2= 2.7 x 10^7 $1/s^2$; s^B, 1.91 x 10^{-13}; D^B = 1.0 x 10^{-7} cm^2/s; c_0^B = 0.5 mg/mL. The time for the graph was the variable in the equation, and increased in increments every 500 s. In the mock up, the cell extended from 6.2-7.2 cm from the the axis of rotation (r_b) and increased in increments of 5.0 x 10^{-3} cm. Figure 2.12 below is a simulation of a two component sample:

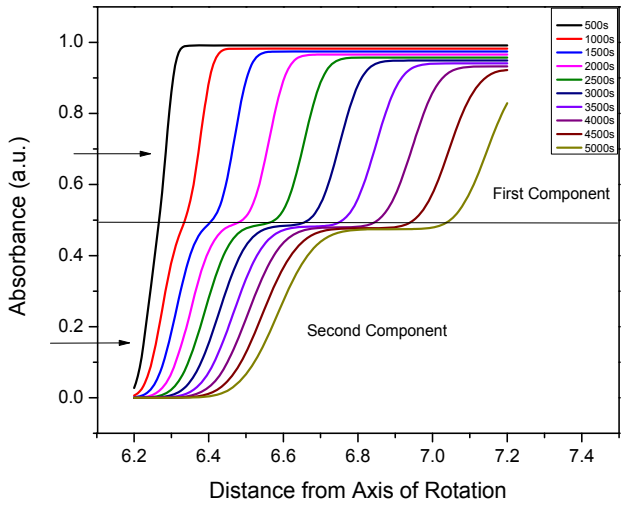

Figure 2.13- Two Component AUC Simulation. The simulation shows 10 scans at 500 s intervals.

Using equations 2.21, 2.9, the $\bar{v}$ values of 0.735 mL/g, and the ρ values of 1.0 g/mL, the molecular weight of the two components were estimated. The molecular weight of the first component is 56.7 g/mol and the molecular weight of the second component is 64.5 g/mol. The difference in the assumed molecular weights can be seen by looking at the sedimentation and diffusion coefficient. Although the second component is shown to sediment less quickly than the first component, it has a

larger molecular weight. This is attributable to the first component having a larger sedimentation coefficient and smaller diffusion coefficient than the second component.

In Figure 2.12, the two samples show distinct distributions; this is seen in breaks in the curve. The two components have different molecular weights and sediment at different rates. The lower molecular weight sample corresponds to the second component from 6.2-6.8 cm, and the higher molecular weight is correlated to the first component from 6.2-7.2 cm. The mockups are ideal systems of behavior of two distinct components in AUC velocity over time.

In actual experiments, the curves would be affected by other factors such as concentration differences. For instance, when the second component sediments, it sediments into the zone where the first component (fast) is concentrated. Depending on the concentration of this first component (fast), this may have an effect on sedimentation of the second component (slow). This is because the sedimentation of the second component will be going into an area of higher concentration and will have its sedimentation affected. This is what is known as the Johnston-Ogston effect. It is an example of an experimental variable which ideal systems are not affected by [40].

Chapter 3: Experimental Section

3.1 Reaction of $[Cu(NH_3)_4]^{2+}$(aq) with m-pbaH$_2$

The square complex $[Cu_4(m\text{-}pba)_4]$ was synthesized following a literature procedure [5].

3.2 Reaction of $[Cu(NH_3)_4]^{2+}$(aq) with MeSi(phacH)$_3$

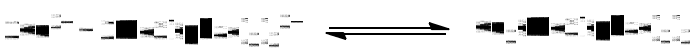

Reaction 3.1

The equation above represents the stoichiometry of the reaction. The reaction occurs in a 3:2 ratio of copper cation to the ligand anion (this is the empirical formula of the product). This is true of all the Si-based β-diketonate ligands used in this research. The empirical formula is used to represent the discrete molecules (i.e. cubic, decahedron, and dodecahedron) for the product in the thesis for the sake of simplicity.

$CuSO_4 \cdot 5H_2O$ (66 mg, 0.264 mmol) was dissolved in 15 mL of deionized water and treated with ca. 0.75 mL concentrated NH_4OH solution (28-30%), which turned the mixture an intense blue. 20 mL of dichloromethane (DCM) was added to the Cu^{2+} mixture, followed by the pre-made MeSi(phacH)$_3$ [51] (50 mg, 0.088 mmol) solution in 20 mL of DCM. Two layers formed an aqueous and an organic layer. The mixture was stirred for 6 hrs at room temperature with magnetic stirring. The organic layer contained the soluble product (the copper complexes), and the aqueous layer contained green polymeric insoluble precipitate. The two layers were separated using a separatory funnel and the aqueous layer was washed three times with 15 mL DCM. The organic layers were dried using sodium sulfate before gravity filtration. The evaporation of solvent afforded 28 mg of solid green film, yield: 48%. The molecular weight of MeSi(phacH)$_3$ is 568.73 g/mol, and the molecular weight of the soluble material $(Cu_3(MeSi(phac)_3)_2$ is 1322.07 g/mol.

3.3 Reaction of $[Cu(NH_3)_4]^{2+}$(aq) with $MeSi(phprH)_3$

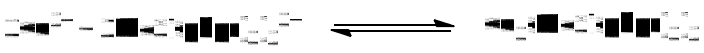

Reaction 3.2

$CuSO_4 \cdot 5H_2O$ (98 mg, 0.39 mmol) was used to prepare $[Cu(NH_3)_4]^{2+}$(aq)] as in Reaction 3.1. 25 mL of DCM was added to the Cu^{2+} solution followed by $MeSi(phprH)_3$ (114 mg, 0.174 mmol) solution in 75 mL of DCM. The mixture was stirred for 6 hrs and an insoluble light green precipitate and a green solution formed. The mixture was then treated similarly to Reaction 3.2. Yield: 94 mg (72 %). The soluble product was a solid green film. The molecular weight for the $MeSi(phprH)_3$ is 653.89 g/mol, and the molecular weight of the soluble material $Cu_3(MeSi(phpr)_3)_2$ is 1490.42 g/mol.

3.4 Reaction of $[Cu(NH_3)_4]^{2+}$(aq) with $MeOC_6H_4(CH_2)_3Si(phacH)_3$

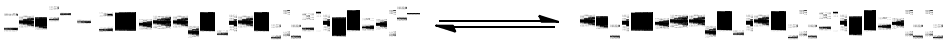

Reaction 3.3

$CuSO_4 \cdot 5H_2O$ (40 mg, 0.16 mmol) was used to prepare $[Cu(NH_3)_4]^{2+}$(aq)] as in Reaction 3.2. 15 mL of DCM was added to the Cu^{2+} solution followed by $MeOC_6H_4(CH_2)_3Si(phacH)_3$ (38 mg, 0.054 mmol) solution in 20 mL of DCM. The mixture was stirred for 6 hrs and an insoluble green precipitate and a green solution formed. The mixture was then treated similarly to Reaction 3.1. Yield: 12mg (28 %). Yield of insoluble precipitate, 28.7 mg (67 %). This soluble product was a solid green film. The insoluble precipitate was a light green flaky substance. The molecular weight for the $MeOC_6H_4(CH_2)_3Si(phacH)_3$ is 702.91 g/mol, and the molecular weight of the soluble material ($Cu_3(MeOC_6H_4(CH_2)_3Si(phac)_3)_2$ is 1590.46 g/mol.

3.5 Reaction of $Cu(NO_3)_2 \cdot 3H_2O$ with $MeSi(phacH)_3$

$Cu(NO_3)_2 \cdot 3H_2O$ (42 mg, 0.18 mmol) was dissolved in 20 mL of Dimethylformamide (DMF). A solution of $MeSi(phacH)_3$ (50 mg, 0.088 mmol) dissolved in 15 mL of DMF was added dropwise into the $Cu(NO_3)_2 \cdot 3H_2O$ solution under magnetic stirring. Upon addition, the solution turned a light green color. Subsequently 0.10 mL (0.72 mmol) of triethyl amine was added to the solution. The solution turned a dark green. The reaction mixture was stirred for 3 hrs, forming a green insoluble precipitate. The

insoluble product was individually washed with 5 mL of acetone, 5 mL of ethyl acetate, and 5 mL of ethyl ether. The insoluble precipitate was dried overnight, yielding 56 mg (96% yield) of insoluble product. The insoluble product was a light green flaky substance. The DMF was evaporated off using a high vacuum pump. 2 mg (3 %) of a dark green film was collected.

3.6 Reflux of Insoluble Material from Reaction 3.4

30 mg of insoluble precipitate from Reaction 3.5 was mixed with 40 mL of DCM in a reaction flask. The insoluble precipitate was refluxed for ~4hrs under nitrogen flow. The mixture was filtered, and the solvent was evaporated to dryness. 2 mg (6.7%) of green film was obtained.

3.7 Conversion of Insoluble Precipitate $Cu_3(MeSi(phac)_3)_2$ to $MeSi(phacH)_3$

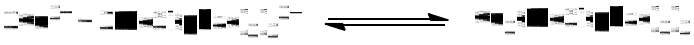

The $MeSi(phacH)_3$ ligand was recovered from the insoluble precipitate of $Cu_3(MeSi(phac)_3)_2$ by acid treatment. 150 mg of insoluble $Cu_3(MeSi(phac)_3)_2$ was treated with 125 mL of 1M HCL. The solution was stirred for 11 hours. After enough time had elapsed, the solution turned a pale blue color, the green precipitate dissolved and a white precipitate formed in solution. The aqueous layer was then washed three times with 20 mL of DCM to extract the ligand. The organic layer was then separated and treated with 100 mL of a 5% solution of sodium bicarbonate. The resulting organic solvent was blue to litmus paper. The aqueous layer was washed three times with 20 mL of DCM, and the organic layer was separated. The organic layer was concentrated down and the remaining material was separated using column chromatography. The volume ratio of the ethyl acetate and hexane used for the running solvent in column chromatography was: 1:4, 1:3, and 1:2 respectively. The solvent was evaporated off and the $MeSi(phac)_3$ ligand was dried overnight, yielding 72.7 mg (57 % yield) of ligand.

3.8 Preparation of Phosphate Buffer Solution for Bovine Serum Albumin

Two separate phosphate solutions were prepared. Table 3.1, Table 3.2, and Table 3.3 below have the quantity of the reagents used for buffer solutions.

Table 3.1: KH_2PO_4 and K_2HPO_4 buffer solutions [52].

Solution of KH_2PO_4	KH_2PO_4 (mass)	KCl (mass)	Water (volume)	KH_2PO_4 (molarity)	KCl (molarity)
	136 mg	1.864 g	100 mL	10 mM	0.25 M
Solution of K_2HPO_4	K_2HPO_4 (mass)	KCl (mass)	Water (Volume)	K_2HPO_4 (molarity)	KCl (molarity)
	174 mg	1.864 g	100 mL	10 mM	0.25 M

Table 3.2: KH_2PO_4 and K_2HPO_4 buffer solution [52].

Buffer Solution	KH_2PO_4 (volume)	KH_2PO_4 (molarity in 45 mL final volume)	K_2HPO_4 (volume)	K_2HPO_4 (molarity in 45 mL final volume)	Buffer Solution (Final Volume)
	40 mL	8.9 mM	5 mL	1.1 mM	45 mL

Table 3.3: Bovine Serum Albumin in Buffer Solution.

BSA solution	Initial Concentration (molarity)	Initial Molarity of BSA in Buffer Solution (molarity)	Dilution of Initial Concentration	BSA (molarity)
	6 mg of BSA in 10 mL of buffer solution	9.02×10^{-6}	No dilution	9.02×10^{-6}

The first solution was made by weighing KH_2PO_4 (136 mg, 1 mmol) and KCl (1.864 g, 25 mmol) in a flask. The flask was then filled to the 100 mL mark with deionized water.

The second solution was made by placing K_2HPO_4 (174 mg, 1 mmol) and KCl (1.864 g, 25 mmol) in a flask. The flask was then filled to the 100 mL mark with deionized water. The KH_2PO_4 (10 mM) solution was poured into a graduated cylinder to the 40 mL mark. 5 mL of KH_2PO_4 (10 mM) was added to the K_2HPO_4 solution by a pipette. The pH was 7.02.

6 mg of BSA (9.02×10^{-6} M) (66.5 kDa) was placed in 10 mL of the phosphate buffer solution for a concentration of 0.3 mg/mL.

3.9 Solubility of Supramolecular Copper Complexes

Solubility of the copper complexes in solution was tested for with various solvents. In the different analysis (i.e., AFM, AUC, and ESI-MS) the copper complexes need to be soluble in solvents in order to ensure the reliability of the results. In the case of ESI-MS, solubility in different solvents may provide a way of getting multiply charged ions in a sample, and allow for the molecular weight to be determined. For analytical ultracentrifugation, using different solvents may allow for more expedient measurements to be made in low density solvents. If the solvents are less dense, than the copper complexes would be able to sediment more quickly decreasing the time it takes to analyze them by AUC. Additionally, for purification purposes, various solvents were tested to see which could be used to remove impurities (such as unreacted ligand) without affecting the soluble copper complexes.

The $Cu_3(CH_3Si(phpr)_3)_2$ was tested for solubility in various solvents. The actual molecular structures are unknown, especially in solution, and thus will be represented by Cu_3L_2. The copper complexes were synthesized according to Reaction 3.3. The dried soluble copper complexes were then analyzed for solubility 20 days later. Table 3.4 that follows lists the density and polarizability of different solvents, and the solubility of $[Cu_3(MeSi(phpr)_3)_2]$ in them:

Table 3.4 Density [53] and polarizability[54] of various solvents. Solubility of $Cu_3(CH_3Si(phpr)_3)_2$ in various solvents.

Solvent	Density of Solvent (g/mL)	Polarizability of Solvent ($C \cdot m^2 . \frac{1}{V}$)	Solubility of $Cu_3(CH_3Si(phpr)_3)_2$ in Solvent
Toluene	0.865	12.4	Soluble
Benzene	0.874	10.44	Soluble
THF	0.889	7.97	Soluble
Dichloromethane	1.325	6.52	Soluble

(Table 3.4 continued)

Solvent	Density of Solvent (g/mL)	Polarizability of Solvent ($C \cdot m^2 . \frac{1}{V}$)	Solubility of $Cu_3(CH_3Si(phpr)_3)_2$ in Solvent
Chloroform	1.492	8.53	Soluble
Chlorobenzene	1.106	12.4	Soluble
Acetone	0.791	6.47	Soluble
Fluorobenzene	1.024	10.33	Soluble
Methanol	0.791	3.26	Partially Soluble
2-propanol	0.785	6.98	Partially Soluble
1-propanol	0.804	6.96	Partially Soluble
Ethanol	0.789	5.13	Partially Soluble
1-Butanol	0.81	8.79	Partially Soluble
Diethyl ether	0.706	8.98	Partially Soluble
Acetonitrile	0.786	4.44	Insoluble
n-hexane	0.659	11.94	Insoluble

In addition to the solubility test with various solvents, different concentrations of $Cu_3(MeSi(phpr)_3)_2$ were tested in ethyl acetate and hexane to examine the effect of concentration on solubility. The compound showed solubility with dilutions of ethyl acetate (EtOAc) and hexane. The compound was soluble in four different mixtures of ethyl acetate and hexane (1:1, 1:3, 1:7, 1:15, 1:31).

1 mL each of hexane and EtOAc was placed in tube 1. The content of tube 1 was mixed, and then 1 mL of the mixture was placed in the tube 2 with 1 mL of hexane. 1 mL of the tube 2 mixture was

put in tube 3 with 1 mL of hexane. This procedure was also followed for tubes 4 and 5. The ratio of the ethyl acetate and hexane in the glass tubes were: 1:1, 1:3, 1:7, 1:15, and 1:31 respectively. After this, approximately 1-2 mg of $Cu_3(CH_3Si(phpr)_3)_2$ was placed in each of the test tubes. In all of these dilutions, the copper complex was soluble. Therefore, it was concluded only pure hexane and acetonitrile could be used as solvents for washing the $Cu_3(CH_3Si(phpr)_3)_2$ complex to remove impurities; addition of even a small amount of another solvent was likely to dissolve some of the complex.

3.10 Stability of Supramolecular Copper Complexes in Various Solvents by UV-Vis Spectroscopy

In the previous section, solubility tests were primarily used to determine if the unknown $Cu_3(CH_3Si(phpr)_3)_2$ sample was soluble in different solvents. Second to this, was to determine what could be used as a wash to remove any unreacted ligand (i.e. hexane) after the compounds are synthesized.

In this section, the stability of the copper complex was examined in different solvents to determine if the soluble $Cu_3(MeSi(phac)_3)_2$ could be analyzed by different analytical techniques. If the copper complexes degrade too quickly in a solvent, they could not be used in AUC, for example. The degradation of the copper complexes can be monitored by UV-Vis analysis. Two distinct peaks around 550 nm and 675 nm are shown for the various known and unknown copper. When degradation occurs for both the known and unknown copper complexes, these peaks are either distorted, or disappear. Additionally, degradation of the soluble copper compounds often (or usually) can be visually recognized by a solid white precipitate appearing in solution as well as the solution changing from a dark green to a light green color. An example of the importance of stability of the copper complexes in suitable solvents can be seen with AUC equilibrium. In order to analyze the unknown copper complexes by AUC equilibrium, they need to be stable in solution for a period of at least 36-48 hours.

In this section, the stability of three different copper compounds in solution will be discussed: $Cu_4(m\text{-}pba)_4$, $Cu_4(m\text{-}pbhx)_4$, and $Cu_3(MeSi(phac)_3)_2$. These copper complexes have shown more stability

when halogenated solvents such as dichloromethane, chloroform, chlorobenzene, and fluorobenzene are present as opposed to solvents not containing halogen atoms. The exact reasons why these copper complexes are more stable in solvents containing a halogen atom are still unknown. The λ_{max} values for the samples are around 550 nm and 675 nm for each of the copper samples tested. The stability tests were performed on the known copper complex to determine what solvent the unknown compounds might be stable in. Because the known $Cu_4(m\text{-}pba)_4$ complex [35] and unknown copper complexes have similar chemical properties, the $Cu_4(m\text{-}pba)_4$ complex was tested first.

Pre-made $Cu_4(m\text{-}pba)_4$ (33.5 mg, 2.5 x 10^{-3}M) was dissolved in 10 mL of chloroform. When the complex was analyzed in chloroform, the $Cu_4(m\text{-}pba)_4$ was stable for the three days it was analyzed. In the different tests performed on the known and unknown complexes, stability tests were all performed for a total of 3 days. This time frame was chosen for the purpose of time sufficient enough to measure the known and unknown compounds by AUC. Figure 3.1 below shows the absorbance measurements:

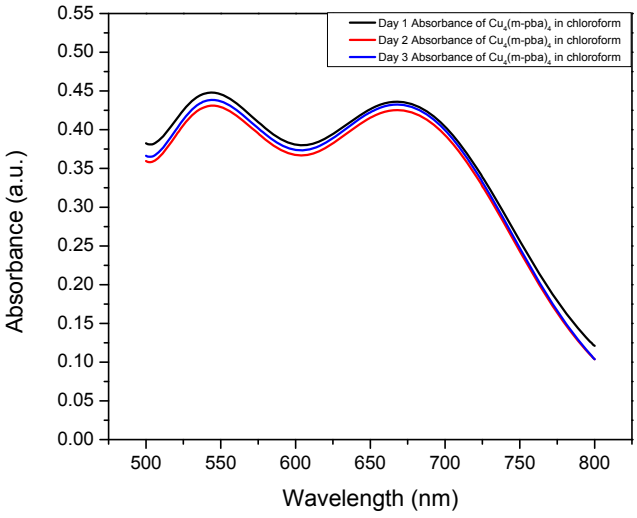

Figure 3.1- Three-day stability measurement of $Cu_4(m\text{-}pba)_4$ (2.5 x 10^{-3}M) in chloroform.

$Cu_4(m\text{-}pba)_4$ (33.5 mg, 2.5 x 10^{-3}M) was also dissolved in 10 mL of DCM. This solution was unstable. Figure 3.2 shows a 2 day absorbance measurement for the compound.

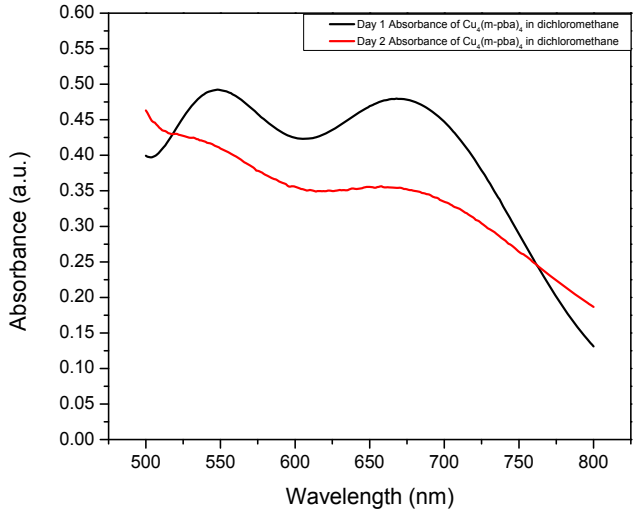

Figure 3.2- Two-day stability measurement of $Cu_4(m\text{-}pba)_4$ (2.5 x 10^{-3}M) in dichloromethane. On day 2, the compound degraded.

Thus, the known $Cu_4(m\text{-}pba)_4$ complex was stable in chloroform, but degraded in dichloromethane. Stability of the other Cu complexes in these solvents also varies. In the stability analysis of the unknown $Cu_3(CH_3Si(phac)_3)_2$ by UV-Vis, four different solvents were used: dichloromethane, chloroform, chlorobenzene, and fluorobenzene. Figure 3.3 shows a 2 day analysis of the sample dissolved in chloroform:

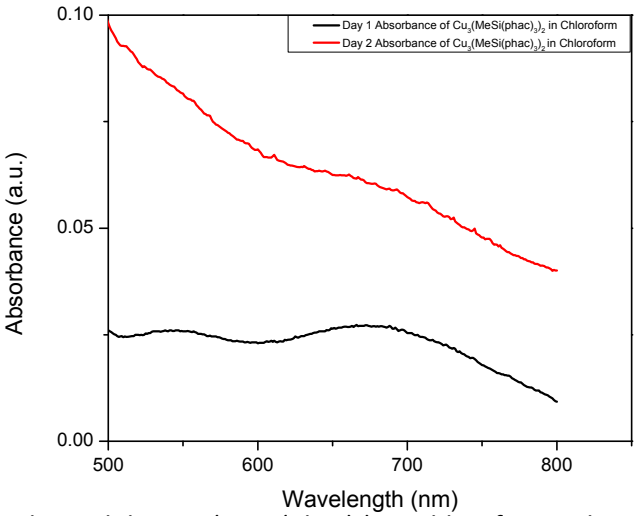

Figure 3.3- Two-day stability $Cu_3(MeSi(phac)_3)_2$ in chloroform. The concentration of the analyzed sample by UV-Vis was 5.3 x 10^{-4} M.

The $Cu_3(CH_3Si(phac)_3)_2$ sample was determined to be unstable in chloroform; therefore it was analyzed by UV-Vis in dichloromethane. Figure 3.4 illustrates a 4 day absorbance of the sample in DCM:

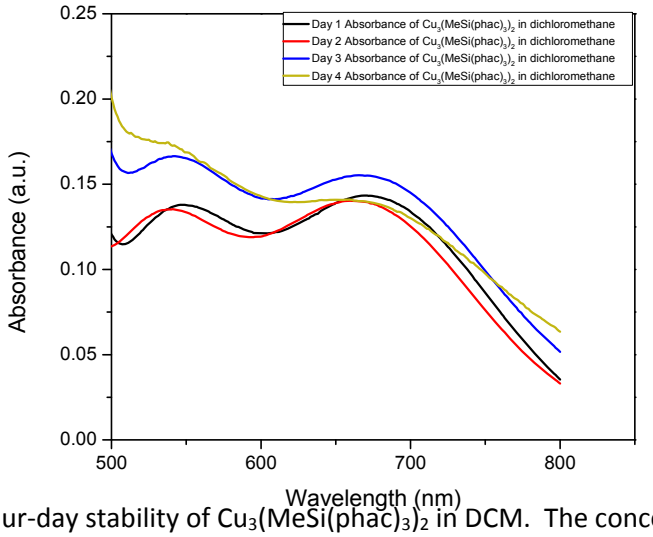

Figure 3.4- Four-day stability of $Cu_3(MeSi(phac)_3)_2$ in DCM. The concentration of the sample analyzed by UV-Vis was 2.1 x 10^{-3} M.

The analysis with DCM as a solvent for $Cu_3(MeSi(phac)_3)_2$ showed it had degraded between day 3 and day 4, and some degradation may be evident at day 3 as well. The sample showed a higher stability in DCM than in chloroform, but a solvent with greater stability was still being pursued for this sample.

There was also concern about the high density of $CHCl_3$ (1.49 g/mL) and CH_2Cl_2 (1.31 g/mL) as solvents for AUC experiments. This is because, in order for a concentration gradient to develop in an AUC experiment, the solute must be denser or less dense than the solvent. Measurements were made in three other solvents: chlorobenzene (1.11 g/mL), fluorobenzene (1.02 g/mL), and toluene (0.867 g/mL) (to be discussed in section 3.10).

The $Cu_3(CH_3Si(phac)_3)_2$ was analyzed in chlorobenzene for 5 days and showed very good stability as shown in Figure 3.5.

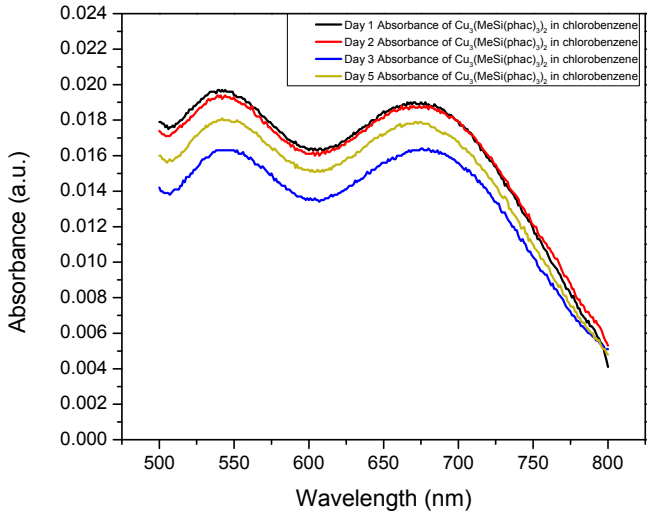

Figure 3.5- Five-day stability of $Cu_3(MeSi(phac)_3)_2$ in chlorobenzene. The concentration of the sample when analyzed by UV-Vis was 5.3 x 10^{-4} M.

$Cu_3(MeSi(phac)_3)_2$ showed good stability in chlorobenzene. The concentration of the sample when analyzed by UV-Vis was 5.3 x 10^{-4} M. As a continuation of the stability measurements, $Cu_3(MeSi(phac)_3)_2$ stability was examined in fluorobenzene shown in Figure 3.6.

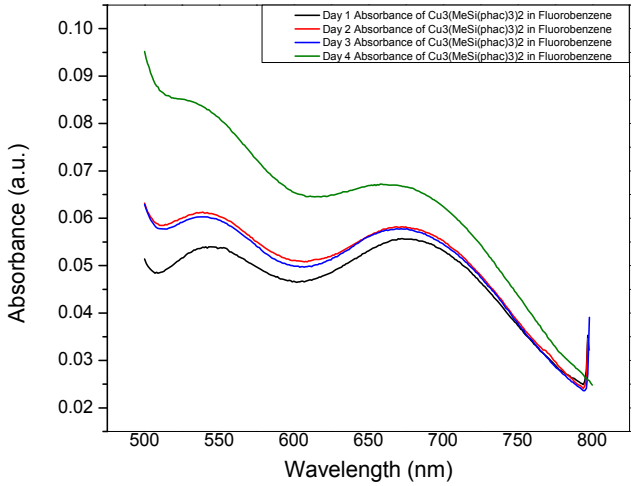

Figure 3.6- Four-day stability measurement of $Cu_3(MeSi(phac)_3)_2$ in fluorobenzene. The stability of the complex was analyzed for ~51 hours (Day3). 12 hours later (~63 hours), on day 4, the $Cu_3(MeSi(phac)_3)_2$ began to decompose. The concentration of the sample was 1.3 x 10^{-3}M.

The resulting conclusion of the stability measurements were the $Cu_3(MeSi(phac)_3)_2$ was most stable in chlorobenzene, but fluorobenzene would give the best AUC measurements due to its density.

Additional measurements by UV-Vis were performed to determine the absorbance maximum of the $Cu_3(MeSi(phac)_3)_2$ in chlorobenzene for AUC measurements. The previous measurements were to determine stability of the copper complexes in various solvents. This UV-Vis measurement was used to determine the concentration the sample-solvent would need to be in order to get a high absorbance value that would give good results for AUC. Figure 3.7 below are absorbance measurements of chlorobenzene and $Cu_3(MeSi(phac)_3)_2$ in chlorobenzene at the following molarities: 1.91×10^{-3} M, 1.91×10^{-4} M, and 1.91×10^{-5} M from the wavelengths of 300 nm to 850 nm:

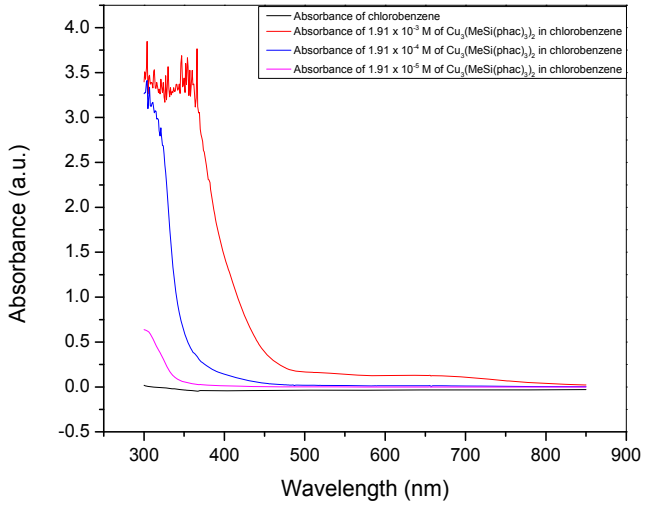

Figure 3.7- Absorbance of $Cu_3(MeSi(phac)_3)_2$ in chlorobenzene at various concentrations.

A high absorbance of the sample was determined to be around 300 nm. The absorbance study provided a suitable range to measuring sample by AUC. The concentration of ~1.91×10^{-5} M was first experimented with by AUC, but too much noise was given. The concentration was later increased and the wavelength of the sample was adjusted for AUC analysis (For a more thorough discussion see Chapter 4 section 4.3). Chlorobenzene was determined to be a solvent where the $Cu_3(MeSi(phac)_3)_2$ was stable in, and could be used for dynamic light scattering and electron paramagnetic resonance experiments, as discussed in Chapter 5.

Cu_4(m-pba)$_4$ is insoluble in chlorobenzene, fluorobenzene, and toluene. Thus it could not be used for AUC analysis. Its role in the research was confined to its stability measurements because of its chemical similarity to the unknown copper complexes. Cu_4(m-pbhx)$_4$ (MW 2241.08 g/mol) [55] is another square complex which is soluble/stable in different solvents (i.e. chlorobenzene, fluorobenzene, and toluene). This complex was tested for stability/solubility in chlorobenzene to determine if it could be used for AUC (for more thorough discussion see Section 4.3). This molecule was tested because it is a known compound, and also because its solubility/stability in different solvents as opposed to Cu_4(m-pba)$_4$. Cu_4(m-pbhx)$_4$ showed outstanding solubility and stability in chlorobenzene when analyzed. Figure 3.8 below shows the stability of Cu_4(m-pbhx)$_4$ over 52 days:

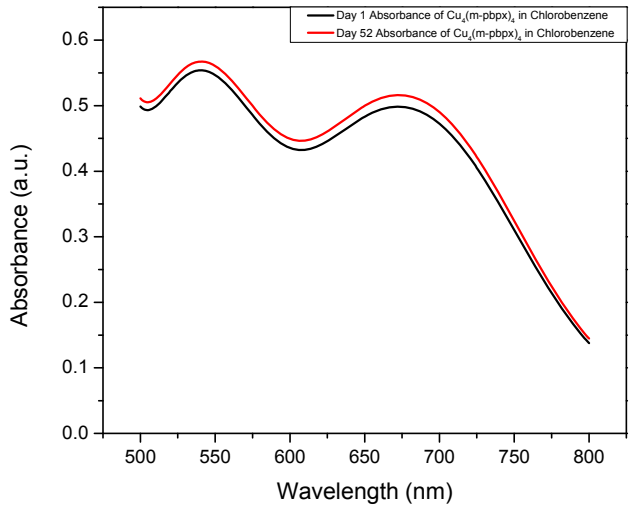

Figure 3.8- Absorbance of Cu_4(m-pbhx)$_4$ in chlorobenzene. Cu_4(m-pbhx)$_4$ (2.5 x 10^{-3}M) in chlorobenzene.

Cu_4(m-pbpx)$_4$ showed good stability/solubility in chlorobenzene. The Cu_4(m-pbpx)$_4$ stability and solubility in various solvents was determined to be a suitable molecule to examine as a standard. The molecular weight, density, and structure of the complex are known, which provides a standard for the unknown copper complexes. Initially experimenting on known molecules by AUC will give a better idea of the challenges arising when examining the unknown complexes by the same technique.

In discovering the optimal conditions (i.e. solvent and stability) to analyzing the unknown and known copper complexes, may provide an effective way to elucidating the unknown compound's structures.

3.11 Stability of $Cu_3(MeSi(phpr)_3)_2$ in Toluene by UV-Vis Spectroscopy

It was discovered serendipitously the stability of the $Cu_3(MeSi(phac)_3)_2$ and $Cu_3(MeSi(phpr)_3)_2$ were not the same in different solvents. For instance, $Cu_3(MeSi(phac)_3)_2$ in pure DCM was stable for three days (see Figure 3.4), while $Cu_3(MeSi(phpr)_3)_2$ showed degradation after one day. In order to ensure a quality analysis for $Cu_3(MeSi(phpr)_3)_2$ by AUC, a stability test was measured in ultrapure toluene. The $Cu_3(MeSi(phpr)_3)_2$ showed good stability in the solvent. Figure 3.9 below shows stability measurements of $Cu_3(MeSi(phpr)_3)_2$ in ultrapure toluene:

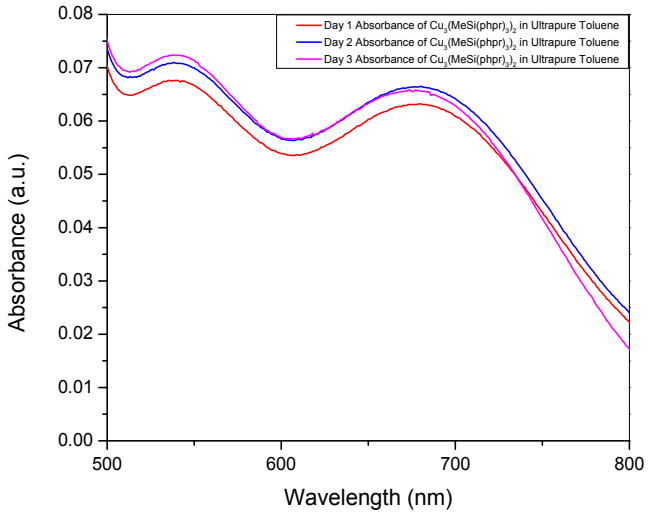

Figure 3.9- Three-day stability measurement of $Cu_3(MeSi(phpr)_3)_2$ in ultrapure toluene. The stability of the complex was measured up to 76 hours. The concentration of the sample was 1.6 x 10^{-3}M.

The stability of the $Cu_3(MeSi(phpr)_3)_2$ in toluene made the choice of the solvents ideal for this AUC analysis. The density of the solvents (toluene (0.867 g/mL); would allow for greater contrast to

emerge for AUC. Chapter 4 describes analysis of these metal organic materials by different analytical techniques.

Chapter 4: Characterization of Copper Complexes

4.1 Atomic Force Microscopy of Unknown Copper Complexes

Two samples were submitted for atomic force microscopy (AFM) analysis: $Cu_3(CH_3Si(phac)_3)_2$ and $Cu_3(CH_3Si(phpr)_3)_2$. The AFM studies were used to analyze the dimensions of the copper complexes. The heights of the two samples were measured to determine if the size distribution of the analyzed samples had heights similar to the projected copper complexes (see Figure 1.3). The possible copper molecules looked for in this study were cubic (2 nm), decahedron (3.5-4.5 nm), and dodecahedron (5 nm).

Tapping mode AFM was used for the analysis of both samples. This technique utilizes the cantilever tip of the AFM instrument that can measure various properties of the material being analyzed. This mode of AFM operates by having the tip move up and down on the sample to determine features such as height, viscoelasticity, and/or even contractile forces of different molecules (i.e. proteins). In this research, tapping mode AFM was used to determine the size of the material analyzed.

The kinds of images taken for these studies were topography and phase imaging. Topography images the height of the sample on the surface of the substrate; this occurs when the AFM tip oscillates up and down touching the sample. In the AFM images, yellow spots (sample) appear when a variation in height is detected on the brown background (the mica substrate). Phase images the viscoelasticity of the sample; it measures the phase lag of the oscillating tip. If the sample distorts when the AFM tip touches it, this will cause a shift in the phase. A sample having more viscoelasticity would cause greater phase lag, where a sample with less viscoelasticity would cause less of a phase lag. Phase imaging gives confirmation the sample being analyzed is the complex, and not a contaminant. A contaminant on a phase image would likely have different color images than the actual sample due to differences in viscoelasticity. In these phase images, the sample (brown spots) appears on the flat mica substrate

(yellow) in the background. Contamination of the sample during synthesis and analysis is always a possibility. Special precautions should be taken to avoid contamination even with different imaging.

In the AFM studies, chloroform was used to prepare the samples submitted. The samples were dissolved in chloroform and immediately analyzed by AFM. Because the samples were analyzed immediately, degradation of the samples in solution was not an issue.

$Cu_3(CH_3Si(phac)_3)_2$ was the first sample analyzed by AFM. The sample was analyzed by AFM ~71 days after its original synthesis. The dry $Cu_3(CH_3Si(phac)_3)_2$ was re-dissolved in $CHCl_3$, and then placed on a mica substrate for analysis. The sample was analyzed by AFM on the same day. Figure 4.1 shows the AFM topography image of the sample (yellow spots) and the substrate (brown background), and a sample point (yellow dot with green line) measured:

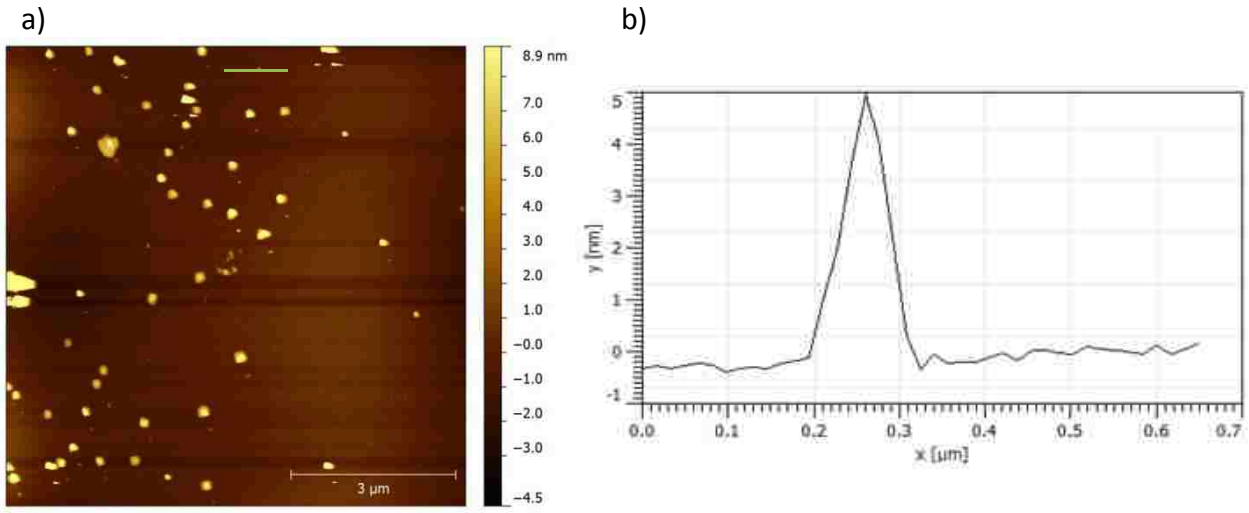

Figure 4.1- a)Topography image of $Cu_3(CH_3Si(phac)_3)_2$. The yellow images are the $Cu_3(CH_3Si(phac)_3)_2$. The dark brown background is the mica substrate. b) Height profile of one $Cu_3(CH_3Si(phac)_3)_2$ molecule, measured along green line in (a). The height profile is a possible dodecahedron at ~5 nm.

The green line in Figure 4.1a shows where the profile in Figure 4.1b was measured. The AFM topography image to the top left measured a ~5 nm complex signifying a possible dodecahedra molecule. In Figure 4.2 below, a different section is shown and it is zoomed in. This was done to show contrast on the sizes of the sample on the substrate. The phase image of the sample is given as well.

Figure 4.2b shows the phase image with similar color spots (black) on the mica (gold background) indicating similar viscoelasticity of the $Cu_3(CH_3Si(phac)_3)_2$ sample. Additionally, a sample measurement was made. The green line in Figure 4.2a is where the profile in Figure 4.2c was measured. Figure 4.2c shows a measurement of 2 nm indicating a possible cubic structure:

a) b)

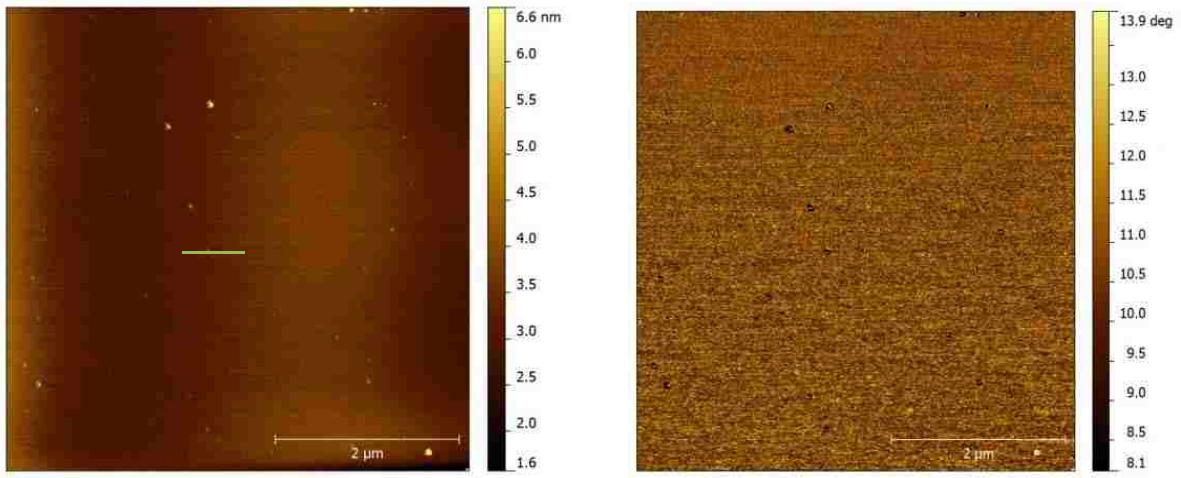

c)

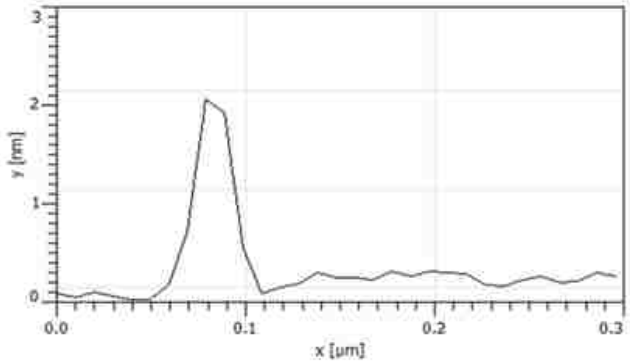

Figure 4.2- a)Topography image of $Cu_3(CH_3Si(phac)_3)_2$. The yellow spots are $Cu_3(CH_3Si(phac)_3)_2$. The dark background is the mica substrate. b) Phase image of $Cu_3(CH_3Si(phac)_3)_2$. The dark spots are the $Cu_3(CH_3Si(phac)_3)_2$. The gold background is the mica substrate. c) Height profile of $Cu_3(CH_3Si(phac)_3)_2$ sample point. The height profile is a possible cubic structure of 2 nm.

A topography image and height profile of a possible aggregate of 2 smaller molecules of $Cu_3(CH_3Si(phac)_3)_2$ is in Figure 4.3 below. The height of 8 nm is a potential aggregation of 2 decahedra complexes (3.5-4.5 nm). Figure 4.3 is unlikely due to the aggregation of other complexes in the sample, given the projected heights of the cubic (2 nm) and dodecahedron complexes (5 nm).

a) b)

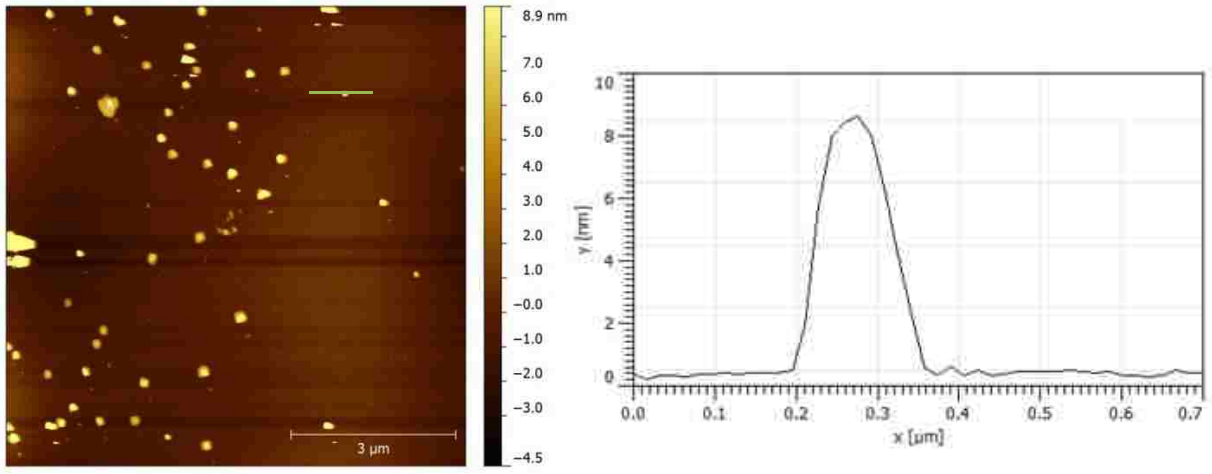

Figure 4.3- a)Topography Image of $Cu_3(CH_3Si(phac)_3)_2$ b) Height profile of $Cu_3(CH_3Si(phac)_3)_2$ sample point. The height profile is a possible aggregation of 2 decahedra (3.5-4.5 nm) of ~ 8 nm.

In Figure 4.4 and Table 4.1 below, show the results of 87 points of the $Cu_3(CH_3Si(phac)_3)_2$ sample taken with AFM. The height distribution shows out of 87 points measured, heights close to 2 nm, 8 nm, and 10 nm.

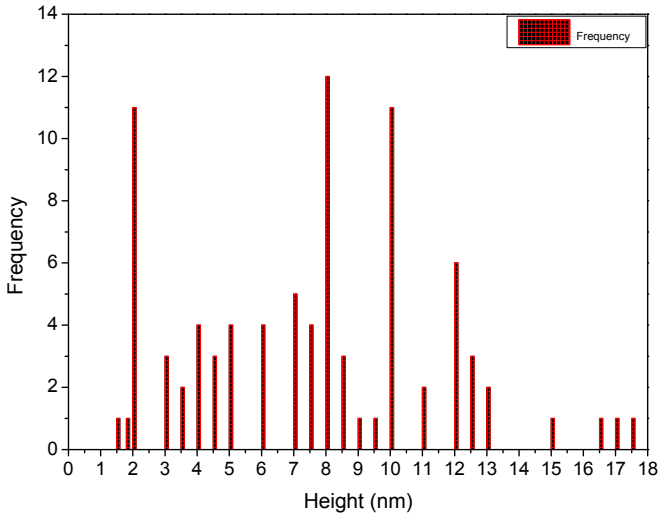

Figure 4.4- Distribution of heights of 87 molecules in a $Cu_3(MeSi(phac)_3)_2$ sample, measured by AFM.

Table 4.1- Atomic Force Microscopy height measurements of $Cu_3(MeSi(phac)_3)_2$. The table lists the frequency of heights out of 101 measurements and its percentage.

Measured Heights (nm)	Occurrence of Height	Percentage of Measured Heights (%)
1.5	1	1.15%
1.8	1	1.15%

(Table 4.1 continued)

Measured Heights (nm)	Occurrence of Height	Percentage of Measured Heights (%)
2	11	12.6%
3	3	3.45%
3.5	2	2.30%
4	4	4.60%
4.5	3	3.45%
5	4	4.60%
6	4	4.60%
7	5	5.75%
7.5	4	4.60%
8	12	13.8%
8.5	3	3.45%
9	1	1.15%
9.5	1	1.15%
10	11	12.6%
11	2	2.30%
12	6	6.90%
12.5	3	3.45%
13	2	2.30%
15	1	1.15%
16.5	1	1.15%
17	1	1.15%
17.5	1	1.15%

In the AFM study of $Cu_3(CH_3Si(phac)_3)_2$, 87 points were measured. Out of the 87 points, 11 points (12.6 %) were measured at 2 nm (possible cubic), 9 points (10.3%) were measured between 3.5-4.5 nm (possible decahedra) and 4 points (4.60 %) were measured at 5 nm (possible dodecahedra). Other heights having a high level of occurrence were 8 nm (13.8 %) and 10 nm (12.6 %) heights. The occurrences of these heights could be attributed to the aggregation of discrete molecules. The 8 nm heights are potential combinations of 2 decahedra complexes, and the 10 nm heights are possible collections of dodecahedra molecules.

The second sample measured by AFM was $Cu_3(MeSi(phpr)_3)_2$. The sample was washed separately with various solvents to determine the effects it would have on the measurements of

complexes by AFM. The soluble $Cu_3(MeSi(phpr)_3)_2$ was first washed with 6 mL of acetone, followed by 6 mL of ethyl acetate, 6 mL of ether, and then a 1:1:1 6 mL solution of acetone, ethyl acetate, and ethyl ether. The $Cu_3(MeSi(phpr)_3)_2$ was treated on day 1. The remaining sample (0.7 mg) was analyzed by AFM ~41 days later. Below is Figure 4.5, a topography image of $Cu_3(CH_3Si(phpr)_3)_2$:

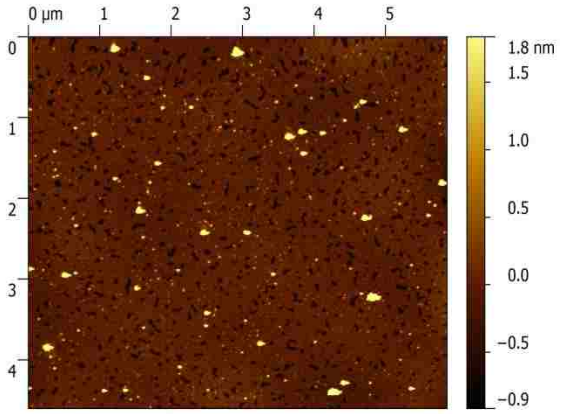

Figure 4.5- Topography Image of $Cu_3(CH_3Si(phpr)_3)_2$. The yellow spots indicate the sample, and the brown background is the mica. This is the area where 101 points were measured by AFM.

Figure 4.6 below is the size distribution for $Cu_3(MeSi(phpr)_3)_2$. This is the 101 points analyzed for the sample. The heights with common occurrence occur at 2, 3, 4, 5, 6, 7, and 8 nm heights. Below Figure 4.6 is Table 4.2 which gives the height, occurrence, and percent of each height measured.

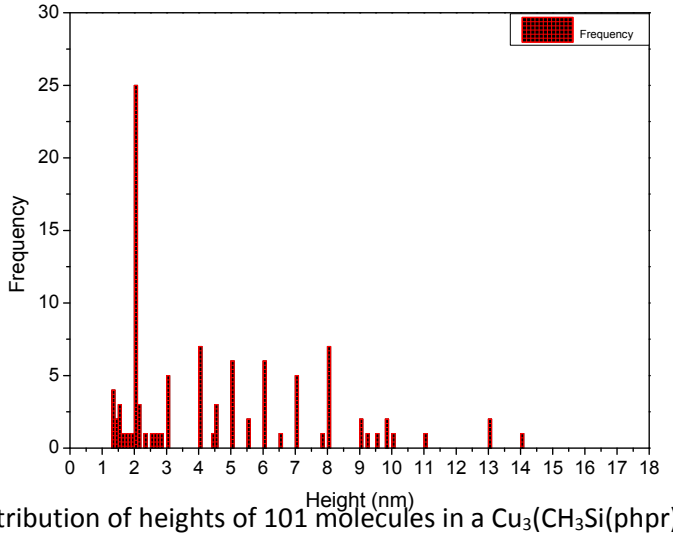

Figure 4.6- Distribution of heights of 101 molecules in a $Cu_3(CH_3Si(phpr)_3)_2$ sample, as measured by AFM.

Table 4.2 - Atomic Force Microscopy height measurements of $Cu_3(CH_3Si(phpr)_3)_2$. The table lists the frequency of heights out of 101 measurements and its percentage.

Measured Heights (nm)	Occurrence of Height	Percentage of Measured Heights (%)
1.3	4	3.96%
1.4	2	1.98%
1.5	3	2.97%
1.6	1	0.99%
1.75	1	0.99%
1.8	1	0.99%
1.9	1	0.99%
2	25	24.7%
2.1	2	1.98%
2.15	1	0.99%
2.3	1	0.99%
2.5	1	0.99%
2.6	1	0.99%
2.75	1	0.99%
2.8	1	0.99%
3	5	4.95%
4	7	6.93%
4.4	1	0.99%
4.5	3	2.97%
5	6	5.94%
5.5	2	1.98%
6	6	5.94%
6.5	1	0.99%
7	5	4.95%
7.8	1	0.99%
8	7	6.93%
9	2	1.98%
9.2	1	0.99%
9.5	1	0.99%
9.8	2	1.98%
10	1	0.99%
11	1	0.99%
13	2	1.98%
14	1	0.99%

$Cu_3(CH_3Si(phpr)_3)_2$ was the second sample examined by AFM and 101 points were measured on the mica substrate. Of the 101 points, 25 points (24.8 %) were measured at 2 nm (cube), 11 points (10.9 %) were measured between 3.5-4.5 nm (decahedron) and 6 points (5.94 %) were measured at 5 nm (dodecahedron). The sample of $Cu_3(MeSi(phpr)_3)_2$ with the washes shows a high number of measurements around 2 nm signifying potential cubic structures. Additionally, there were 7 points at 8 nm (6.93%). The 5 nm points may be dodecahedra structures, while 8 nm may be possible aggregates of 2 decahedra complexes. The washes from the sample may have been more effective at dissolving the decahedra and dodecahedra molecules compared to dissolving the cubic complexes.

The discrete molecules of cube (2 nm), decahedron (3.5-4.5 nm), and dodecahedron (5 nm) were the complexes whose frequency of height was being determined. In the two AFM studies, Table 4.3 offers a comparison of the points measured:

Table 4.3- Frequency of measured height of copper complexes using atomic force microscopy for $Cu_3(CH_3Si(phac)_3)_2$ and $Cu_3(CH_3Si(phpr)_3)_2$.

	Points Measured	Possible Cube (2 nm)		Possible Decahedron (3.5-4.5 nm)		Possible Dodecahedron (5 nm)	
$Cu_3(CH_3Si(phac)_3)_2$	87	11	13%	9	10%	4	5%
$Cu_3(CH_3Si(phpr)_3)_2$	101	25	25%	11	11%	6	6%

In the AFM studies that were performed, the $Cu_3(CH_3Si(phac)_3)_2$ was analyzed ~71 days after synthesis, and the $Cu_3(CH_3Si(phpr)_3)_2$ was analyzed ~41 days after synthesis. In having established a histogram of the $Cu_3(CH_3Si(phac)_3)_2$ and $Cu_3(CH_3Si(phpr)_3)_2$ material, offers a better idea of the complexes remaining after time has elapsed. These AFM studies provide a basis of comparison for future studies. The longevity of the complexes stability outside of solution has not been determined. It would be beneficial to submit freshly synthesized samples of each compound for AFM analysis to determine the initial distribution of heights.

Additionally, it would be advantageous to test the affects particular solvents have on the solubility of the copper molecules. Using different solvents may provide an effective separation technique for the complexes. When the samples are freshly prepared, the copper complexes in solution completely dissolve in the solvents shown in Table 3.4. When time has elapsed, the copper complexes show only partial solubility with some of the solvents (i.e. ethyl acetate and acetone). In the study of $Cu_3(CH_3Si(phpr)_3)_2$, the high frequency of 2 nm heights demonstrates some kind of complex (i.e. cubic) remaining. This demonstrates that some of the copper complex is partially soluble in these solvents (the washes turned green) after time has elapsed, while some unknown copper material becomes insoluble (a light green film).

4.2 Electrospray Ionization Time of Flight Mass Spectrometry of Copper Complexes

In this section, ESI-TOF MS has been used as a characterization technique for the unknown copper complexes. The two samples discussed in this section are the known square complex of $Cu_4(m\text{-}pba)_4$ and the unknown compound of $Cu_3(MeSi(phac)_3)_2$.

The natural abundance of copper (^{63}Cu, 69.17%; ^{65}Cu, 30.83%) [37] leads to distinctive mass spectrometry patterns. This is a way to determine if copper is in a sample and an aid in structure determination. Additionally, the monoisotopic ion was used in analyzing the copper complexes for ESI-TOF MS. The monoisotopic ion is when every atom in the ion is the most abundant isotope for that element. The $Cu_4(m\text{-}pba)_4$ and $Cu_3(MeSi(phac)_3)_2$ compounds are composed of C, H, O, and Cu atoms (the $Cu_3(MeSi(phac)_3)_2$ also contains Si atoms); for these atoms, the most abundant isotope is the lightest. The distinctive isotopic features of the copper atom and the monoisotopic ion of the complexes could allow for the samples to be accurately analyzed.

An analysis of the known $Cu_4(m\text{-}pba)_4$ by ESI-TOF MS was tested first. This sample was used as a reference compound, whose structure is known, to establish what the mass spectrometry data might

resemble for the larger unknown molecules of $Cu_3(MeSi(phac)_3)_2$. In Figure 4.7 below, the ESI-TOF MS of the $Cu_4(m\text{-}pba)_4$ complex is shown:

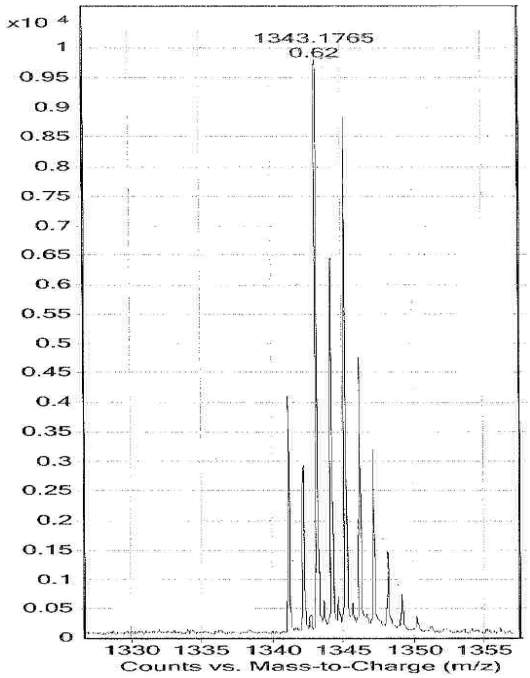

Figure 4.7- Mass spectrum of $Cu_4(m\text{-}pba)_4$ analyzed in methanol at 215V. The monoisotopic ion (M+H) is shown at 1341.17 amu.

The $Cu_4(m\text{-}pba)_4$ was analyzed by ESI-TOF MS. A peak occurred at mass to charge (m/z) = 1341.17 atomic mass unit (amu) which is the monoisotopic ion (M+H) of the square complex; shown in Figure 4.7. The mass spectrum showed a distinct copper isotopic distribution indicative of 4 copper isotopes.

In the mass spectrometry studies of the $Cu_3(MeSi(phac)_3)_2$ sample, multiply charged ions were looked for. The unknown complexes (i.e. cubic, decahedra, and dodecahedra) for this research have masses above 3000 amu. Therefore, singly charged molecular ions would be too large for detection with the ESI-TOF MS instrument. If the $Cu_3(MeSi(phac)_3)_2$ complexes had multiply charged ions, then the discrete molecules of the cube, decahedron, and dodecahedron could be identified. The complexes

could be characterized if they were multiply charged because it could be brought into the range of detection by the mass spectrometer.

Multiply charged ions M^{2+} give individual peaks separated by 1/2 amu in their mass spectra. We recorded mass spectra for $Cu_3(MeSi(phac)_3)_2$, but did not see any signals attributable to multiply charged ions. In the study of the $Cu_3(MeSi(phac)_3)_2$ sample, a possible signal was looked for at 1322.25 amu and other points where multiply charged species may have been found. There were no multiply charged signals in the samples examined (nor a m/z signal at 1322.25 amu). Different solvents and treatments of the samples were performed, but the discrete molecules of the cube, decahedron, and dodecahedron were not able to be characterized by ESI-TOF. Various samples of $Cu_3(MeSi(phac)_3)_2$ were submitted for mass spectrometry analysis using different solvents (such as dichloromethane and acetone) and voltages. No multiply charged ion peaks were discovered. Table 4.4 gives the monoisotopic ion of the complexes with only the peak occurrence of $Cu_4(m\text{-}pba)_4$ occuring.

Table 4.4- The monoisotopic ion for and peak occurrence for $Cu_4(m\text{-}pba)_4$. The monoisotoic ion for $Cu_3(MeSi(phac)_3)_2$, $Cu_{12}(MeSi(phac)_3)_8$, $Cu_{24}(MeSi(phac)_3)_{16}$, and $Cu_{30}(MeSi(phac)_3)_{20}$. There were no peak occurrences for $Cu_3(MeSi(phac)_3)_2$ in ESI-TOF MS. There was no multiply charged peaks for $Cu_{12}(MeSi(phac)_3)_8$, $Cu_{24}(MeSi(phac)_3)_{16}$, and $Cu_{30}(MeSi(phac)_3)_{20}$.

	Monoisotopic Ion	Peak Occurrence
$Cu_4(m\text{-}pba)_4$	1340.14 amu	1341.17 amu
$Cu_3(MeSi(phac)_3)_2$	1319.20	-------
Cube- $Cu_{12}(MeSi(phac)_3)_8$	5276.79	-------
Decahedron- $Cu_{24}(MeSi(phac)_3)_{16}$	10553.58	-------
Dodecahedron- $Cu_{30}(MeSi(phac)_3)_{20}$	13191.98	-------

The ESI-MS TOF showed no multiply charged ion that was indicative of the proposed polyhedra cages being formed. Further test using ESI-TOF do not appear likely to give multiply charged ions given the different solvents used in this study.

4.3 Analytical Ultracentrifugation of Copper Complexes

AUC Equilibrium was performed on $Cu_4(m\text{-}pbhx)_4$ to test a known copper complex in an organic solvent before the unknown copper complexes of $Cu_3(MeSi(phac)_3)_2$ and $Cu_3(MeSi(phpr)_3)_2$ were attempted. Two different solvent systems were used for the analysis of the $Cu_4(m\text{-}pbhx)_4$: fluorobenzene and toluene. The wavelength values used for AUC were not λ max values. When experimental test were performed on $Cu_4(m\text{-}pbhx)_4$ in fluorobenzene for highly dilute samples (9.5×10^{-6} M) the noise from the samples was too much to receive quality data for the AUC experiment. It was determined that higher concentration would be better for AUC analysis. The absorbance of $Cu_4(m\text{-}pbhx)_4$ was measured with the concentration of the sample at 2.94×10^{-5} M in both fluorobenzene and toluene. Figure 4.8 below is the measured absorbance:

a)

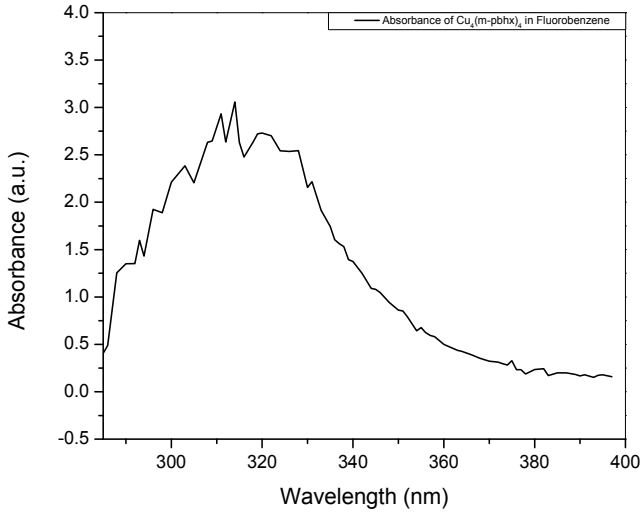

(Figure 4.8 continued)

b)

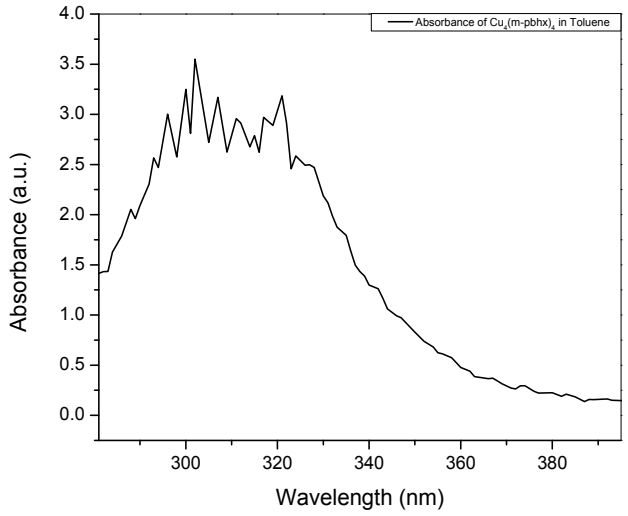

Figure 4.8- Measured absorbance of $Cu_4(m\text{-}pbhx)_4$ in fluorobenzene and toluene. The wavelength used in the measurements was 360 nm due to its reasonable absorbance in AUC. The concentration of both samples were 2.94 x 10^{-5} M. a)Measured absorbance of $Cu_4(m\text{-}pbhx)_4$ in fluorobenzene for AUC equilibrium 320-400 nm. b) Measured absorbance of $Cu_4(m\text{-}pbhx)_4$ in toluene for AUC equilibrium 320-400 nm.

Both samples were analyzed at 360 nm by AUC. The next step was determining the proper rotation speed for AUC equilibrium analysis of $Cu_4(m\text{-}pbhx)_4$. If the speed was too low, then not enough contrast will be produced to get quality data. If it is too high, then the sample may sediment to the bottom, lowering the accuracy of the results. When using different solvents with different densities, determining an appropriate speed was a necessity. Equilibrium was achieved for $Cu_4(m\text{-}pbhx)_4$ at 60 krpm (the ω^2 value was 3.9 x 10^7 rad^2/sec^2) in fluorobenzene at 36 hours. Equilibrium was achieved for $Cu_4(m\text{-}pbhx)_4$ in toluene at 50 krpm (the ω^2 value was 2.7 x 10^7 rad^2/sec^2) 18 hours (after the rotor was de-accelerated from equilibrium at 60 krpms). Sedimentation was a factor with the $Cu_4(m\text{-}pbhx)_4$ in toluene at 60 krpm. When the data were analyzed for the sample in toluene, it was determined the speed was too much to produce accurate data for equilibrium. The cell measured for the $Cu_4(m\text{-}pbhx)_4$ analysis in both solvents were measured from 5.9- 7.2 cm (above the meniscus to the end of the cell)

where there was no further absorption by the $Cu_4(m\text{-}pbhx)_4$. Figure 4.9 below shows the equilibrium curve in fluorobenzene and toluene for the $Cu_4(m\text{-}pbhx)_4$ complex:

a)

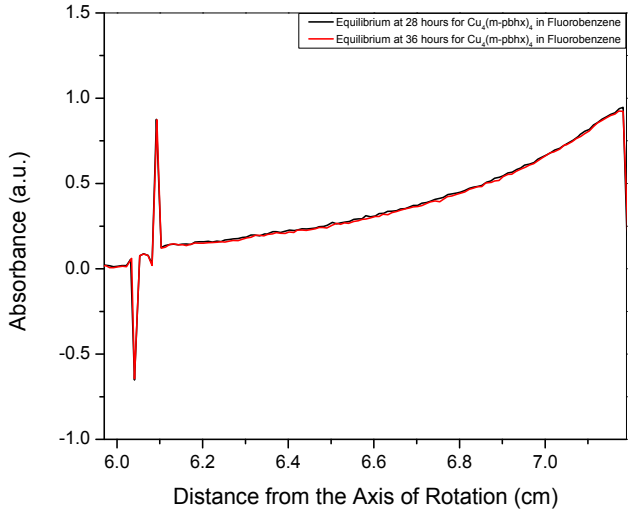

b)

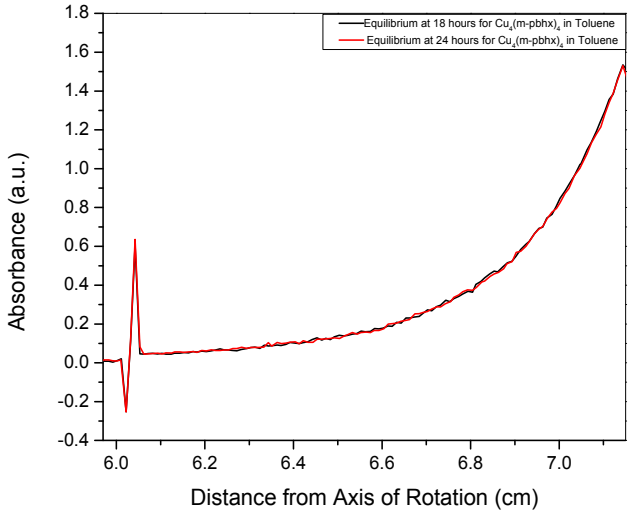

Figure 4.9- AUC Equilibrium data for $Cu_4(m\text{-}pbhx)_4$. a) Equilibrium of the sample was achieved at 60 krpm at 36 hours in fluorobenzene. b) Equilibrium achieved at 50 krpm at 18 hours (after the de-acceleration from equilibrium at 60 krpm) in toluene.

The raw data from the two graphs from Figure 4.9 were converted into logarithmic plots for further analysis (See section 2.6 for details). The $\log_{10}$(absorbance) for the Cu_4(m-pbhx)$_4$ in fluorobenzene was taken at the rb (distance from axis of rotation) from 6.223-7.182cm. The $\log_{10}$(absorbance) for the Cu_4(m-pbhx)$_4$ in toluene was taken at the rb from 6.404-7.047cm. This conversion was performed to linearize the data, and to determine if further information could be established. Figure 4.10 below is the $\log_{10}$ plot of the two graphs from Figure 4.9:

a)

b)

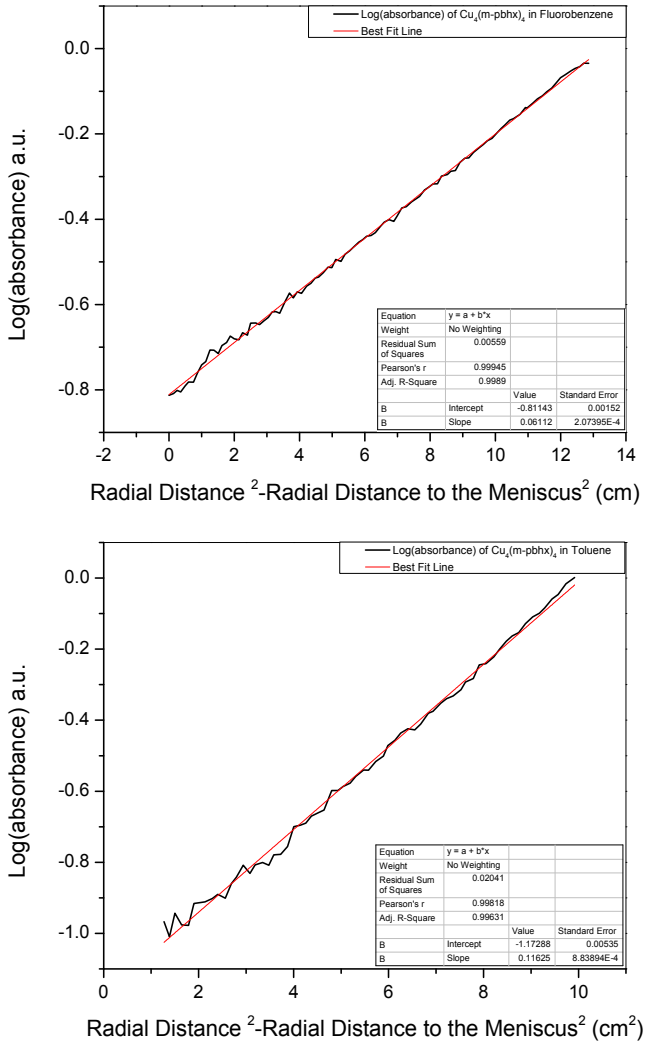

Figure 4.10- Log_{10}(absorbance) vs. rb^2-rm^2 plot for Cu_4(m-pbhx)$_4$ in toluene and fluorobenzene. Using the partial specific volume of 0.90220 mL/g derived from AUC measurements in different solvents (see p. 66)- and their calculated slope, it was determined that the molecular weight of the square was ~2274 g/mol in fluorobenzene and 2183 g/mol in toluene. a) The $\log_{10}$(absorbance) for the Cu_4(m-pbhx)$_4$ in fluorobenzene. b) The $\log_{10}$(absorbance) for the Cu_4(m-pbhx)$_4$ in toluene.

The straight lines in Figure 4.10 a and b indicate dispersion of a single entity of Cu_4(m-pbhx)$_4$ in fluorobenzene and toluene. The analysis does not indicate other species contained in the solvents. The molecular weight of the square is 2241 g/cm^3 as determined by X-ray crystallography [55]. The density was calculated by performing AUC runs with Cu_4(m-pbhx)$_4$ in different solvents and speeds to receive a close value of the actual density of the Cu_4(m-pbhx)$_4$. Below is Table 4.5 that show the AUC runs performed for the density measurements:

Table 4.5- AUC Data for Cu_4(m-pbhx)$_4$ in different solvents and speeds for density measurement.

Solvent	Solvent Density	rpm	rpm/100000	slope	slope/ω^2
toluene	0.865	50000	0.5	0.11625	0.465
toluene	0.865	50000	0.5	0.1176	0.4704
toluene	0.865	40000	0.4	0.083	0.51875
toluene-d8	0.943	50000	0.5	0.0763	0.3052
toluene-d8	0.943	40000	0.4	0.0583	0.364375
tetralin	0.973	40000	0.4	0.0639	0.399375
fluorobenzene	1.024	60000	0.6	0.06112	0.169778

The data from the AUC experiments were put into a plot so an approximate density of the Cu_4(m-pbhx)$_4$ could be established. Figure 4.11 below is the scatter plot of density vs. slope/ω^2:

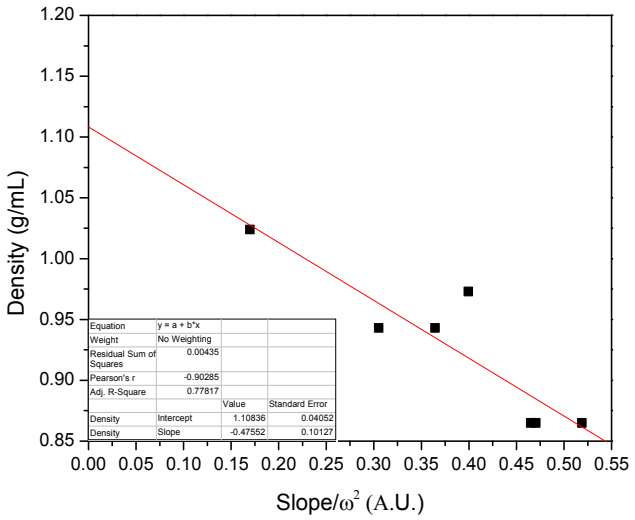

Figure 4.11- Density vs. slope/ω^2 of AUC experiments from Table 4.4. The best fit line of the plot gives the y-intercept of 1.1084 g/mL which is the approximated density of the square.

In Figure 4.11 the data from the AUC experiments were used to get a close estimation of the actual density value. The y-intercept from the curve gives the value of 1.1084 g/mL which is the estimated density of Cu_4(m-pbhx)$_4$ from multiple experiments. The unknown metal organic materials of Cu_3(MeSi(phac)$_3$)$_2$ and Cu_3(MeSi(phpr)$_3$)$_2$ were examined next.

The unknown copper complexes of Cu_3(MeSi(phac)$_3$)$_2$ and Cu_3(MeSi(phpr)$_3$)$_2$ density used for all of the analysis were based on assumed molecular weights based on the sedimentation of the sample in the solvent. Given the sedimentation rate of the sample in solution and Cu_3(MeSi(phac)$_3$)$_2$ sedimenting in chlorobenzene (density of 1.11 g/mL), the density of the copper complexes was assigned a value of 1.138 g/mL. Although the density assigned is an approximate value, the results provide the type of complexes possibly forming in solution. The density of the Cu_4(m-pbhx)$_4$ square was 1.1084 g/mL, and the Cu_3(MeSi(phac)$_3$)$_2$ and Cu_3(MeSi(phpr)$_3$)$_2$ complexes will possibly be more dense. The reason is the proposed complexes are more heavily aromatic; so the density of 1.138 g/mL is a good approximation to work with.

Still, in order to receive a more accurate value for the density of the compounds (to get a more accurate molecular weight) further test have to be done. Either a direct density measurement by a density meter could be performed, or running the sample in deuterated solvent could give a direct value for the density. The difficulty in a direct density measurement by the density meter is having sufficient amount of material to measure. The ligand that makes each of the respected compounds requires a minimum of a month's time to synthesize. In the case of using deuterated solvent (i.e. fluorobenzene-d5 or toluene-d8) in analyzing the sample, the unknown organic copper complex would first have to be synthesized, tested for stability, and then run by AUC. For these studies an approximate density value for the unknown complexes were assigned.

The initial step in the AUC analysis of the $Cu_3(MeSi(phac)_3)_2$ consisted of determining the proper wavelength for the complex in fluorobenzene and toluene. Figure 4.12 is the absorption spectrum of the $Cu_3(MeSi(phac)_3)_2$ in the two solvents:

a)

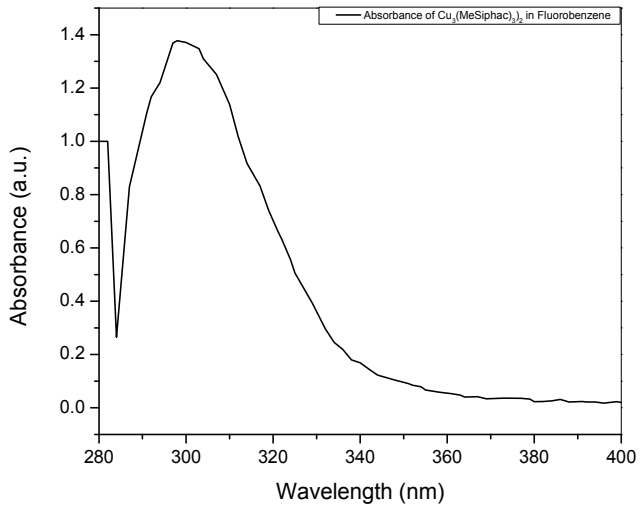

b)

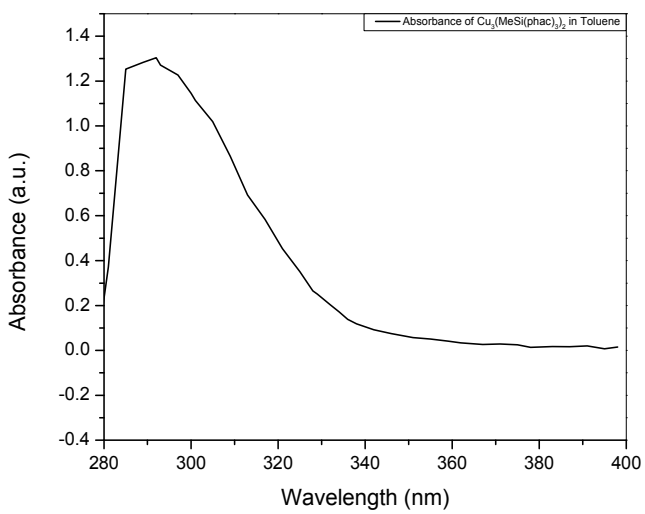

Figure 4.12- Measured absorbance of $Cu_3(MeSi(phac)_3)_2$ in fluorobenzene and toluene. The max wavelength was not used due to noise interference and the concentration being too low. The concentration for the analysis in both solvents was 3.02×10^{-5}M. a) Measured absorbance of $Cu_3(MeSi(phac)_3)_2$ in fluorobenzene (wavelength used 320 nm). b) Absorbance of $Cu_3(MeSi(phac)_3)_2$ in toluene (wavelength used 315 nm).

The $Cu_3(MeSi(phac)_3)_2$ complex was measured at 320 nm in fluorobenzene and 315 nm in toluene at 60krpm. In the study of the unknown copper complex, the speed of 60krpm was determined to be sufficient to analyzing the sample in both solvents. The cell measured for the $Cu_3(MeSi(phac)_3)_2$ analysis in both solvents were measured from 5.9- 7.2 cm (above the meniscus to the end of the cell). Figure 4.13 below shows the AUC equilibrium analysis of the $Cu_3(MeSi(phac)_3)_2$ in fluorobenzene and toluene:

a)

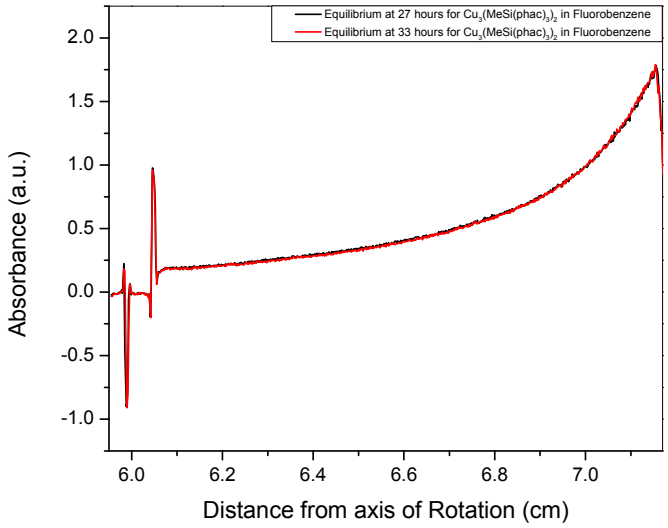

b)

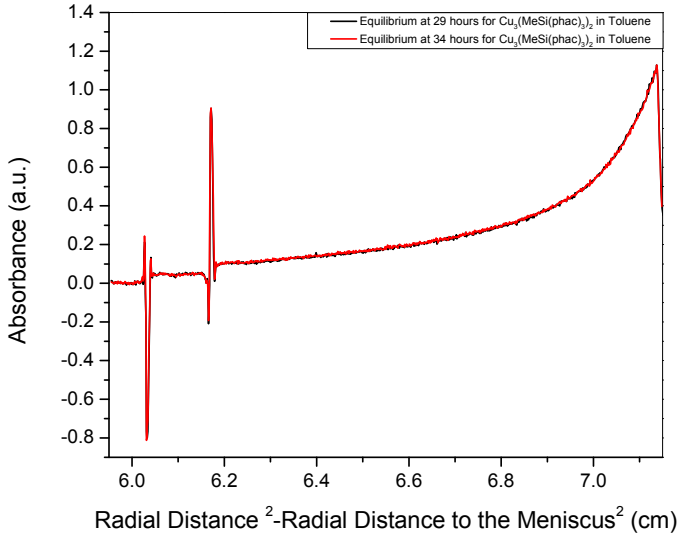

Figure 4.13- AUC Equilibrium for $Cu_3(MeSi(phac)_3)_2$. a) Equilibrium of the sample was achieved at 60 krpm at 27 hours in fluorobenene. b) Equilibrium achieved at 60 krpm at 29 hours in toluene.

The raw data from the two graphs from Figure 4.13 were converted into $\log_{10}$ forms below. In the data set for both $Cu_3(MeSi(phac)_3)_2$ samples, two exponential fits were made for the analysis based on the fit of the whole raw data set. Two exponential fits were made to determine if multiply dispersed sample existed in solution.

The $\log_{10}$(absorbance) for the $Cu_3(MeSi(phac)_3)_2$ in fluorobenzene was taken at the rb from 6.3-7.144cm. The 1st exponential fit was taken from 6.3-6.717cm and the 2nd exponential fit was taken at 6.717-7.144cm. The exponential fits were performed to linearize the data, and to determine if at least two species could be identified. The AUC equilibrium graph in Figure 4.13a was converted into the $\log_{10}$ plots in Figure 4.14 below:

a)

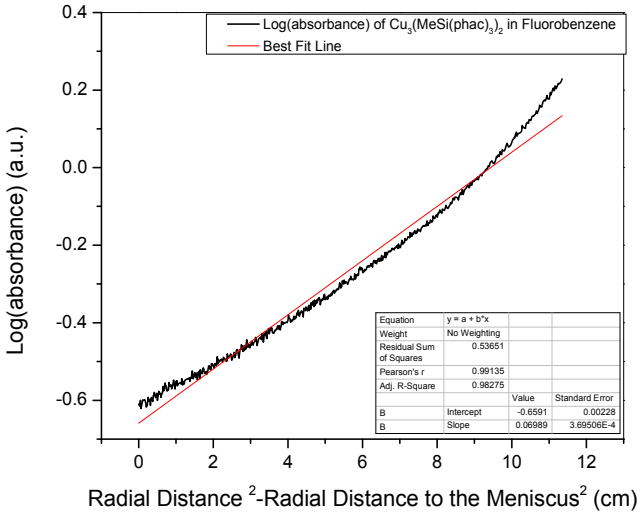

b)

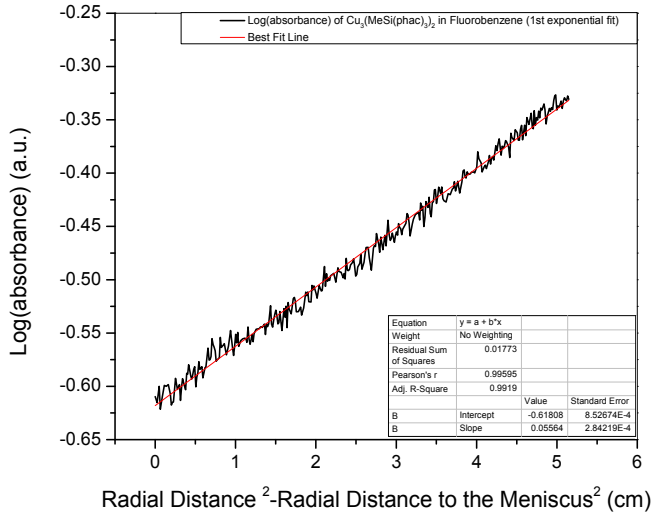

(Figure 4.14 continued)
c)

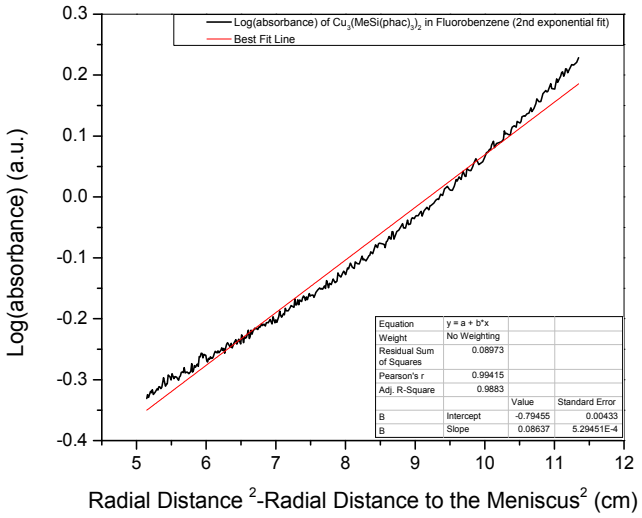

Figure 4.14- Log_{10}(absorbance) vs. rb^2-rm^2 plot for $Cu_3(MeSi(phac)_3)_2$ and two exponential fits in fluorobenzene. Using the density of 1.138 g/mL and the slope of the curves, it was determined that the molecular weight was 1920.71 g/mol (entire curve), 1541.41 g/mol (1st exponential fit), and 2407.07 g/mol (2nd exponential fit). The calculated molecular weight are close to the empirical formula of 1322.07 g/mol, the molecular weight of $Cu_3(MeSi(phac)_3)_2$. The different exponential fits show at least two components are in the sample. a) The entire log_{10}(absorbance) plot of $Cu_3(MeSi(phac)_3)_2$ in fluorobenzene. b) The 1st exponential fit log_{10}(absorbance) plot of $Cu_3(MeSi(phac)_3)_2$ in fluorobenzene. c) The 2nd exponential fit log_{10}(absorbance) plot of $Cu_3(MeSi(phac)_3)_2$ in fluorobenzene.

The arched line for the entire log_{10}(absorbance) curve in Figure 4.14 indicates dispersion of multiple entities of the $Cu_3(MeSi(phac)_3)_2$ in fluorobenzene. Fitting the early and late parts of the curve yield molecular weights of 1541.41 g/mol and 2407.07 g/mol. Thus, it is possible that the sample contains several different sizes of molecules. The large difference in the two values signify different compounds in solution. The overall molecular weight was calculated using the assumed density of 1.138 g/mL. The analysis shows close molecular weight to the molecular weight of the empirical formula $Cu_3(MeSi(phac)_3)_2$ (1322.07 g/mol).

The analysis of $Cu_3(MeSi(phac)_3)_2$ was also performed in toluene. The log_{10}(absorbance) for the entire $Cu_3(MeSi(phac)_3)_2$ in toluene was taken at the rb (distance from axis of rotation) from 6.404-

7.047cm. The $\log_{10}$(absorbance) for the 1st exponential was taken at rb 6.426-6.775cm. The $\log_{10}$(absorbance) for the 2nd exponential was taken at rb 6.775-7.137cm. The AUC equilibrium graph in Figure 4.13b was converted into $\log_{10}$ plots shown in Figure 4.15 below:

a)

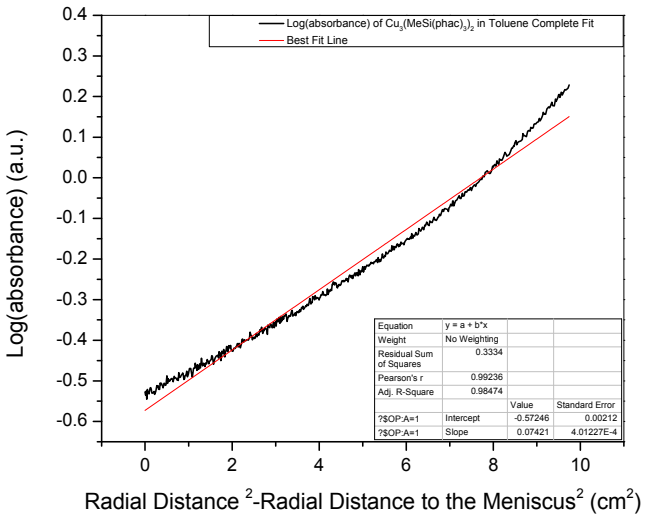

b)

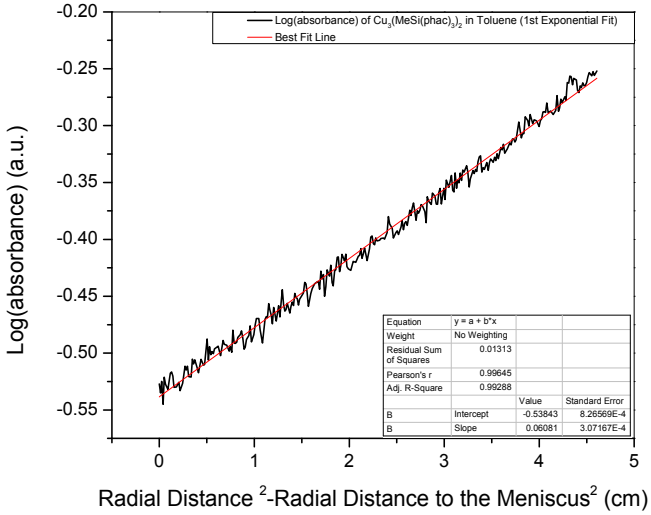

(Figure 4.15 continued)
c)

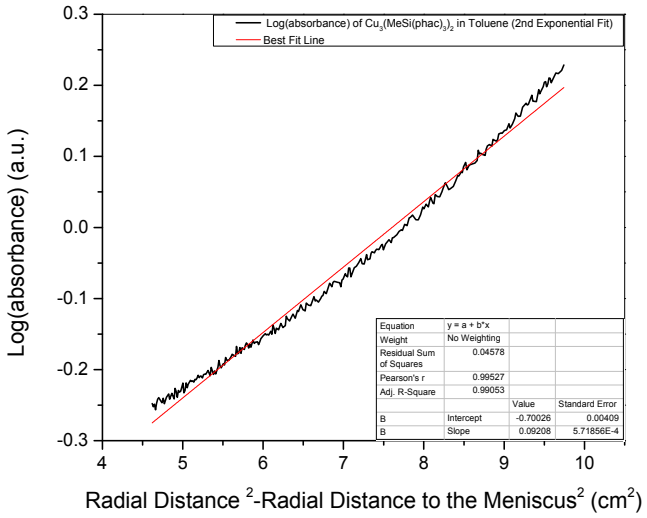

Figure 4.15- Log_{10}(absorbance) vs. rb^2-rm^2 plot and two exponential fits for $Cu_3(MeSi(phac)_3)_2$ in toluene. Using the assumed density of 1.138 g/mL (and the slope of the curve), it was determined that the molecular weight was 886.31 g/mol (entire curve), 726.24 g/mol (1st exponential fit), and 1098.93 g/mol (2nd exponential fit). The calculated moleculare weight of the 2nd exponential fit is closest to the empirical formla of 1322.07 g/mol, the molecular weight of $Cu_3(MeSi(phac)_3)_2$. The exponential fits also indicate at least two distinct species in the sample. a) The entire log_{10}(absorbance) plot of $Cu_3(MeSi(phac)_3)_2$ in toluene. b) The 1st exponential fit log_{10}(absorbance) plot of $Cu_3(MeSi(phac)_3)_2$ in toluene. c) The 2nd exponential fit log_{10}(absorbance) plot of $Cu_3(MeSi(phac)_3)_2$ in toluene.

The curved line for the entire log_{10}(absorbance) curve in Figure 4.15 indicates dispersion of multiple entities of $Cu_3(MeSi(phac)_3)_2$ in toluene. The low calculated molecular weights of 886.31 g/mol (entire curve), 726.24 g/mol (1st exponential fit), and 1098.93 g/mol (2nd exponential fit) indicate possible degradation of the sample during analysis. The second exponential fit is near the molecular weight of the empirical formula of $Cu_3(MeSi(phac)_3)_2$ (1322.07 g/mol).

The next set of AUC equilibrium experiments were performed on $Cu_3(MeSi(phpr)_3)_2$ in toluene and fluorobenzene. Since the experiment was time sensitive, the samples were analyzed immediately. The wavelengths used for AUC analysis were first established before running the samples. The measured absorbance of the samples were taken from 280nm-400nm. The concentration of the $Cu_3(MeSi(phpr)_3$

in both solvents were 4.23 x 10^{-5}M. Figure 4.16 show the absorbance of the unknown copper complex in the two solvents:

a)

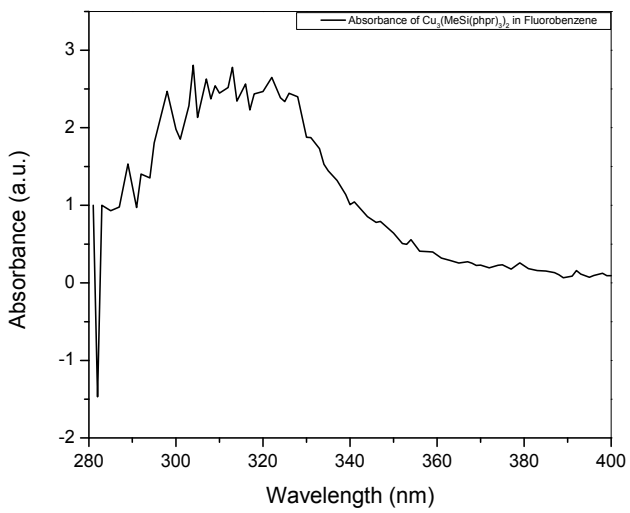

b)

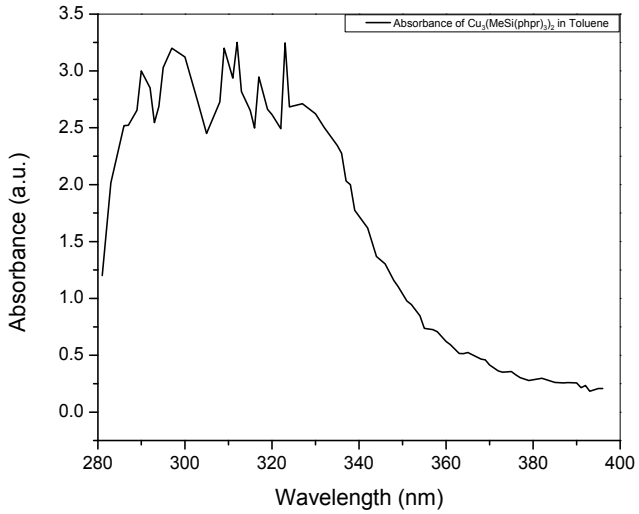

Figure 4.16- Measured absorbance of $Cu_3(MeSi(phpr)_3)_2$ in fluorobenzene and toluene. The max wavelength was not used due to noise interference and the concentration being too low. The concentration for the analysis in both solvents was 4.23 x 10^{-5}M. a) Absorbance of $Cu_3(MeSi(phpr)_3)_2$ in fluorobenzene (wavelength used 350 nm). b) Absorbance of $Cu_3(MeSi(phpr)_3)_2$ in toluene (wavelength used 355 nm).

$Cu_3(MeSi(phpr)_3)_2$ was measured by AUC at 350 nm in fluorobenzene and 355 nm in toluene at 60krpm. The rotor speed of 60krpm was determined to be sufficient to analyzing the sample in both solvents. The cell measured for the $Cu_3(MeSi(phpr)_3)_2$ analysis in both solvents were measured from

5.9- 7.2 cm (above the meniscus to the end of the cell). Figure 4.17 shows the AUC equilibrium analysis of the $Cu_3(MeSi(phpr)_3)_2$ in toluene and fluorobenzene.

a)

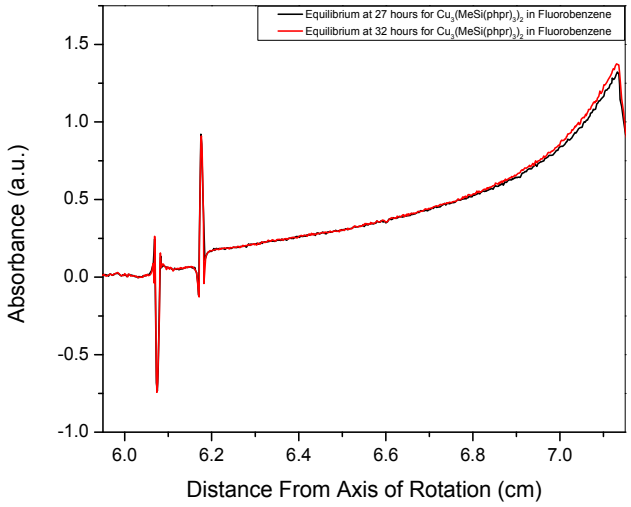

b)

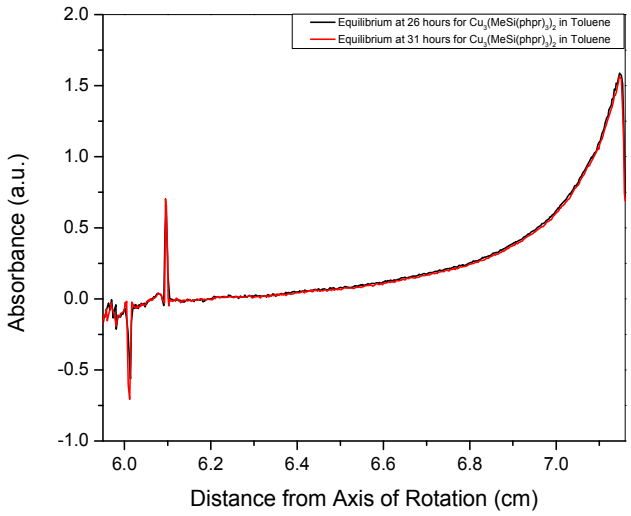

Figure 4.17- AUC Equilibrium $Cu_3(MeSi(phpr)_3)_2$. a) Equilibrium of the sample was achieved at 60 krpm at 27 hours in fluorobenene. b) Equilibrium achieved at 60 krpm at 26 hours in toluene.

The data from the graphs in Figure 4.17 were converted into logarithmic plots for the fluorobenzene sample in Figure 4.18 and for the toluene sample Figure 4.18. The data set for the $Cu_3(MeSi(phpr)_3)_2$ were converted into exponential fits to determine if multiple species occurred. The log_{10}(absorbance) for the $Cu_3(MeSi(phpr)_3)_2$ in fluorobenzene was taken at the rb from 6.322-7.132cm.

The 1st exponential fit was taken from 6.322-6.596cm and the 2nd exponential fit was taken at 6.596-7.132cm. The conversion was performed to linearize the data, and to determine if at least two species could be identified. Figure 4.18 is the $\log_{10}$ plot of $Cu_3(MeSi(phpr)_3)_2$ in fluorobenzene:

a)

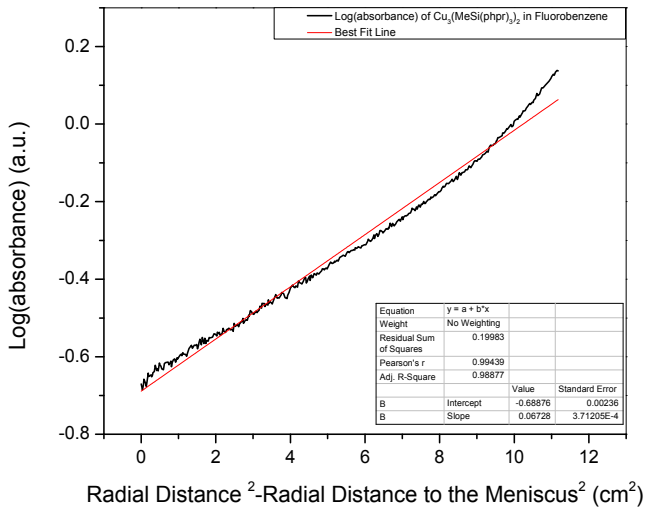

b)

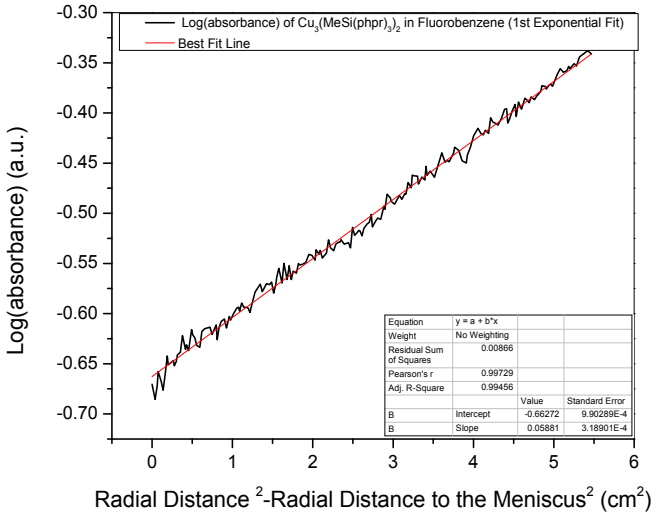

(Figure 4.18 continued)
c)

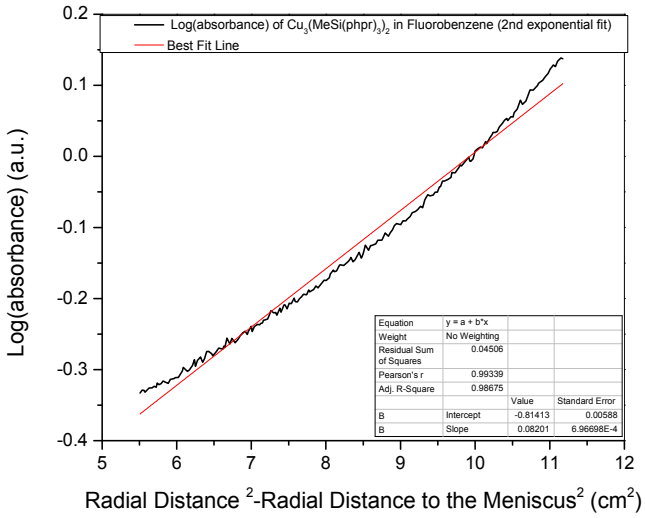

Figure 4.18- Log_{10}(absorbance) vs. rb_2-rm_2 plot and two exponential fits of $Cu_3(MeSi(phpr)_3)_2$ in fluorobenzene. Using the assumed density of 1.138 g/mL (and the slope of the curve), it was determined that the molecular weight was 1848.72 g/mol (entire curve), 1615.98 g/mol (1st exponential fit), and 2253.47 g/mol (2nd exponential fit). The plots in this figure have calculated molecular weights near the molecular weight of 1490.42 g/mol which is the empirical formula of $Cu_3(MeSi(phpr)_3)_2$. The analysis also shows at least two distinct species in the sample by the separation of values of the exponential fits. a) The entire log_{10}(absorbance) plot of Cu3(MeSi(phpr)$_3$)$_2$ in fluorobenzene. b) The 1st exponential fit log_{10}(absorbance) plot of $Cu_3(MeSi(phpr)_3)_2$ in fluorobenzene. c) The 2nd exponential fit log_{10}(absorbance) plot of $Cu_3(MeSi(phpr)_3)_2$ in fluorobenzene.

Figure 4.19 is the is the log_{10} plot of $Cu_3(MeSi(phpr)_3)_2$ in toluene:

a)

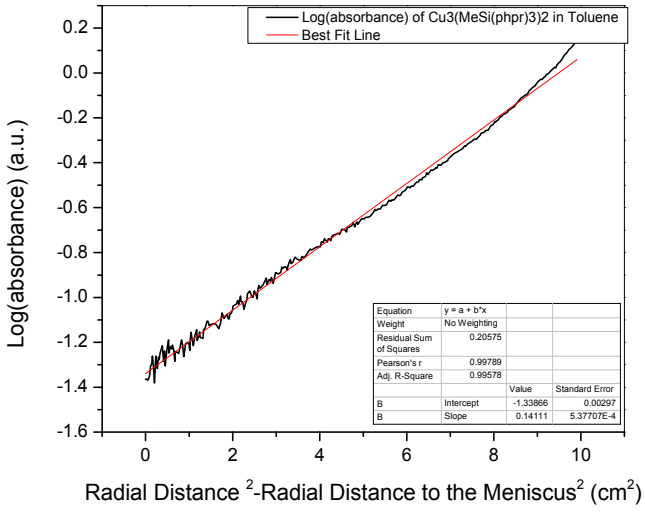

(Figure 4.19 continued)
b)

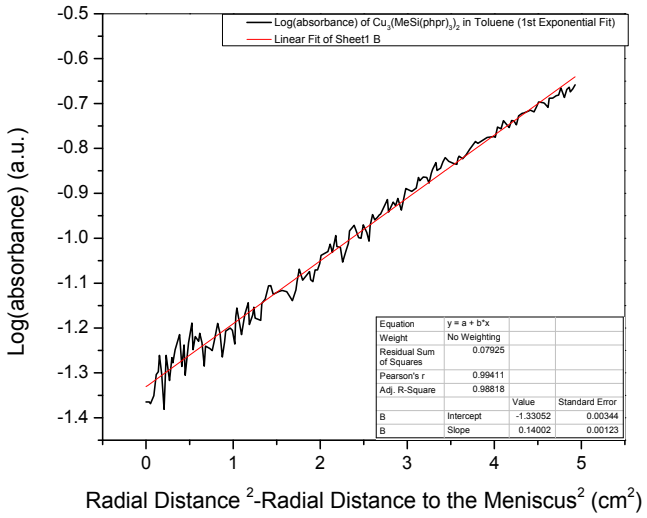

c)

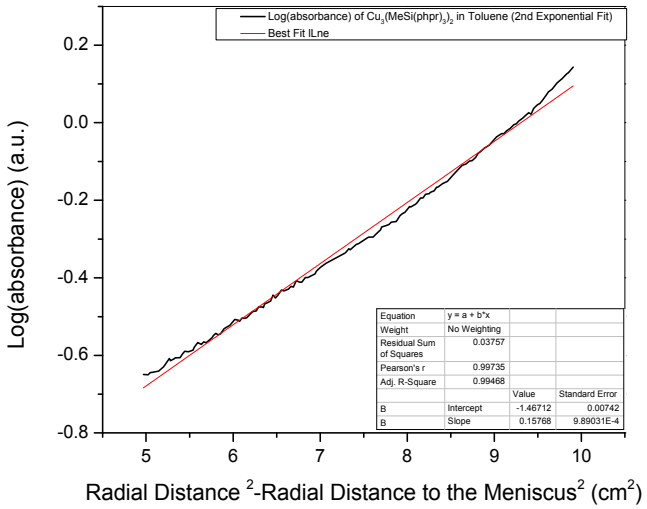

Figure 4.19- Log_{10}(absorbance) vs. rb^2-rm^2 plot of $Cu_3(MeSi(phpr)_3)_2$ and two exponential fits in toluene. Using the assumed density of 1.138 g/mL (and the slope of the curve), it was determined that the molecular weight was 1680 g/mol, 1670 g/mol for the 1st exponential fit, and 1880 for the 2nd exponential fit. The calculated molecular weight are close to the empirical formula of 1490.42 g/mol, the molecular weight of $Cu_3(MeSi(phpr)_3)_2$. The analysis also shows at least two distinct species in the sample by the separation of values of the exponential fits. a) The entire log_{10}(absorbance) plot of $Cu_3(MeSi(phpr)_3)_2$ in toluene. b) The 1st exponential fit log_{10}(absorbance) plot of $Cu_3(MeSi(phpr)_3)_2$ in toluene. c) The 2nd exponential fit log_{10}(absorbance) plot of $Cu_3(MeSi(phpr)_3)_2$ in toluene.

The analysis of the unknown copper complexes shows at least two components existing in the different solvents. In addition, the approximated molecular weights are near the empirical formula of the unknown copper complexes. In order to give a direct comparison, Table 4.6 provides AUC results for all of the copper complexes studied in fluorobenzene and toluene:

Table 4.6-Calculated molecular weights of the copper complexes based on approximated densities. The density of the unknown compounds were given estimated densities of 1.138 g/mL for the calculation of the MW of the $Cu_3(MeSi(phac)_3)_2$ and $Cu_3(MeSi(phpr)_3)_2$. The density of the square is put at 1.11 g/mL.

	Fluorobenzene			Toluene		
	Molecular Weight of Complete Fit (g/mol)	Molecular Weight of 1st Exponential Fit (g/mol)	Molecular Weight of 2nd Exponential Fit (g/mol)	Molecular Weight of Complete Fit (g/mol)	Molecular Weight of 1st Exponential Fit (g/mol)	Molecular Weight of 2nd Exponential Fit (g/mol)
$Cu_4(m\text{-}pbhx)_4$	2140	N/A	N/A	2170	N/A	N/A
$Cu_3(MeSi(phac)_3)_2$	1920	1540	2410	890	730	1100
$Cu_3(MeSi(phpr)_3)_2$	1850	1620	2250	1680	1670	1880

The AUC analysis of the copper complexes of $Cu_4(m\text{-}pbhx)_4$, $Cu_3(MeSi(phac)_3)_2$, and $Cu_3(MeSi(phpr)_3)_2$ have produced varying results. The known copper complex of $Cu_4(m\text{-}pbhx)_4$ has given results of a mono-dispersed sample for the AUC analysis. Additionally, the two solvents used for the analysis of $Cu_4(m\text{-}pbhx)_4$ had similar molecular weights for the copper square analyzed. The results of the analysis give validity and credence to using AUC as a tool for analysis on metal organic materials.

The $Cu_3(MeSi(phac)_3)_2$ had different results in the two solvents observed. In the study both fluorobenzene and toluene had exponential fits indicating at least two distinct species. But, in the case of toluene, the calculated molecular weight was overall lower than in fluorobenzene. In the case of toluene, only the last exponential fit (1100 g/mol) was close to the molecular weight of the empirical formula ($Cu_3MeSi(phac)_3)_2$ = 1322.07g/mol). The difference behind the discrepancy may be due to the more expedient degradation of $Cu_3(MeSi(phac)_3)_2$ in toluene as opposed to fluorobenzene.

The unknown complex of $Cu_3(MeSi(phpr)_3)_2$ have produced results showing distinct species in solution and molecular weights close to unknown copper complex's empirical formula (1490.42 g/mol). The similarities in the studies were the distinct species which were determined by the variation of molecular by the exponential fits. The difference in the study of $Cu_3(MeSi(phpr)_3)_2$ in fluorobenzene versus toluene are the different molecular weights of the sample. The sample in fluorobenzene has a larger overall molecular weight value than toluene. The differences in molecular weight may be attributable to the type of species in solution as well as different solvents used. A possible explanation for the differences in molecular weights of the samples may be slow degradation of the material in solution; another may be aggregation of species in solution.

Chapter 5: Other Techniques

5.1- Other Techniques Used for Analyzing the Structures of the Cu(II) complexes of Silicon-Based Multidentate β-Diketonate Ligands

Various efforts have been made to characterize the Cu(II) complexes of silicon-based multidentate β-diketonate ligands. Beyond the experiments discussed, other forms of analysis of the copper complexes have been made. Among the other methods studied were transmission electron microscopy (TEM), matrix assisted laser desorption ionization (MALDI), electron paramagnetic resonance (EPR), and dynamic light scattering (DLS).

Transmission Electron Microscopy (TEM) was attempted to characterize the $Cu_3(MeSi(phac)_3)_2$ to determine if the polyhedral cages could be identified. The results were that no distinct features of the molecules were visible in the TEM images. An explanation for the inability of TEM to characterize the structure is the low amount of copper metal making up these complexes. The amount more atoms of high atomic number in a sample, the higher contrast the sample provides for TEM. The amount of copper metal in the sample may have been too low for it to be observed. In addition, staining the $Cu_3(MeSi(phac)_3)_2$ with 2% uranyl acetate in H_2O, which can improve contrast due to its uranium atoms, did not yield any observable molecules.

The $Cu_3(MeSi(phac)_3)_2$ was investigated with by matrix assisted laser desorption ionization time of flight mass spectrometry (MALDI-TOF MS). In these studies, various matrixes were tested to determine if the various proposed polyhedral structures could be identified. The matrices experimented with were anthracene, dithranol, 2,6-dihydroxyacetophenone (DHA), 1,7-dimethoxynaphthalene (DMN), terthiophene (THP), and 2-cyano-4-hydroxycinnamic acid (HCCA). In addition to this, a matrix-free sample of $Cu_3(MeSi(phac)_3)_2$ was also tested. The choices of using different matrices for MALDI-TOF MS came from different papers cited in the literature which analyzed metal complexes [56-58]. Ramanjaneyulu and coworkers analyzed different metal complexes (including copper) of benzimidazole thiosemicarbazones with MALDI [58]. The matrices used in their study were polar (i.e. HCCA) and non-

polar (i.e. DMN and THP) yielded results. It was from this study, that THP was discovered, used, and gave a signal for the $Cu_3(MeSi(phac)_3)_2$.

All of the matrices except terthiophene (THP) produced no discernible signal for the complex. With terthiophene as the matrix, the spectrum showed a series of peaks separated by ~162, ~100, and ~63 amu. These are approximately correct for Cu(acac), acacH, and Cu respectively. However, there are too many of them (~36 peak seperations) to make sense with any logical structure for the complex, and the peaks were unable to be identified. Thus, MALDI-TOF MS also did not provide useful structural information for $Cu_3(MeSi(phac)_3)_2$. Below is Figure 5.1 the ligand $Cu_3(MeSi(phac)_3)_2$ coordinating to copper metal, and Figure 5.2 fragments from the ligand $Cu_3(MeSi(phac)_3)_2$ coordinating to copper metal:

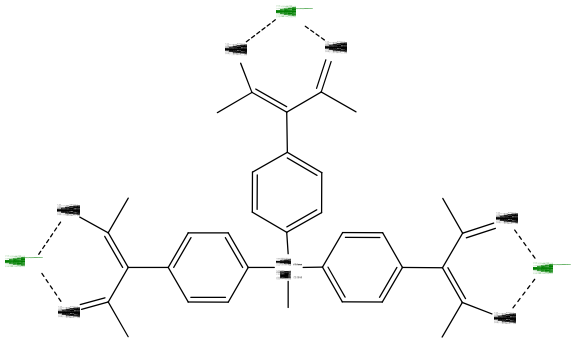

Figure 5.1- β-diketonate ligand $MeSi(phacH)_3$ coordinating to copper metal.

a) **b)** **c)**

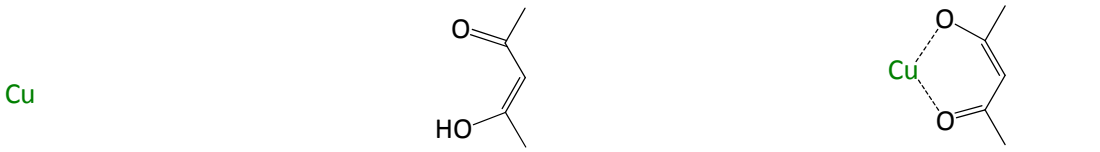

Molecular Weight: 63.55 Molecular Weight: 100.12 Molecular Weight: 162.65

Figure 5.2- Fragments of β-diketonate ligand $MeSi(phacH)_3$ coordinating to copper metal.
a) Copper Atom
b) β-Diketonate Ligand
c) β-Diketonate Ligand Cooridinated to Copper Atom

The complex may have degraded into these fragments. Although the separation between the peaks of the MALDI-TOF MS could be assigned, no clear structure was able to be determined from MALDI-TOF MS. The peaks themselves were not able to be identified as any particular molecules. Future work for MALDI-TOF MS does not appear likely to yield satisfactory results given the variety of matrices used and the indiscernible data from the terthiophene matrix.

Electron paramagnetic resonance (EPR) spectroscopy was used to analyze 6 mM solution of $Cu_3(MeSi(phac)_3)_2$ in chlorobenzene. The EPR spectrum of $Cu(acac)_2$ (see Figure 1.5) shows four lines, because the unpaired electron couples to the Cu nucleus (spin 3/2). EPR spectra of polynuclear Cu(II) complexes often show more than four lines, because the unpaired electrons can couple to more than one Cu nucleus. Thus, in a molecule like "$Cu_3(MeSi(phac)_3)_2$", if you saw hyperfine coupling in the EPR spectrum, you might be able to interpret it in terms of the proposed polyhedral structures. However, when the spectrum was recorded, only a broad peak near g = 2 was observed which did not show any hyperfine coupling. Future analysis on the unknown copper complex appears unlikely given the results of the EPR.

Analysis of $Cu_3(MeSi(phpr)_3)_2$ was performed using dynamic light scattering (DLS) in chlorobenzene to determine the size of the molecule. DLS can measure particles with diffusion coefficients of 10^{-6}-$10^{-9}cm^2/s$ (or even less). The $Cu_3(MeSi(phpr)_3)_2$ was used instead of the $Cu_3(MeSi(phac)_3)_2$ because the size is expected to be larger than the $Cu_3(MeSi(phac)_3)_2$. Two samples were analyzed by DLS. The first sample analyzed had a concentration of 1.7 mg/mL, the second sample had a concentration of 11.6 mg/mL. The first sample analyzed produced no signal for the red, green, and blue wavelengths; therefore a more concentrated sample was attempted. When the second sample of $Cu_3(MeSi(phpr)_3)_2$ was analyzed by DLS, the sample absorbed the laser light. DLS operates by measuring the intensity of light scattered, therefore absorbance adversely affects the analysis. The copper in the sample was causing a significant absorption of light and what made the analysis by DLS

problematic. Future work with DLS is unlikely given the inherent problems associated with the absorbance features of the complex.

Chapter 6: Conclusion

The copper complexes "$Cu_3(MeSi(phac)_3)_2$" and "$Cu_3(MeSi(phpr)_3)_2$" have been examined by several techniques that might reveal their molecular structure. It was anticipated that the new results might support the existence of cubes, decahedra, and dodecahedra molecules in the samples. So far the only technique performed for the research showing any possibility of the proposed polyhedral cages forming is atomic force microscopy. The following techniques used to examine the unknown organic copper complexes have not provided information about their molecular structure: nuclear magnetic resonance (NMR), electron paramagnetic resonance (EPR), electrospray ionization (ESI) and matrix assisted laser desorption ionization (MALDI) time of flight mass spectrometry, transmission electron microscopy (TEM), and dynamic light scattering (DLS).

Analysis of the compounds with analytical ultracentrifugation (AUC) has given estimates of the molecular weights of the molecules, though the results indicate that a mixture of molecules with different sizes may be present. These estimated molecular weights are too small to suggest the formation of these particular complexes (with the possible exception of the cube). In order to determine the molecular weight of the $Cu_3(MeSi(phac)_3)_2$ and $Cu_3(MeSi(phpr)_3)_2$ complexes, the density of the copper organic complexes need to be determined. The density of the two samples can be determined by using deuterated solvents with AUC. Additional details, such as what portion of the samples exists in small or large aggregates, may be gained by applying nonlinear least squares fitting algorithms to the data.

Future work on the unknown copper complexes does not seem likely given the thorough analysis of the compounds, the inherent instability of the materials, and the small amounts available. As the research has demonstrated, analysis of some closely related metal organic materials (i.e. Cu_4(m-pbhx)$_4$) by AUC has been effective. Work analyzing other metal organic materials using AUC may provide structural elucidation for other unknown systems resistant to the usual forms of analysis.

References

1. Eddaoudi, M. and J.F. Eubank, *Insight into the Development of Metal-Organic Materials (MOMs): At Zeolite-Like Metal-Organic Frameworks (ZMOFs)*, in *Metal-Organic Frameworks*. 2010, John Wiley & Sons, Inc. p. 37-89.

2. Barrer, R.M., *Zeolites and their synthesis.* Zeolites, 1981. **1**(3): p. 130-140.

3. Mumpton, F.A., *La roca magica: Uses of natural zeolites in agriculture and industry.* Proceedings of the National Academy of Sciences, 1999. **96**(7): p. 3463-3470.

4. Kuznicki, S.M., et al., *Macroscopic aggregates of microcyrystalline zeolites for static water softening applications. US Pat. Appl. US 2002077245, 2002.*

5. Kuznicki, S.M., et al., *Porous static water softener containing hybrid zeolite-silicate composition. US Pat. Appl. US 20020074293, 2002.*

6. Mao, L.V., *R.Zeolite materials with enhanced ion exchange capacity. Can. Pat. Appl. CA 2125314, 1995.*

7. Le Van Mao, R., et al., *Modified zeolites for the removal of calcium and magnesium from hard water.* Journal of Materials Chemistry, 1994. **4**(7): p. 1143-1147.

8. Yang, X.-p., *Latest advances in application of zeolites in oil refining and petrochemical industry.* Industrial Catalysis, 2003. **11**(6): p. 19.

9. Maxwell, I.E., *Hydrocarbon processing with zeolites.* Studies in Surface Science and Catalysis, 2001. **137**(Introduction to Zeolite Science and Practice (2nd Edition)): p. 747.

10. Corma, A., *Zeolites in oil refining and petrochemistry.* NATO ASI Series, Series C: Mathematical and Physical Sciences, 1992. **352**(Zeolite Microporous Solids: Synth., Struct., React.): p. 373.

11. Glaeser, R., *The application of zeolites in catalysis.* Springer Series in Chemical Physics, 2004. **75**(Basic Principles in Applied Catalysis): p. 161.

12. Hagiwara, K., et al., *Effect of vanadium on USY zeolite destruction in the presence of sodium ions and steam—studies by solid-state NMR.* Applied Catalysis A: General, 2003. **249**(2): p. 213-228.

13. Claridge, R.P., et al., *Faujasite catalysis of aromatic nitrations with dinitrogen pentoxide. The effect of aluminium content on catalytic activity and regioselectivity. The nitration of pyrazole.* Journal of the Chemical Society, Perkin Transactions 2, 2001(2): p. 197-200.

14. Robert, M.M., *Molecular Sieve Science and Technology*, in *Zeolite Synthesis*. 1989, American Chemical Society. p. 1-10.

15. Contreras Niño, V.D., et al., *Application of faujasite synthesized from illite to the removal of Cr3+ and Ni2+ from electroplating wastewater.* Revista ION, 2013. **26**: p. 7-16.

16. Kondo, M., et al., *Three-Dimensional Framework with Channeling Cavities for Small Molecules: {[M2(4, 4'-bpy)3(NO3)4]·xH2O}n (M = Co, Ni, Zn).* Angewandte Chemie International Edition in English, 1997. **36**(16): p. 1725-1727.

17. Kaye, S.S., et al., *Impact of Preparation and Handling on the Hydrogen Storage Properties of Zn4O(1,4-benzenedicarboxylate)3 (MOF-5).* Journal of the American Chemical Society, 2007. **129**(46): p. 14176-14177.

18. Evans, O.R., H.L. Ngo, and W. Lin, *Chiral Porous Solids Based on Lamellar Lanthanide Phosphonates.* Journal of the American Chemical Society, 2001. **123**(42): p. 10395-10396.

19. Sawaki, T. and Y. Aoyama, *Immobilization of a Soluble Metal Complex in an Organic Network. Remarkable Catalytic Performance of a Porous Dialkoxyzirconium Polyphenoxide as a Functional Organic Zeolite Analogue.* Journal of the American Chemical Society, 1999. **121**(20): p. 4793-4798.

20. Gomez-Lor, B., et al., *In2(OH)3(BDC)1.5 (BDC = 1,4-Benzendicarboxylate): An In(III) Supramolecular 3D Framework with Catalytic Activity.* Inorganic Chemistry, 2002. **41**(9): p. 2429-2432.

21. Zou, R.-Q., H. Sakurai, and Q. Xu, *Preparation, Adsorption Properties, and Catalytic Activity of 3D Porous Metal–Organic Frameworks Composed of Cubic Building Blocks and Alkali-Metal Ions.* Angewandte Chemie International Edition, 2006. **45**(16): p. 2542-2546.

22. Horcajada, P., et al., *Metal–Organic Frameworks as Efficient Materials for Drug Delivery.* Angewandte Chemie International Edition, 2006. **45**(36): p. 5974-5978.

23. Eddaoudi, M., *Molecular Building Block Approach to the Assembly of Zeolite-like Metal-Organic Frameworks (ZMOFs) with Extra-Large Cavities.* Abstracts, 34th Northeast Regional Meeting of the American Chemical Society, Binghamton, NY, United States, October 5-7, 2006.

24. Fujita, M., *From Hofmann Complexes to Organic Coordination Networks*, in *Metal-Organic Frameworks*. 2010, John Wiley & Sons, Inc. p. 1-35.

25. Isaeva, V.I. and L.M. Kustov, *Metal-organic frameworks—New materials for hydrogen storage.* Russian Journal of General Chemistry, 2007. **77**(4): p. 721-739.

26. Collins, D.J., S. Ma, and H.-C. Zhou, *Hydrogen and Methane Storage in Metal-Organic Frameworks*, in *Metal-Organic Frameworks*. 2010, John Wiley & Sons, Inc. p. 249-266.

27. Fujita, M., et al., *Spontaneous assembly of ten components into two interlocked, identical coordination cages.* Nature, 1999. **400**(6739): p. 52.

28. Xiaofei, K., et al., *Assembly of a metal–organic framework by sextuple intercatenation of discrete adamantane-like cages.* Nature Chemistry, 2010. **2**(6): p. 461-465.

29. Dincă, M., A.F. Yu, and J.R. Long, *Microporous Metal−Organic Frameworks Incorporating 1,4-Benzeneditetrazolate: Syntheses, Structures, and Hydrogen Storage Properties.* Journal of the American Chemical Society, 2006. **128**(27): p. 8904-8913.

30. Rowsell, J.L.C. and O.M. Yaghi, *Strategies for Hydrogen Storage in Metal–Organic Frameworks.* Angewandte Chemie International Edition, 2005. **44**(30): p. 4670-4679.

31. Rowsell, J.L.C., et al., *Hydrogen Sorption in Functionalized Metal−Organic Frameworks.* Journal of the American Chemical Society, 2004. **126**(18): p. 5666-5667.

32. Han, S.S., W.-Q. Deng, and W.A. Goddard, *Improved Designs of Metal–Organic Frameworks for Hydrogen Storage.* Angewandte Chemie International Edition, 2007. **46**(33): p. 6289-6292.

33. Han, S.S. and W.A. Goddard, *Lithium-Doped Metal-Organic Frameworks for Reversible H2 Storage at Ambient Temperature.* Journal of the American Chemical Society, 2007. **129**(27): p. 8422-8423.

34. Dincă, M., et al., *Observation of Cu2+–H2 Interactions in a Fully Desolvated Sodalite-Type Metal–Organic Framework.* Angewandte Chemie International Edition, 2007. **46**(9): p. 1419-1422.

35. Pariya, C., et al., *Copper β-Diketonate Molecular Squares and Their Host–Guest Reactions.* Angewandte Chemie, 2007. **119**(33): p. 6421-6424.

36. Pieratteli, R. and I. Bertini, *Pure Appl. Chem., Vol. 76, No. 2, pp. 321–333, 2004.© 2004 IUPAC 321 Copper(II) proteins are amenable for NMR investigations* Department of Chemistry and Magnetic Resonance Center (CERM), University of Florence, Via Luigi Sacconi 6, 50019 Sesto Fiorentino (Florence), Italy*

37. http://www.webelements.com/copper/, *Copper: the essentials.* (accessed on 11/2/2013).

38. Alday, P.H. and J.J. Correia, *Macromolecular Interaction of Halichondrin B Analogues Eribulin (E7389) and ER-076349 with Tubulin by Analytical Ultracentrifugation.* Biochemistry, 2009. **48**(33): p. 7927-7938.

39. Koehler, C.S.W., *Developing the Ultracentrifuge.* American Chemical Society, 2003(February 2003).

40. Cantor, C.R. and P.R. Schimmel, *Biophysical Chemistry. Part II: Techniques for the Study of Biological Structure and Function*. 1969: W. H. Freeman and Company. 591-641.

41. Cantor, C.R. and P.R. Schimmel, *Biophysical Chemistry. Part II: Techniques for the Study of Biological Structure and Function*. 1969: W. H. Freeman and Company. 593.

42. Cantor, C.R. and P.R. Schimmel, *Biophysical Chemistry. Part II: Techniques for the Study of Biological Structure and Function*. 1969: W. H. Freeman and Company. 595.

43. Van Holde, K.E., C. Johnson, and H.P. Shing, *Principles of Physical Biochemistry Second Edition*. 1998. 237-241.

44. Probstein, R.F., *Physicochemical Hydrodynamics*. 1994. p. Chapter 5 pp.109-162.

45. Van Holde, K.E., C. Johnson, and H.P. Shing, *Principles of Physical Biochemistry 2nd Edition © 2006, pp. 215, 216, 224. Reprinted by permission of Pearson Education, Inc., Upper Saddle River, NJ*.

46. Stewart, J.S., *Calculus Early Transcendentals*. 2003: Thomson Brooks/Cole.

47. Feng, R., Y. Konishi, and A.W. Bell, *High accuracy molecular weight determination and variation characterization of proteins up to 80 ku by ionspray mass spectrometry.* Journal of the American Society for Mass Spectrometry, 1991. **2**(5): p. 387-401.

48. http://www.sigmaaldrich.com/content/dam/sigma-aldrich/docs/Sigma/Product_Information_Sheet/b4287pis.pdf, *Product Information on Bovine Serum Albumin.* (accessed on 11/2/2013).

49. http://www.analyticalultracentrifugation.com/LammEqSolutions.htm, *Solving the Lamm equation.* (accessed on 11/2/2013).

50. http://en.wikipedia.org/wiki/Error_function, *The Error Function.* (accessed on 11/2/2013).

51. Marcos, Y.S., *Beta-Diketone and Beta-Ketoenamine Building Blocks For Porous Metal-Organic Materials.* Louisiana State University, 2009.

52. http://www.medicago.se/sites/default/files/pdf/productsheets/PBS_Buffer_v._01.pdf. *Phosphate Buffer Saline* (accessed on 4/14/2014).

53. *Sigma Aldrich Corporation, Aldrich chemistry: handbook of fine chemicals.* 2007-2008.

54. Bosque, R. and J. Sales, *Polarizabilities of Solvents from the Chemical Composition.* Journal of Chemical Information and Computer Sciences, 2002. **42**(5): p. 1154-1163.

55. Jackson, J.K., *Beta-Diketone and Beta-Ketoenamie Based Molecular Squares.* Louisiana State University, 2012.

56. Nunez, C., et al., *Structural, MALDI-TOF-MS, Magnetic and Spectroscopic Studies of New Dinuclear Copper(ii), Cobalt(ii) and Zinc(ii) Complexes Containing a Biomimicking [small mu]-OH bridge.* Dalton Transactions, 2010. **39**(48): p. 11654-11663.

57. Ivanova, B. and M. Spiteller, *Silver(I) and zinc(II) organometallic intermediates, catalysing coupling reactions of polysubstituted benzoic acids – Experimental and theoretical study.* Chemical Engineering Journal, 2013. **232**(0): p. 118-127.

58. Bhaskar, G., et al., *Matrix-assisted laser desorption/ionization studies on transition metal complexes of benzimidazole thiosemicarbazones.* European Journal of Mass Spectrometry, 2007. **13**(2): p. 135-145.

Appendix A: Letters of Permission for Copyrighted Material

PEARSON

Legal/Permissions
One Lake Street
Upper Saddle River, NJ 07458
Fax: 201-236-3290
Phone: 201-236-3281
Vineta.Lewis@Pearson.com

Sep 30, 2013 PE Ref # 180245

Jonathan Stephen Casey
LOUISIANA STATE UNIVERSITY
4010 Gourrier Avenue
Baton Rouge, LA 70808

Dear Jonathan Stephen Casey:

You have our permission to include content from our text, ***PRINCIPLES OF PHYSICAL BIOCHEMISTRY, 2nd Ed. by VAN HOLDE, KENSAL E; JOHNSON, CURTIS; HO, PUI SHING,*** in your masters thesis at LOUISIANA STATE UNIVERSITY.

Content to be included is:
pp. 215, 216, 224 Figs. 5.2, 5.4, 5.8

Please credit our material as follows:
VAN HOLDE, KENSAL E; JOHNSON, CURTIS; HO, PUI SHING, PRINCIPLES OF PHYSICAL BIOCHEMISTRY, 2nd Edition, © 2006, pp. 215, 216, 224. Reprinted by permission of Pearson Education, Inc., Upper Saddle River, NJ

Sincerely,
Vineta Lewis, Permissions Supervisor

Thank you for your message.

W.H. Freeman and Company/Worth Publishers grants you permission to use in your educational paper a maximum of three illustrations from the Cantor, Schimmel, Paul Reinhard 1980. Biophysical Chemistry PartII: Techniques for the Study of Biological Structure and Function title.

This permission is granted with the following conditions:

Photographs of any type are excluded.

Any third-party content (any material credited or attributed to another party) is excluded.

Use is limited to the details of your request and to educational, non-commercial purposes.

No other rights may be assumed.

Best Regards,

Felice Pilchik

Appendix B: List of Acronyms and Symbols

A	Perpendicular Cross-Sectional Area to the Direction of Flow
a	Radius of Sphere
a.u.	Arbitrary Unit
AFM	Atomic Force Microscopy
amu	Atomic Mass Unit
AUC	Analytical Ultracentrifugation
AΔx	Total Volume of an Object
BDC	1,4-benzenedicarboxylate
BDT	1,4-benzeneditetrazolate
BSA	Bovine Serum Albumin
C	Concentration
cm	Centimeter
D	Diffusion Coefficient
Da	Daltons
DCM	Dichloromethane
DEF	N,N-Diethylformamide
DMF	Dimethylformamide
ESI-TOF MS	Electrospray Ionization Time of Flight Mass Spectrometry
EtOAc	Ethyl Acetate
f	Frictional Coefficient
F_b	Buoyancy Force
F_c	Centrifugal Force
F_d	Frictional Force

F_o	Frictional Coefficient
g	Grams
J	Flow
J(x)	Flow Rate
J(x+Δx)	Flow Rate of Mass Out of a Volume
J_s	Sedimentation Flow
k	Boltzmann Constant
L	Ligand
m	Mass
M	Molarity
M	Molecular Weight
M	Monoisotopic Ion
m/z	Mass to Charge
mg	Milligram
min	Minutes
mL	Milliliter
m_o	Mass of Solvent Displaced
MOF	Metal Organic Framework
mol	Moles
MOMs	Metal Organic Materials
MS	Mass Spectrometry
nm	Nanometers
NMR	Nuclear Magnetic Resonance
r	Distance from the Rotation Center
R	Ideal Gas Constant

R_b	Distance from the Axis of Rotation
r_m	Distance of Meniscus from the Axis of Rotation
rpm	Rotations per Minute
s	Seconds
s	Sedimentation Coefficient
S	Svedberg
T	Temperature
UV-Vis	Ultraviolet Visible Spectroscopy
µm	Micrometer
v	Velocity
v_s	Velocity of Sedimentation
$\bar{v}$	Partial Specific Volume
α	Half the Length of the Major Axis
β	Radius of the Minor Axis
Δw	Change in Mass
δx	Change in Distance
η	Viscosity of Solvent
λ_{max}	Wavelength Max
π	Pi
ρ	Density
ϕ	Error Function
ω	Angular Velocity
$\mathcal{N}$	Avogadro ’s Number

Appendix C: NMR Spectrum of $Cu(acac)_2$ and MALDI of Terpthiophene

NMR Spectrum of $Cu(acac)_2$

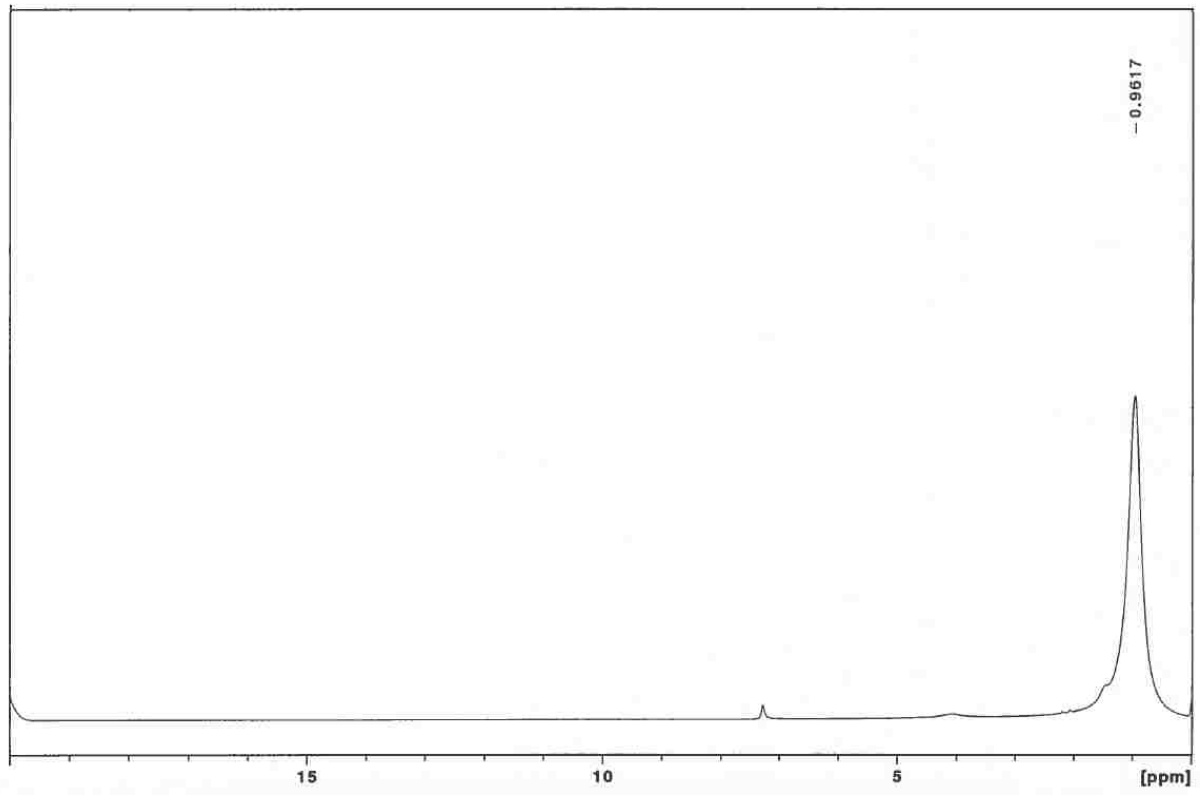

MALDI of terpthiophene low mass range

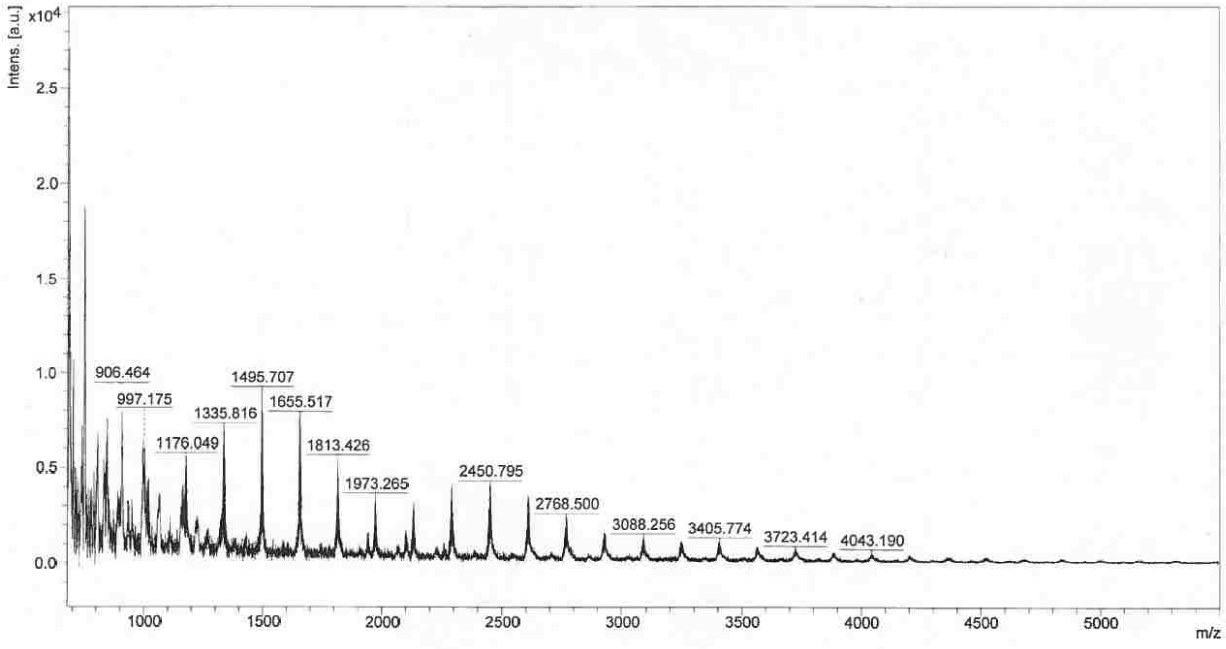

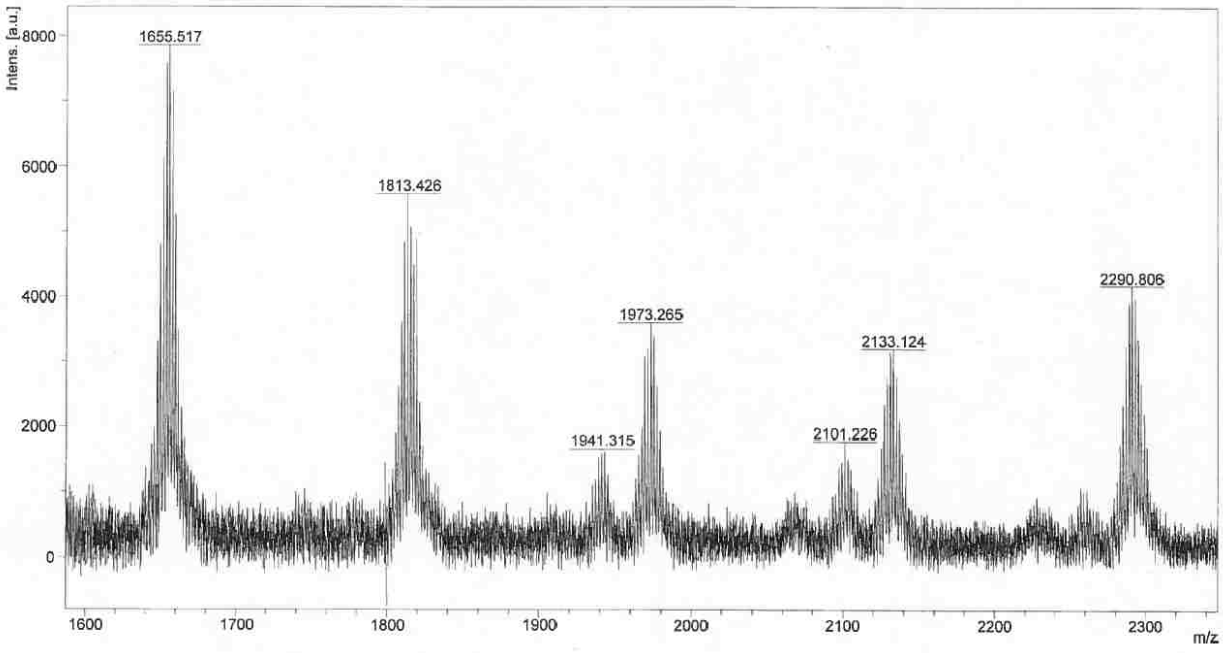

MALDI of terpthiophene high mass range

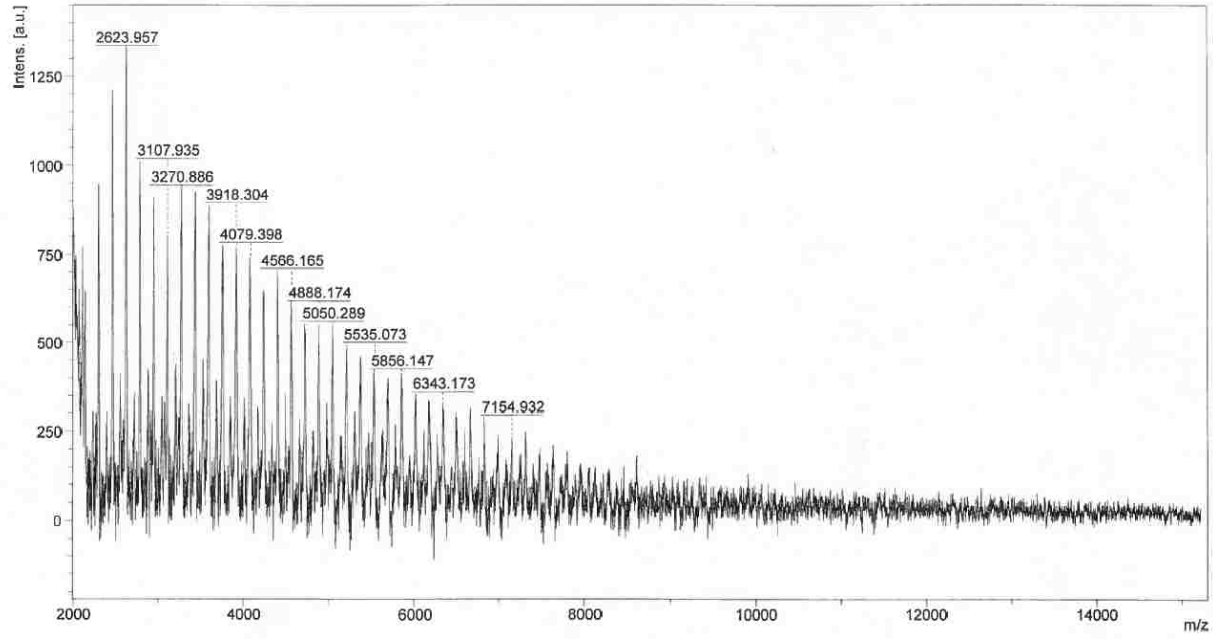

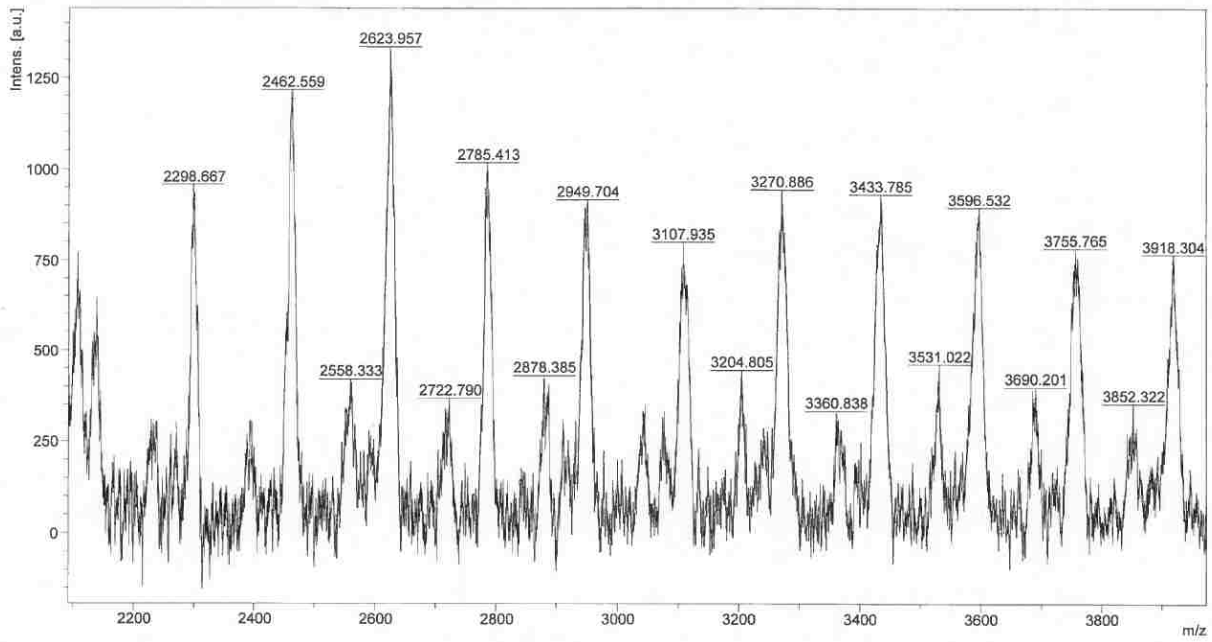
Intens. [a.u.]
1250
1000
750
500
250
0
2623.957
2462.559
2785.413
2298.667
2949.704
3270.886
3433.785
3596.532
3107.935
3755.765
3918.304
2558.333
2878.385
3204.805
3531.022
2722.790
3690.201
3852.322
3360.838
2200
2400
2600
2800
3000
3200
3400
3600
3800
m/z

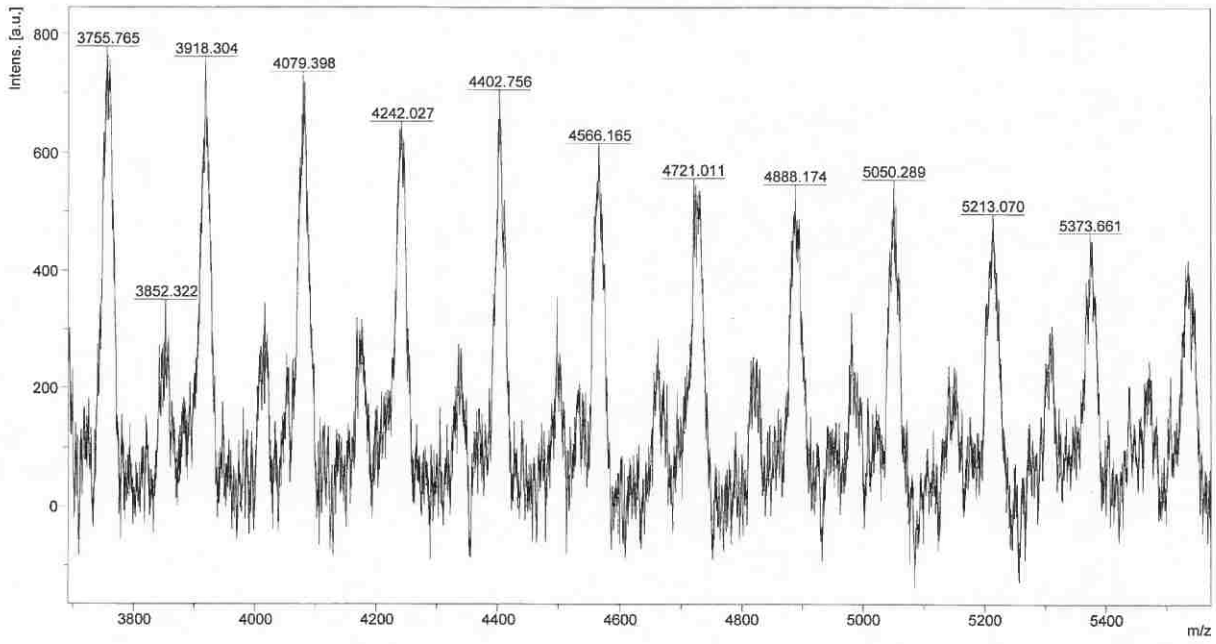
Intens. [a.u.]
800
600
400
200
0
3755.765
3918.304
4079.398
4402.756
4242.027
4566.165
4721.011
4888.174
5050.289
5213.070
5373.661
3852.322
3800
4000
4200
4400
4600
4800
5000
5200
5400
m/z

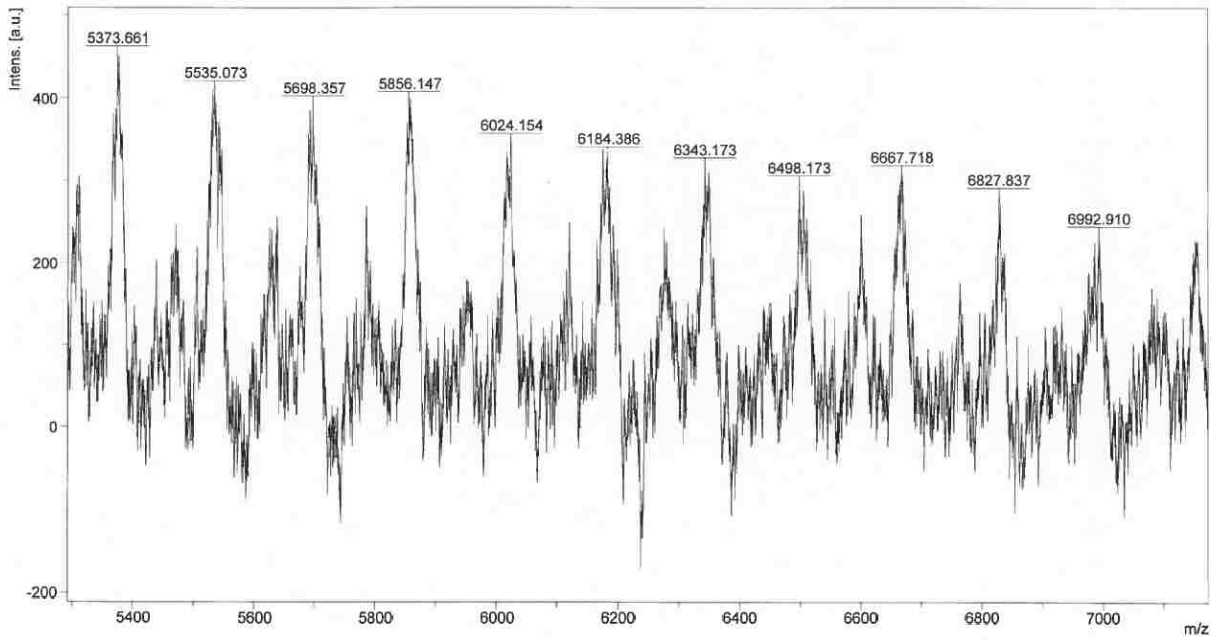
Intens. [a.u.]
400
200
0
-200
5373.661
5535.073
5698.357
5856.147
6024.154
6184.386
6343.173
6498.173
6667.718
6827.837
6992.910
5400
5600
5800
6000
6200
6400
6600
6800
7000
m/z

Vita

Jonathan Casey was born in New Orleans Louisiana. He obtained his Bachelor of Science in Chemistry and Biology in 2010 from the University of New Orleans. In the fall of 2011 he began work towards his master's degree.